CATALYTIC OXIDATION OF ETHYLENE AND PROPYLENE IN A SOLID ELECTROLYTE CELL

by

MICHAEL STOUKIDES

Diploma of Chem. Eng., Nat. Tech. Univ., Athens 1978

Submitted to the Department of
Chemical Engineering on January 26, 1982
in partial fulfillment of the requirements of
the Degree of

Doctor of Philosophy

at the

MASSACHUSETTS INSTITUTE OF TECHNOLOGY

January 1982

Signature of the Author _____
Department of Chemical Engineering

Certified By _____
Prof. Costas Vayenas
Thesis Supervisor

Accepted By _____
Prof. Glenn C. Williams
Departmental Committee on
Graduate Theses

ACKNOWLEDGEMENTS

Many thanks to my advisor, Costas, with whom cooperation was unusually successful. In addition, many people helped me reach this point in my career that I am sure to forget to mention some if I try to list them all. All those who helped me will not be forgotten, and to them I dedicate this thesis.

TABLE OF CONTENTS

ABSTRACT

The silver catalyzed gas phase oxidation of ethylene and propylene was studied in the solid electrolyte cell

$$O_2, C_2H_4 \text{ (or } C_3H_6), CO_2, H_2O, C_2H_4O \text{ (or } C_3H_6O), Ag \mid ZrO_2 (Y_2O_3) \mid Ag, air$$

at temperatures between 200 and 450°C and atmospheric pressure. The new technique of Solid Electrolyte Potentiometry (SEP) was used to monitor the chemical potential of oxygen adsorbed on the metal catalyst. To this end the silver film catalyst also served as one of the electrodes of a solid electrolyte oxygen concentration cell and the open-circuit emf of the cell was monitored during reaction. Thus the dependence of the thermodynamic surface oxygen activity on the gas phase composition and the rate of the reaction was studied and important imformation for the behavior of various species adsorbed on the catalyst surface was obtained. Isothermal rate and oxygen activity oscillations were observed during the oxidation of propylene oxide to CO_2 and H_2O.

During the study of ethylene oxidation it was found that when external voltages were applied to the cell and O^{2-} was "pumped" to the catalyst, the ethylene oxide selectivity and yield increased considerably. The opposite effect was observed upon inversion of the voltage polarity. A similar behavior was observed during propylene oxidation. The increase in the rate of C_2H_4O production exceeded the rate of O^{2-} pumping by two orders of magnitude, indicating a dramatic change in the properties of the silver catalyst. A simple model was proposed in order to explain this new phenomenon.

A. INTRODUCTION - THE SCOPE OF THIS STUDY

A.1 The catalytic oxidation of Ethylene on silver

The gas phase oxidation of ethylene on silver catalysts is the dominant industrial process for ethylene oxide formation, a chemical intermediate with an annual production of the order of 6 billion lbs. (1). Ethylene oxide is a highly reactive chemical. It is probably the most versatile petrochemical at the disposal of industry today (2). The most important products in terms of volume are the glycols. The table below summarizes the utilization of ethylene oxide on a percentage basis for the major applications in U.S. and Western Europe in (1980) (1,2).

	U.S.A.	Western Europe
Ethylene glycols	69	55
Polyglycols		4
Ethanolamines	6	7
Surfactants	13	12
Glycol ethers	7	12
Others	5	10

Ethylene and oxygen react on silver catalysts to produce ethylene oxide, carbon dioxide and water. No other products are formed except in trace amounts, although there is some evidence that acetaldehyde is formed as an intermediate which is rapidly oxidized to CO_2 and water (3, 4).

Typical industrial operating conditions involve temperatures between 220 and 300°C and total pressures of 150-300 psig with usual air-ethylene ratios of 10 to 1 or equivalently Po_2/P_{ET}

∿ 2 (5). All the industrial processes now in use apply fixed bed operation. This is because in a gas-solid fluid-bed operation, problems of attrition of the active silver surface are such as almost to dictate the fixed-bed alternative (2). Other considerations unfavorable to a fluidized catalyst system are: loss of selectivity because of backmixing and channeling, catalyst life and recovery problems which are more critical with an expensive catalyst and narrow range of flow conditions possible with a fluidized catalyst. Furthermore the advantages of a fluidized catalyst for regeneration are of no value here since regeneration of silver is not needed (6).

Due to its great industrial importance a very large number of investigators have studied the gas phase oxidation of ethylene on silver. Despite the large number of kinetic and mechanistic investigations, no generally accepted mechanism has yet been established. The first thorough study was done by Twigg (3 , 4) in the late 1940s. He suggested the following triangular reaction network:

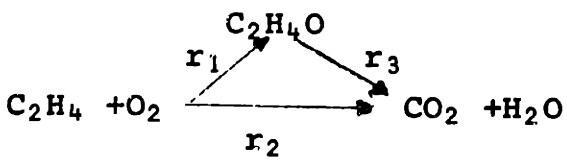

according to which CO_2 can be produced either directly from ethylene or by the oxidation of ethylene oxide. Twigg proposed that only atomic oxygen is adsorbed on silver. When ethylene reacts with one adsorbed oxygen atom ethylene oxide (ETO) is produced, while when it reacts with two adsorbed oxygen atoms CO_2 is produced. Twigg reported both r_1 and r_2 (rates of ETO and CO_2 formation respectively) to be first order in

gaseous ethylene, i.e.

$$r_1 = k_1 P_{ET} \theta_O$$

$$r_2 = k_2 P_{ET} \theta_O$$

He also found the secondary ethylene oxide oxidation to be zero order in oxygen and proportional to the coverage of the adsorbed ethylene oxide:

$$r_3 = k_3 \theta_{ETO}$$

Since the early work of Twigg, numerous studies have been reported and today it is almost generally accepted that besides atomic oxygen, several other species are adsorbed on the catalyst during reaction (7, 8, 9,10,11).

Voge and Adams (7) have reviewed work prior to 1967 and work prior to 1974 has been summarized by Kilty and Sachther (10). Sachther et al. (10,11) proposed the existence of both molecular and atomic oxygen adsorbed on silver. Molecular oxygen reacts with ethylene to produce ethylene oxide while CO_2 is formed from atomic oxygen. Both reactions were proposed to proceed via an Ealy-Rideal mechanism. It was proposed that molecular oxygen requires only one surface Ag site for adsorption while four adjacent sites are required for dissociative adsorption. One can thus explain the observation that chlorinated compounds increase the selectivity to ethylene oxide by assuming that adsorged chlorine atoms, even at low coverages, destroy significant numbers of quadraplets of Ag atoms required for the dissociative adsorption of oxygen.

His mechanism is in basic agreement with that of Imre (12) who suggested the existence of adsorbed atomic oxygen plus two forms of adsorbed molecular oxygen, one parallel (O_2-) and one perpendicular to the surface ($O_2\perp$), the latter being responsible for ETO formation.

Voge and Adams (7), summarizing the work of numerous investigators, suggest a Langmuir-Hinselhood rather than an Ealy-Rideal type of mechanism. However, they also agree with the existence of both atomic and molecular oxygen adsorbed on silver, the former producing CO_2 and the latter ethylene oxide. Apparent activation energies reported are in the range of 13-18 kcal/mole for ETO formation, 19-23 kcal/mol for direct CO_2 formation and 20$\pm$5 kcal/mol for the secondary ethylene oxide oxidation (4, 7). Considerable disagreement exists between previous investigators about the dependence of the rates of ethylene epoxidation (r_1) and combustion (r_2) on P_{ET} and P_{O_2}. various orders between 0 and 1 have been reported for either P_{ET} or P_{O_2} (7,13).

The role of various substances used as moderators is an interesting subject and has been studied by a large number of investigators (7,11,14,15,16). Metal oxides such as BaO, MgO CaO and BaO_2 as well as Se, Te, S and Au-Ag alloys have been reported as having promoting effects on the yield or the selectivity of ethylene oxidation on Ag. Nitrous oxide (17) has been found to cause a decrease on r_1 shifting the selectivity to values close to zero at low temperatures. Nevertheless the moderators that are most frequently used are halogen compounds and specifically chlorinated hydrocarbons.

They are used as gas phase promoters introduced in the reactor feed stream in a concentration of some ppm's. The use of chlorinated compounds for moderating silver has been known for many years from the patent of Law and Chitwood (18). Furthermore since it is not easy to prepare silver completely free from chlorine or sulfur, or other moderating elements, many catalysts used in experimental work have apparently been moderated unintentionally to some extent (7).

The inhibition effect caused by either reactants or products is another subject of considerable study (19-24). Ethylene oxide (23) and hyrodrocarbons (20) have been reported to retard both ethylene epoxidation and combustion rates. Kurilenko et al. (21) and Metcalf and Harriot (19) have suggested that CO_2 inhibits both epoxidation and deep oxidation reactions. Hayes, however, has found that CO_2 has an inhibiting effect on ethylene epoxidation only (22). Hayes also suggested that water vapor has not any effect on either epoxidation or complete oxidation reactions. Metcalf and Harriot however observed that by adding water in the reactor feed the epoxidation rate declines in proportion to the -.25 power of P_{H_2O} and the CO_2 formation rate falls off with the -.20 power of P_{H_2O} (19). In a recent work, Wachs and Kelemen studied the interaction of ethylene with surface carbonate and hydroxide intermediates on silver using spectroscopic techniques (25). They suggested that CO_{3ads} and OH_{ads} on the silver surface are responsible for the inhibiting effects of CO_2 and H_2O.

A large number of investigators have studied the behavior of various species adsorbed on the silver surface during ethylene

oxidation using modern surface techniques. Force and Bell used infrared spectroscopy in order to study the various species adsorbed on silver during ethylene oxidation (8). They also examined the relationship of these species to the reaction mechanism (9). Kummer has studied the reaction kinetics on different silver crystallographic planes and found little difference in activity and selectivity (26). Carberry et al. (27) have found that the selectivity to ethylene oxide increases by γ-preirradiation of the catalyst. Clarkson and Cirillo (28) studied the electron paramagnetic reasonance signals of oxygen adsorbed on silver and suggested that at room temperature most O_2 adsorbed is in the molecular form. Sato and Seo found that emission of exo-electrons from the Ag surface is proportional to the rate of ethylene oxide formation (29). Harriot et al. (30,31) have studied support and crystal size effect on the activity and selectivity of ethylene oxidation. They found that by increasing the crystal size from 20Å to 500Å the selectivity increases from almost zero to 60%. Verykios et al. (32) investigated the kinetic effects of total surface area, average silver crystallite size and silver crystallite morphology of supported silver catalysts under ethylene oxidation conditions. They found that the specific activity and selectivity of the catalysts were strong functions of the total surface area and that the specific rates to ethylene oxide and to CO_2 and H_2O formation exhibited strong structure sensitivity with minimum rates at crystallite sizes in the range of 500-700 Å. Cant and Hall (33) used C^{14} to study oxygen exchange between ethylene and ethylene oxide and found

that ethylene oxide oxidation to CO_2 is much slower than direct CO_2 formation from ethylene oxidation, in agreement with previous workers (3, 4, 5). In a recent communication, Dettwiller et al. (34)provided detailed kinetic expressions for the three reactions r_1, r_2, r_3 for silver supported on pumice. They suggested that for constant P_{O_2}, both r_1 and r_2 can be expressed as

$$r_i = k_i \frac{k_{ET}P_{ET}}{1+k_{ET}P_{ET}}$$

where $K_{ET} = 1.84 \cdot 10^{-4} \exp\left[\frac{53550}{RT}\right] \text{bar}^{-1}$. They also report that the rate of ethylene oxide oxidation r_3 is first order in ethylene oxide and zero order in oxygen.

A.2. The catalytic oxidation of propylene to propylene oxide

Propylene oxide, the third large volume chemical derivative of propylene, trailing polypropylene at 28% and acrylonitrile at 17% accounts for about 13% of propylene consumption for chemical use. The annual production of propylene oxide is in the range of 2 billion lbs. (1). Propylene oxide is a chemical intermediate used primarily for producing polyether polyols and propylene glycol. Urethane polyols account for about 65% of U.S. PrO consumption in today's market. About 80% of the urethane polyols are used to produce flexible foam for use in furniture, automobile seats, carpet underlay, and the like. Ten per cent or polyols consumption ends up in rigid foam used primarily for insulation purposes such as surface coatings, high performance elastomers and mircocellular resins. The other major use for propylene oxide is propylene glycol which accounts for 25% of production. Propylene glycol is used in a number of markets including polyester resins, pet food, cosmetics and tobacco(1).

Unlike ethylene oxide production, the main routes for propylene oxide production are not based on direct catalytic oxidation of propylene, mainly because of the low selectivities to propylene oxide. The major industrial processes currently used for propylene oxide formation are

a) The "chlorination process" according to which propylene is reacted with hypochlorous acid to produce propylene chlorohydrin. The chlorohydrin is then reacted with slaked lime or caustic soda to form propylene oxide.

b) The "Oxirane process" in which isobutane and oxygen are

reacted to form tertiary butyl hydroperoxide and tertiary butyl alcohol. Propylene is then reacted with the hydroperoxide to form propylene oxide. In 1977 Oxirane added new peroxidation technology which uses ethylbenzene instead of isobutane as a feedstock. Today peroxidation accounts for 45% of the total U.S. propylene oxide capacity(1).

It has to be pointed out, however, that propylene oxide formation by direct oxidation of propylene on silver would be financially preferable if high yield and selectivity to propylene oxide could be achieved (1,35). Therefore a large number of investigators have studied the optimal conditions for direct propylene oxidation (36-42). Propylene and oxygen react on silver catalysts at 250-350°C and 1-10 atm total pressure to produce propylene oxide, carbon dioxide and water. Without the use of promoters, total conversion to partially oxygenated products is of the order of 10-15% with a selectivity to propylene oxide of the order of 5-6%. The use of various promoters increases both yield and selectivity by a factor of 2-3 (43,44).

The kinetics of the reaction have been studied in the past but there is no general agreement. Kano and Masatoshi studied the oxidation of propylene in the presence of a mixture of Ag_2O, NaCl and Na_2SO_4. Their reaction rates were expressed as $r_1 = k_1 P_{Pr} P_{O_2}^{.5} - k_1 P_{CO_2}^{.5} P_{Pro}$ for the epoxidation reaction and $r_2 = k_3 P_{Pr} P_{O_2} P_{CO_2}^{-n}$ for the CO_2 formation reaction, where n is between zero and unity depending on the propylene-oxygen ratio (43). Kaliberdo et al. (45) studied the above reaction

system at 280-400°C and concluded that both propylene oxide and CO_2 are formed in a parallel scheme:

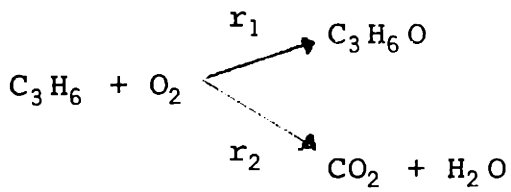

The activation energies for both reactions are reported to be between 9 and 16 kcal/mole (46,47). In general the rate dependence of r_1, r_2 on P_{O_2}, P_{Pr} is reportedly between zero and one for both reactants (46,47,43).

The promoting effect of various compounds is an interesting subject of study. As in the case of ethylene oxidation chlorinated hydrocarbons are reported to have a promoting effect on the selectivity to PrO (37,48). Besides Chlorine compounds, CaO and BaO were also found to have a promoting effect. Sulfure, however, decreases the catalyst activity (37). Yamanato et al. studied the effect of the catalyst modification with sodium halides. Catalytic activity was decreased in the order of NaF > NaCl > NaI while the selectivity to propylene oxide was increased (49). Kaliberdo et al. suggested that a propylene-propane mixture provides a selectivity of 30% with respect to propylene oxide while other products besides CO_2, H_2O and PrO were formed: acetaldehyde, propionaldehyde etc. (37).

The effect of reaction products on the rates of the reaction is another interesting subject of study. Propylene oxide was found to inhibit both the epoxidation and the complete oxidation to CO_2. Carbon dioxide was found to decrease both those rates at temperatures above 330°C (50).

Kaliberdo et al. also studied the oxidation of propylene oxide on pure silver and on silver supported on various carriers (38). They found that on pure silver only CO_2 and water are produced below 420°C. Isomerization products including propionaldehyde, acetone and acetaldehyde were found as products when α-Al_2O_3 and silicon carbide were used as carriers. Cant and Hall (33) studied the oxidation of ethylene and propylene labeled with deuterium as well as cooxidation of unlabeled olefins with the corresponding ^{14}C labaled epoxides at temperatures 200-220°C. They found that in both instances most of the undesirable CO_2 originates from direct oxidation of the olefins and thus the reason for low selectivity of silver for propylene oxide formation is not primarily due to the instability of propylene oxide under reaction conditions. The stereochemistry of the epoxidation of CiS-propylene - 1,2-d_2 to propylene oxide was studied recently by Imachi et al. (51) over supported and unsupported silver catalysts. They also examined similarities between ethylene and propylene epoxidation on silver.

In a number of recent communications partial surface polymerization of adsorbed propylene or propylene oxide has been suggested (51,52). Freriks et al. (51) suggested that the low selectivity of propylene to propylene oxide is caused by the formation of acrolein which polymerizes and is deeply oxidized by gaseous oxygen to CO_2 and H_2O. The existence of a surface intermediate has also been suggested by Kobayashi (52). Kobayashi reported that the ratio of C:H in the structure of this intermediate is 1:2. The rate of decomposition of this adsorbed intermediate was

found to be first order with respect to its coverage and proportional to the partial pressure of oxygen in the gas phase (52).

A.3. Oxygen ion conducting solid Electrolytes

Solid electrolytes are solid state materials with an electric conductivity partly or wholly due to ionic displacement. Point defects are primarily responsible for electrical conduction in solid electrolytes. Presence of ionic defects gives rise to ionic conductivity, while that of electronic defects results in electronic conductivity, which is undesirable in a solid electrolyte. In practice, for a solid electrolyte to be useful, the ratio of ionic to electronic conductivity should be 100 or greater (53).

Research on solid electrolyte properties and applications is continually expanding. Both cations are anions may be the conducting species of the solid electrolyte. Various compounds have been reported to be pure Ag^+, H^+, K^+, Na^+, $10Li^+$, Cu^+, NH_4^+, Al^{3+}, Mg^{2+} or Rb^+ conductors. On the other hand the following anions are reported to be the conducting species of several solid state materials: F^-, Cl^-, Br^-, I^-, O^{2-} and 5^{2-} (53).

Of particular interest in the present research is the class of oxygen ion conducting solid electrolytes. These are solid solutions formed between oxides containing di- and trivalent cations such as CaO, Sc_2O_3, Y_2O_3 or La_2O_3 with oxides containing tetravelent cations such as ZrO_2, ThO_2 and CeO_2 (54). Their high ionic conductivity is due to the existence of O^{2-} site vacancies. One O^{2-} vacancy occurs for each divalent or each two trivalent cations that are substituted for a tetravelent ion in the lattice. Of special interest is a solid solution containing 15 mol % CaO in ZrO_2 (calcia stabilized zirconia)

as well as a solid solution containing 8 mol % Y_2O_3 in ZrO_2 (yttria stabilized zirconia). The importance of these two solid electrolytes is due to their high inoic conductivity, their pure oxygen-ion conduction over wide ranges of temperature and oxygen pressure (55) as well as their relatively low cost.

Several investigators including Schmalzreid (56), Steele and Alcock (57) and Baker and West (58) have determined the temperature and P_{O_2} limits of the purely anionic conduction of calcia and yttria stabilized zirconia. As a general conclusion they found that as long as the partial pressure of oxygen in contact with stabilized zirconia is higher than the oxygen partial pressure defined by the Cr/Cr_2O_3 equilibrium, then the transference number of O^{2-} in stabilized zirconia is essentially unity. Since the Cr/Cr_2O_3 equilibrium defines extremely low oxygen partial pressures ($P_{O_2} \sim 10^{-30}$ atm of 1000°K), the range over which stabilized zirconia can be used as a purely anionic conductor is very wide. For all practical purposes, calcia or yttria stabilized zirconia is a purely ionic conductor for temperatures below 1200°C. For these temperatures, the conductivity of yttria and calcia stabilized zirconia is given approximately by:

$$K_{\text{yttria-zirconia}} = 240 \exp\left(-\frac{9700}{T}\right) (\text{Ohm}\cdot\text{cm})^{-1}$$

$$K_{\text{calcia-zirconia}} = 2800 \exp\left(-\frac{15130}{T}\right) (\text{Ohm}\cdot\text{cm})^{-1}$$

where T is °K.

The pure ionic conduction of stabilized zirconia enabled

Wagner and Kiukkola to construct a high temperature stabilized zirconia concentration electrochemical cell and use it to obtain accurate free energies of formation of several metal oxides (54). Similar experiments were carried out by Peters and Mobius (59) and Peters and Mann (60) with stabilized zirconia and thoria. Weissbart and Ruka (61) tested experimentally a similar cell of the type O_2 (anode), Pt $|(ZrO)_{.85}(CaO)_{.15}|$ Pt, O_2 (cathode) and verified that the open circuit EMF was in very good agreement with the Nernst equation

$$E_o = \frac{RT}{4F} \ln\left[\frac{P_{O_2}\ (anode)}{P_{O_2}(cathode)}\right] \qquad [A.3.1]$$

where F is the Faraday constant, and R is the ideal gas constant.

A.4. Solid Electrolyte Potentiometry (SEP) and Oxygen "Pumping"

The important role that solid electolytes can play in the effort for a better understanding of heterogeneous catalytic oxidations was first realized by C . Wagner (69) who proposed the new technique.

The basic principle of solid electrolyte potentiometry (SEP) is as follows: two thin ($\sim$ 1-10 μm) porous metal film electrodes are deposited on the two sides of a thin ($\sim$ 100-1000 μm) stabilized zirconia disc (Fig. 1). One electrode is exposed to a reference gas, like O_2 or air, and the other electrode is exposed to a reactive gas mixture and serves as the catalyst as well. At sufficiently high temperatures (i.e. above approximately 250°C), the mobility of oxygen ions in the elctrolyte becomes significant so that under zero-current conditions a constant electrochemical potential for oxygen ions is established throughout the electrolyte. Under these conditions the steady-state electromotive force of the cell is given by

$$E = \frac{1}{4F} \left[\mu_{O_2}(\text{catalyst}) - \mu_{O_2}(\text{reference})\right] \qquad [A.4.1]$$

where F is the Faraday constant, provided both electrodes are made of the same metal and are at the same temperature. One can define the oxygen activity on the catalyst a_{O_2} (catalyst) as follows:

$$\mu_{O_2}(\text{catalyst}) = \mu^{\circ}_{O_2}(g) + RT \ln a_{O_2}(\text{catalyst}) \qquad [A.4.2]$$

i.e. a_{O_2} (catalyst) expresses the partial pressure of gaseous oxygen (in atmospheres) that would be in equilibrium with oxygen adsorbed on the catalyst at the given temperature. For Pt, Ag or Au in contact with air, equilibrium is rapidly

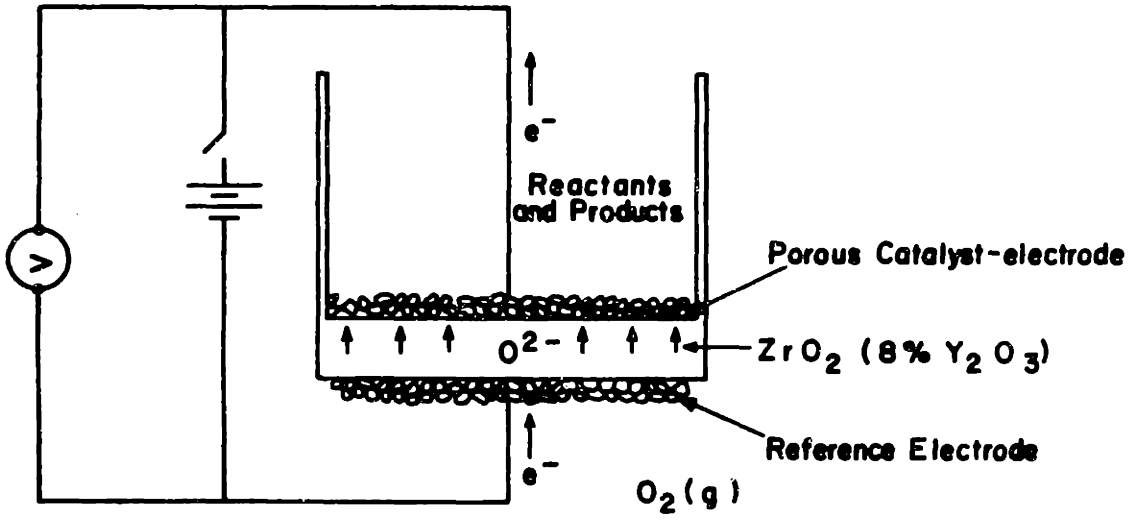

Figure 1: Schematic diagram of apparatus for oxygen activity measurement

established between O_2 in air and O_2 on the metal electrode (63), under zero-current conditions, therefore, we can write:

$$\mu_{O_2}(\text{reference}) = \mu^{\circ}_{O_2}(g) + RT \ln P_{O_2} = \mu^{\circ}_{O_2}(g) + RT \ln (.209) \qquad [A.4.3]$$

Combining (A.4.1), (A.4.2) and (A.4.3), one obtains

$$E = \frac{RT}{4F} \ln \left(\frac{a_{O_2 \text{catalyst}}}{.209} \right) \qquad [A.4.4]$$

for air as the reference gas.

The last equation shows that by simply measuring the open-circuit EMF and the temperature, one can immediately calculate a_{O_2} (catalyst) and therefere directly determine whether or not equilibrium is established between oxygen in the gas phase of the reacting mixture and oxygen on the surface of the catalyst, provided one knows or can independently measure P_{O_2} in the gas phase.

This technique of solid electrolyte potentiometry originally proposed by Wagner (62) has been used in conjunction with kinetic measurements to study the mechanism of SO_2 oxidation on noble metals (63,64) and of the oxidation of ethylene on platinum (65).

A second important application of oxygen ion conducting solid electrolyte cells is their use as oxygen "pumps". When a voltage is applied to a stabilized zirconia cell, a current flows and oxygen is transferrred accordingly from one side of the electrolyte to the other. This device has been used by Weiss-hart and Smart (66), and Mason, Huggins et al. (67,68) as a means to dissociate compounds containing oxygen such as CO_2, H_2O and NO. Stabilized zirconia cells with catalytic electrodes operating in the fuel cell mode have been used to cogenerate electrical energy and nitric oxide (69,70).

A.5 The Scope of This Study

A considerable improvement in the understanding of heterogeneous catalysis would be achieved if the properties of reactants, intermediates and products, present on the catalyst surface, could be measured during reaction. In particular, knowledge of the properties and the concentration of oxygen adsorbed on the catalytic surface is of crucial importance in determining the oxidation mechansim.

In the previous sections of the introduction two industrially important catalytic systems were presented, the oxidations of ethylene and propylene on silver. Despite the large number of investigations and the various spectroscopic and high vacuum techniques that have been used, much remains still unknown about the mechansim of these reactions - information which would be very useful for the rational design of catalysts as well as for the effective reduction of the undesirable byproducts.

Solid electrolyte Potentiometry is a technique recently developed in order to monitor the thermodynamic activity of oxygen adsorbed on metal surfaces. The advantages of this technique are

a) Operation under industrially important temperature and pressure conditions. High vacuum conditions are thus not required.

b) The oxygen activity measurement is continuous.

In the present study SEP will be used in conjunction with kinetic measurements in order to elucidate the mechanism of the

above mentioned catalytic oxidations. To that end both reactions will be carried out in an oxygen concentration solid electrolyte cell with silver electrodes. This mechanistic investigation is the first goal of the present research.

As it has already been mentioned both the selectivity of the catalytic oxidation of ethylene and propylene to their epoxides is limited by their complete oxidation to CO_2 and H_2O. A number of different approaches have been examined so far in order to increase the selectivity to the epoxides including alloying silver with other metals, using different catalyst supports and promoters as well as adding gas phase moderators (sect. A.1, A.2). In the present study an electrochemical approach will be examined. By applying an external voltage across the solid electrolyte cell oxygen will be pumped electrochemically to or from the catalyst surface causing an increase or decrease to the activity of oxygen species adsorbed on the catalyst. Thus the investigation of the effect of oxygen "pumping" on the yield and the selectivity of ethylene and propylene epoxidation is the second goal of the present research.

B. EXPERIMENTAL APPARATUS

A schematic diagram of the apparatus is given in Fig. 2. It consists basically of the flow system, the reactor cell and the analytical system.

Reactants and diluents were Matheson certified standards of ethylene, ethylene oxide, propylene, propylene oxide, nitrogen, carbon dioxide and zero grade air. All reactants were diluted in nitrogen. Reactants and diluents passed through the calibrated flowmeters where the flowrates were accurately measured. Then the gases were mixed and entered the reactor cell. The effluent stream passed through the IR CO_2 analyzer before being vented (Fig. 2). Sample valves were located before and after the reactor cell in order to take samples of either reactants or products and pass them through the Gas Chromotograph. The G.C. was operating on line and a sample loop of 2 ml volume was used.

The reactor cell configuration is shown in Fig. 3. The silver catalyst film was deposited on the flat bottom of a 8% Y_2O_3 stabilized zirconia tube. The stabilized zirconia tubes obtained from Zircoa Products, Corning Glass Works, were .15m long and of $2 \cdot 10^{-4}$ m^3 internal cross sectional area with a corresponding volume of $3.03 \cdot 10^{-5}$ m^3 (30.3 cm^3). The flat bottoms of the tubes were diamond polished to a thickness of approximately 200 microns in order to reduce the resistance of the oxygen concentration cell. To deposit the silver film at the bottom of the tube, a few drops of a silver suspension in butul acetate was used. (See section C1.c). An appropriately machined stainless steel cap was clamped to the open end of

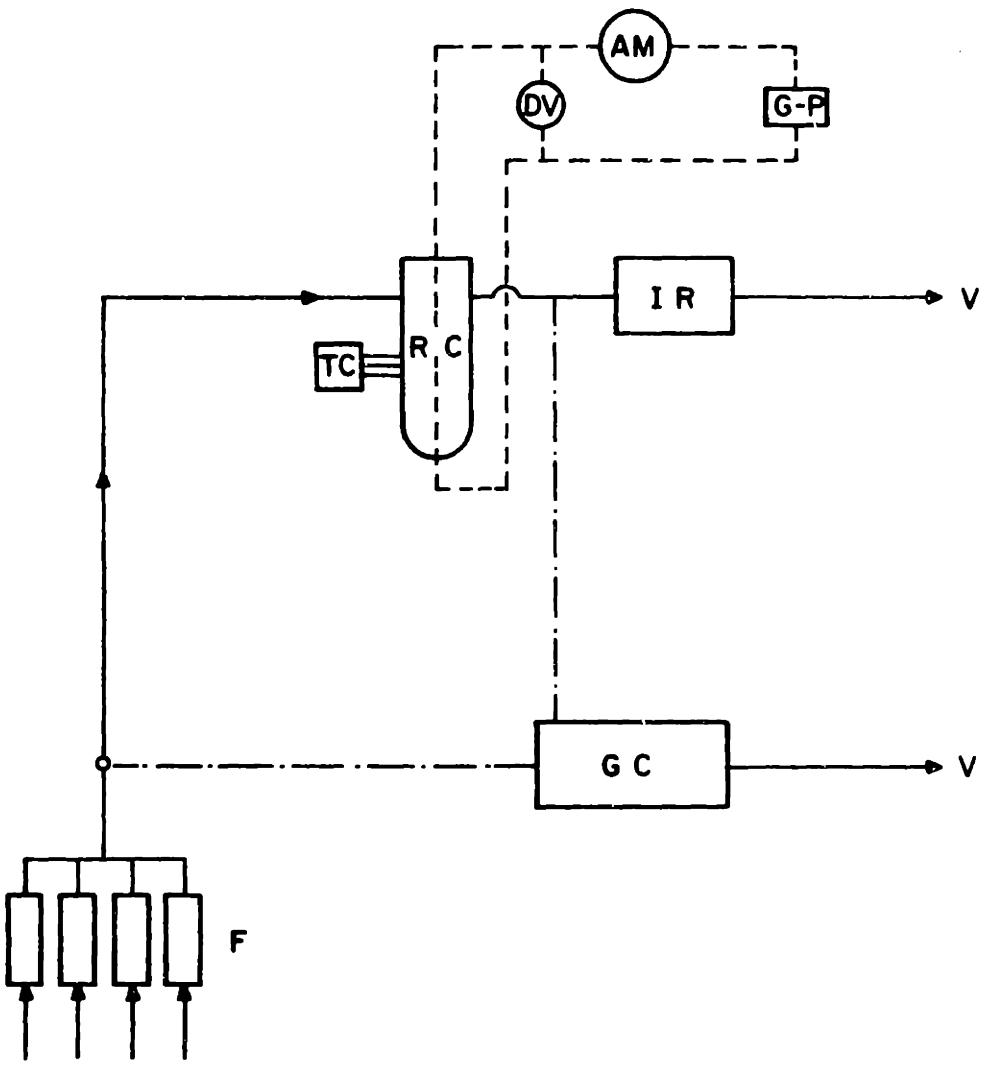

Figure 2: Schematic diagram of the apparatus

(F) Calibrated feed flow meters (RC) Reactor cell (TC) Temperature controller (IR) Infrared analyzers (GC) Gas chromatograph (DV) Differential voltmeter (AM) Multimeter (G-P) Galvanostat-Potentiostat (V) Vent

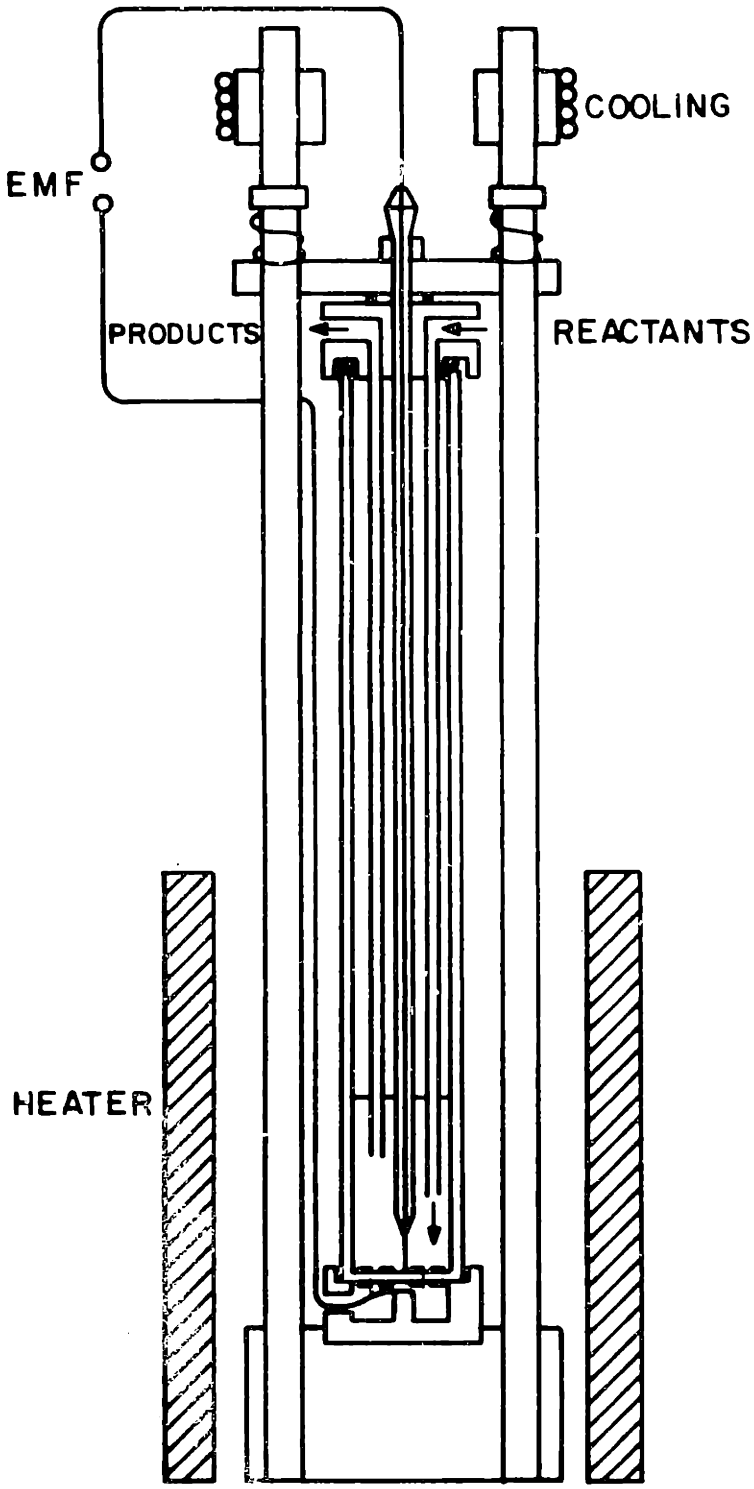

Figure 3: Reactor-cell configuration

the tube. The cap had provision for introduction of reactants, removal of products as well as for introduction of a Ag wire, enclosed in a Pyrex tube to make contact with the internal film catalyst-electrode. The cap was water cooled. The reactor cell was placed in a resistively heated furnace. The catalyst temperature was controlled within 1-2°C by means of a Leeds and Northrup temperature controller and was also measured with a second thermocouple touching the wall of the stabilized zirconia tube 1 mm from the reference electrode.

Reactants and products were analyzed by means of a Perkin-Elmer Gas Chromatograph with a Thermal Conductivity detector. A Poropak Q column was used to separate air, CO_2, and hydrocarbons. Air, CO_2 and Ethylene could be easily separated at 25-30°C column temperature. For separating ethylene and ethylene oxide a 90°C column temperature was used while Propylene oxide was separated at a 100°-110°C. A molecular sieve 5A column was used to separate N_2 and O_2, operating at room temperature. The concentration of CO_2 in the products was also monitored by a Beckman 864 Infrared Analyzer.

For the measurement of the open circuit EMF of the oxygen concentration cell, a J. Fluke 981A differential voltmeter was used with an input resistance of 10^8 Ohms and infinite resistance at null. An AMEL 549 Potentiostat-Galvanostat was used for the application of external voltages and current measurement through the electrolyte. The voltmeter reading as well as those of the IR CO_2 Analyzer and the Gas Chromatograph were recorded using Houston Instruments model B5111-5 one pen and model B5216-2 two pen chart recorders.

C. EXPERIMENTAL RESULTS AND DISCUSSION

c.1 Reactor Design Characteristics

Catalyst preparation and characterization

C1.a Reactor characteristics

The continuous flow reactor used throughout this study is a zirconia tube shown in figure 3 and described in chapter B. Over the range of flowrates employed in the present study the reactor has been shown to be well mixed (CSTR). This was found using the IR CO_2 analyzer as follows:

CO_2 free air was introduced in the reaction at a constant flowrate. At t=0, the air stream was cut off and replaced by an equal flowrate of 1% CO_2 in Nitrogen. The IR CO_2 analyzer was monitoring the concentration of CO_2 in the effluent stream. Figure 4 shows this transient response in comparison with the F curve of an ideal CSTR. For all practical purposes the zirconia reactor can be considered well mixed.

C1.b External and internal mass transfer limitations

It was necessary to verify that the experimental measurements during the studies of ethylene and propylene oxidation represented intrinsic kinetics and that external or internal diffusion limitations were negligible. It was also desirable to determine the flowrate limits below which mass transfer limitations started to be significant.

For the above purpose the total rate of ethylene consumption r_t was measured by varying the total flowrate during ethylene oxidation at 440°C, which was the highest temperature employed in our study (see sections C2 and C3).

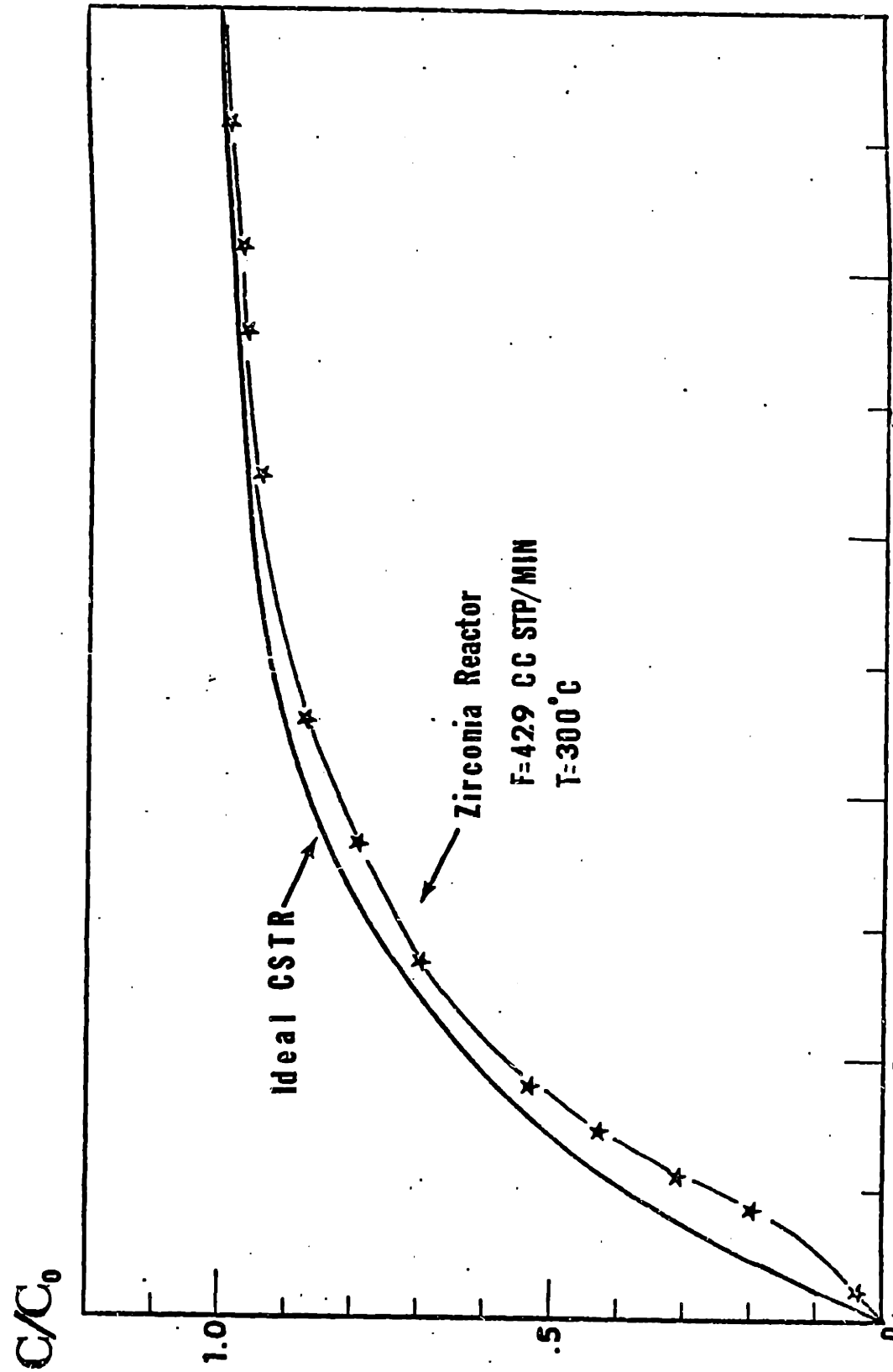

Figure 4: Reactor response to a step change in inlet CO_2 concentration

At this temperature the reaction rate is linearly dependent on the partial pressure of ethylene. Thus the reaction rate r_t satisfies the equation

$$r_t = K_t \; P_{ET} \qquad [C1.1]$$

In the general case the reaction rate constant K_t can be written as:

$$K_t = \frac{1}{\frac{1}{K_R} + \frac{1}{K_M}} \qquad \text{where } K_R \text{ is} \qquad [C1.2]$$

the intrinsic reaction rate constant and K_M is the overall mass transfer coefficient. Thus the reaction rate has the general form:

$$r_t = \frac{1}{\frac{1}{K_R} + \frac{1}{K_M}} \; P_{ET} \qquad [C1.3]$$

When mass transfer limitations are absent

$$r_t = \frac{1}{\frac{1}{K_R}} \; P_{ET} = K_R P_{ET} \qquad [C1.4]$$

and when mass transfer is dominant

$$r_t = K_M \; P_{ET} \qquad [C1.5]$$

The reaction rate was calculated by measuring the total flowrate and the inlet and outlet concentrations of ethylene:

$$r_t = F(P_{ET_1} - P_{ET}) \qquad [C1.6]$$

where P_{ET_1} is the inlet concentration of ethylene. Combining eqns [C1.3] and [C1.6] one gets:

$$F[P_{ET_1} - P_{ET}] = \frac{1}{\frac{1}{K_R} + \frac{1}{K_M}} P_{ET} \qquad [C1.7]$$

Thus $$\frac{P_{ET_1}-P_{ET}}{P_{ET}} \cdot = \frac{1}{\frac{1}{K_R} + \frac{1}{K_M}} \cdot \frac{1}{F} \qquad [C1.8]$$

If the flowrate is sufficiently high, so that no mass transfer limitations exist $\frac{P_{ET_1}-P_{ET}}{P_{ET}} = K_R \cdot \frac{1}{F}$. When the flowrate decreases diffusion problems will eventually arise below some value of the flowrate.

Table 1 contains experimental data at 440°C and flowrate variations between 720 and 165 cm^3/min. In figure 5 the expression $\frac{P_{ET_1}-P_{ET}}{P_{ET}}$ is plotted vs. $\frac{1}{F}$ using the data of table 1. From that figure it is concluded that diffusion limitations are not significant at flowrates above 200-250 cm^3/min for this particular reaction.

The same procedure was followed for the study of propylene oxidation. . Figure 6 shows a similar plot of $\frac{P_{Pr_1}-P_{pr}}{P_{Pr}}$ vs. $\frac{1}{F}$ for data obtained at 420°C. At this temperature diffusion limitations are neglible for flowrates higher than 540-580 cm^3/min. The absence of internal diffusional effects was verified by using three different reactors with porous Ag films thicknesses verying roughly between 3 and 20 μm and observing no difference (< 1-2%) in the surface oxygen activity at the same temperature and gas phase composition. Since the surface oxygen activity a_o is measured at the bottom of the porous Ag film, i.e., at the gas-metal-zirconia interline, this proves that internal diffusional effects were neglible.

Table 1

Effect of flowrate on the reaction rate

(T = 440°C)

P_{ET_1} ($x10^3$bar)	P_{ET} ($x10^3$bar)	F_{tot} cm^3/min	$\frac{\Delta P_{ET}}{P_{ET}}$	$\frac{1}{F}.10^3$ min/cm^3
10.79	9.15	720	.179	1.39
10.79	8.96	640	.204	1.56
10.98	8.48	565	.275	1.77
10.40	8.19	490	.270	2.04
10.31	7.99	425	.290	2.35
10.79	7.80	360	.383	2.78
10.79	7.56	312	.427	3.21
10.59	7.18	254	.475	3.94
10.21	6.50	204	.571	4.90
10.35	6.16	164	.680	6.09

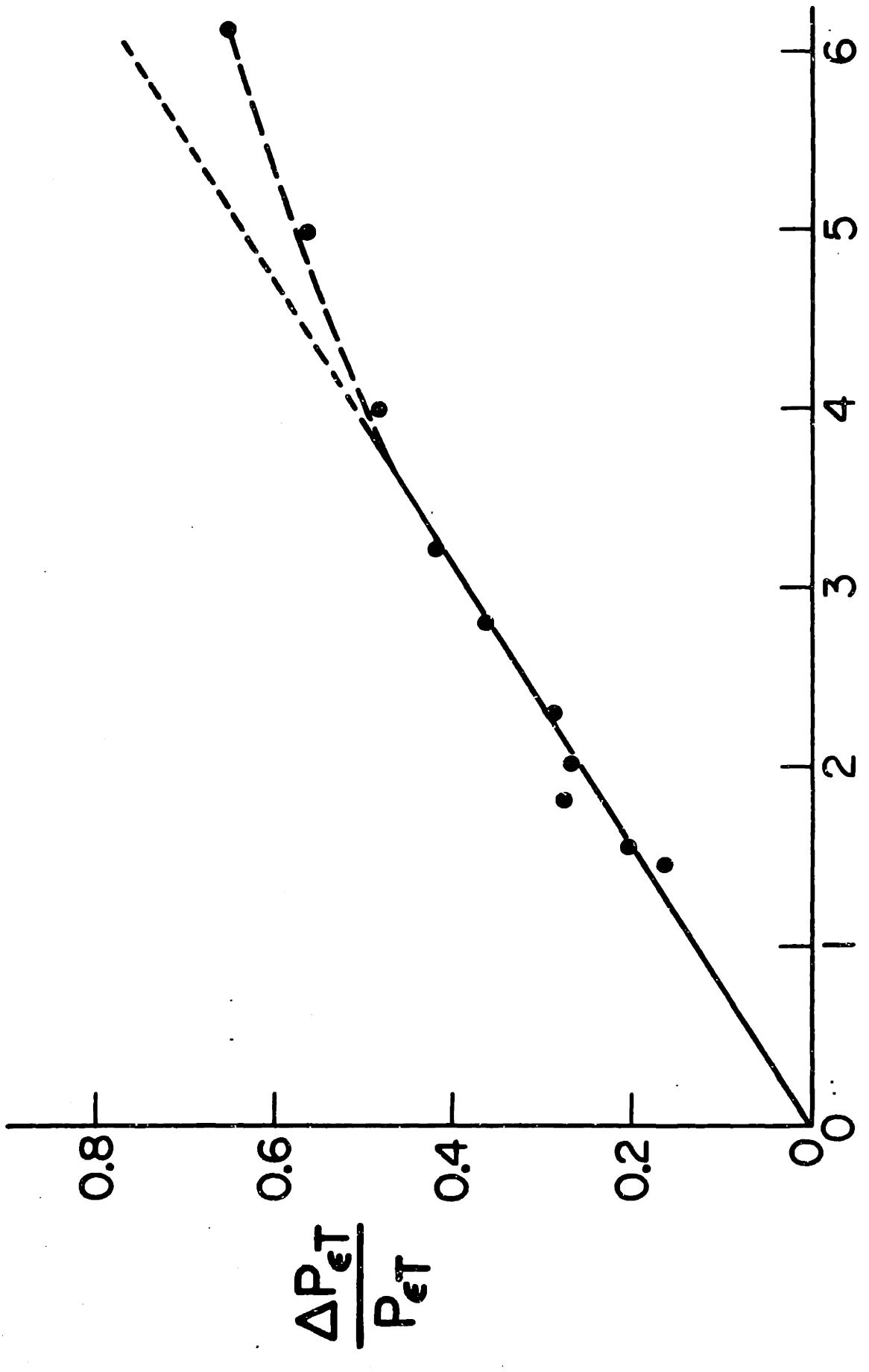

Figure 5: Effect of flowrate on the reaction rate

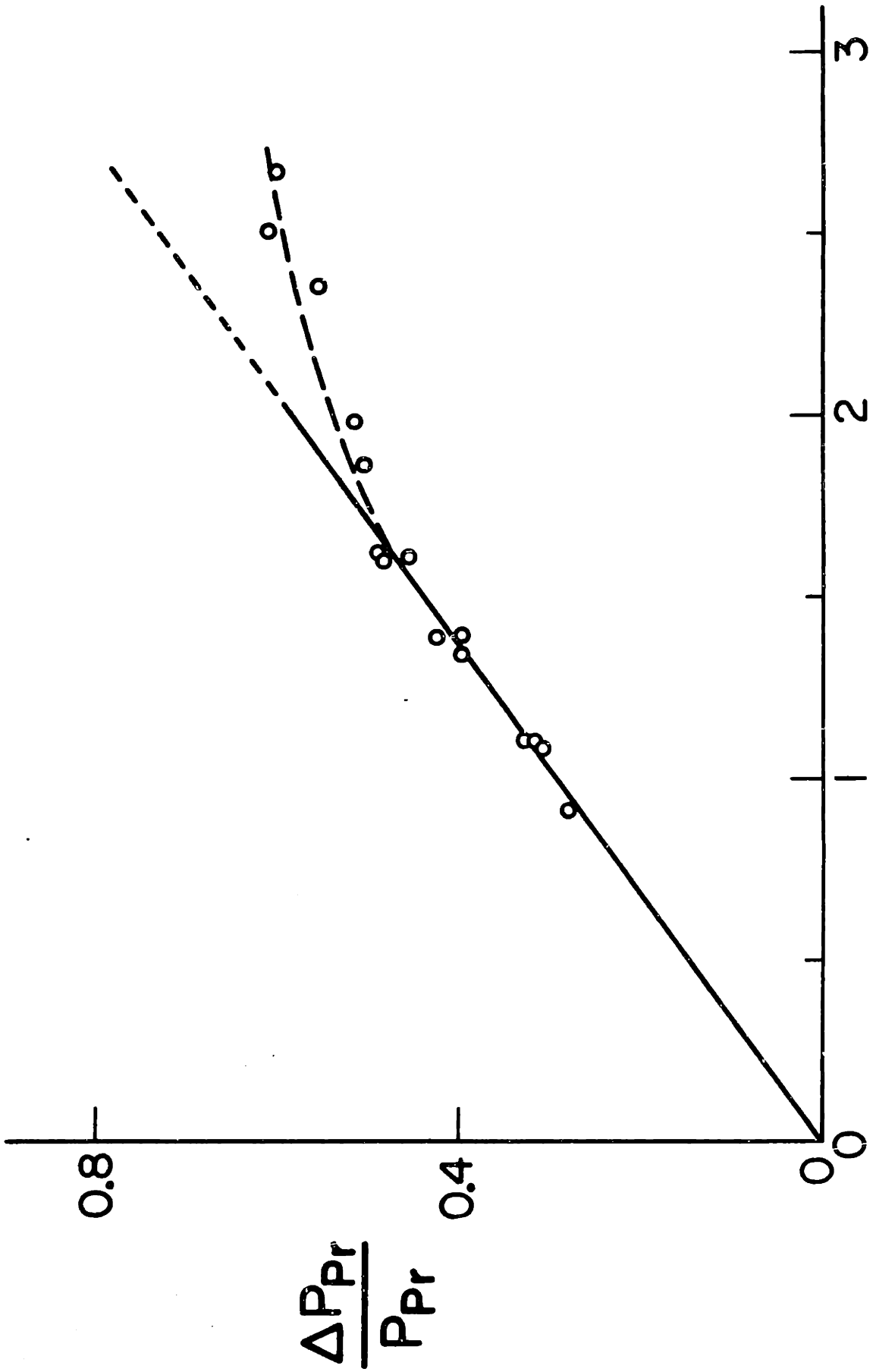

Figure 6: Region of external mass transfer limitations

C.1c Catalyst preparation and characterization

The Ag catalyst film that was deposited on both walls on the flat bottom of the zirconia tube (fig . 3) was prepared from a silver suspension in butyl acetate, obtained from GC Electronics. To deposit the film a few drops of the silver suspension were used, followed by drying at 70-80°C for 2 hours. Then the catalyst was calcined at 400°C for four hours.

The catalyst surface was examined using Auger Electron Spectroscopy and Scanning Electron Microscopy. The Auger spectrum of one of the catalysts used for the present research is exhibited in fig. 7. The spectrum shows that the silver surface impurities include some Cl (probably less than .5% of a monolayer) which might be responsible to some extent for the observed high selectivity of this catalyst for the ethylene oxidation to ethylene oxide. A typical scanning electron micrograph of the catalyst is shown in fig. 8. It can be seen that the catalyst film is fairly porous with an average diameter of pores of 1-2 microns.

C1.d. Catalyst Initial Transient Operation.

Oxygen desorption experiments

When a freshly calcined catalyst is placed on stream in an ethylene/O_2 mixture the catalyst activity and selectivity as well as the surface oxygen activity a_o change considerably during the first 10 h and approach steady state only after 30 h on stream. The selectivity usually passes through a maximum. A typical case is shown in figure 9. The catalyst activity, selectivity and oxygen activity were then found to remain

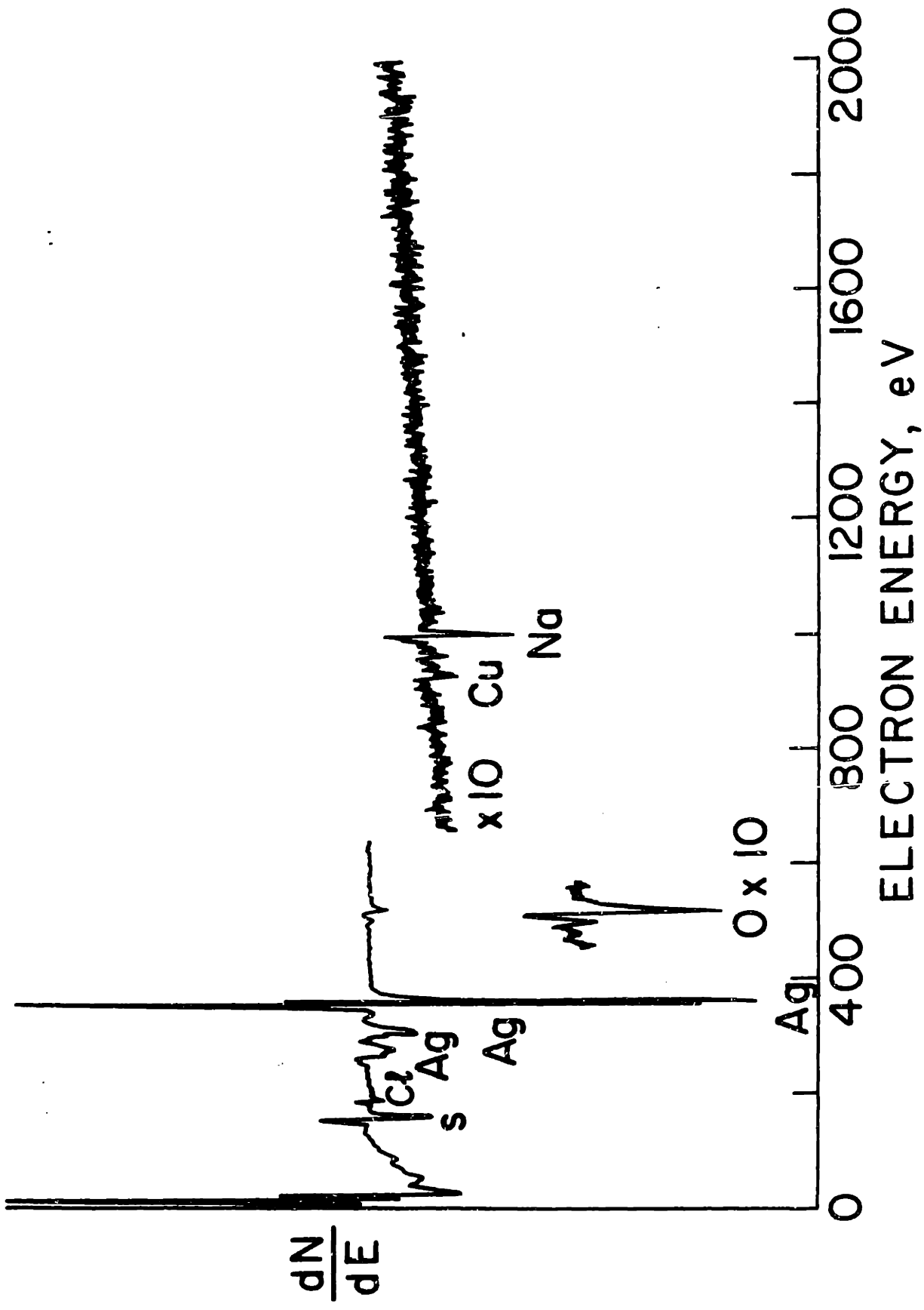

Figure 7: Auger Spectrum of the catalyst.

Figure 8: Scanning Electron Micrograph of a catalyst sample.

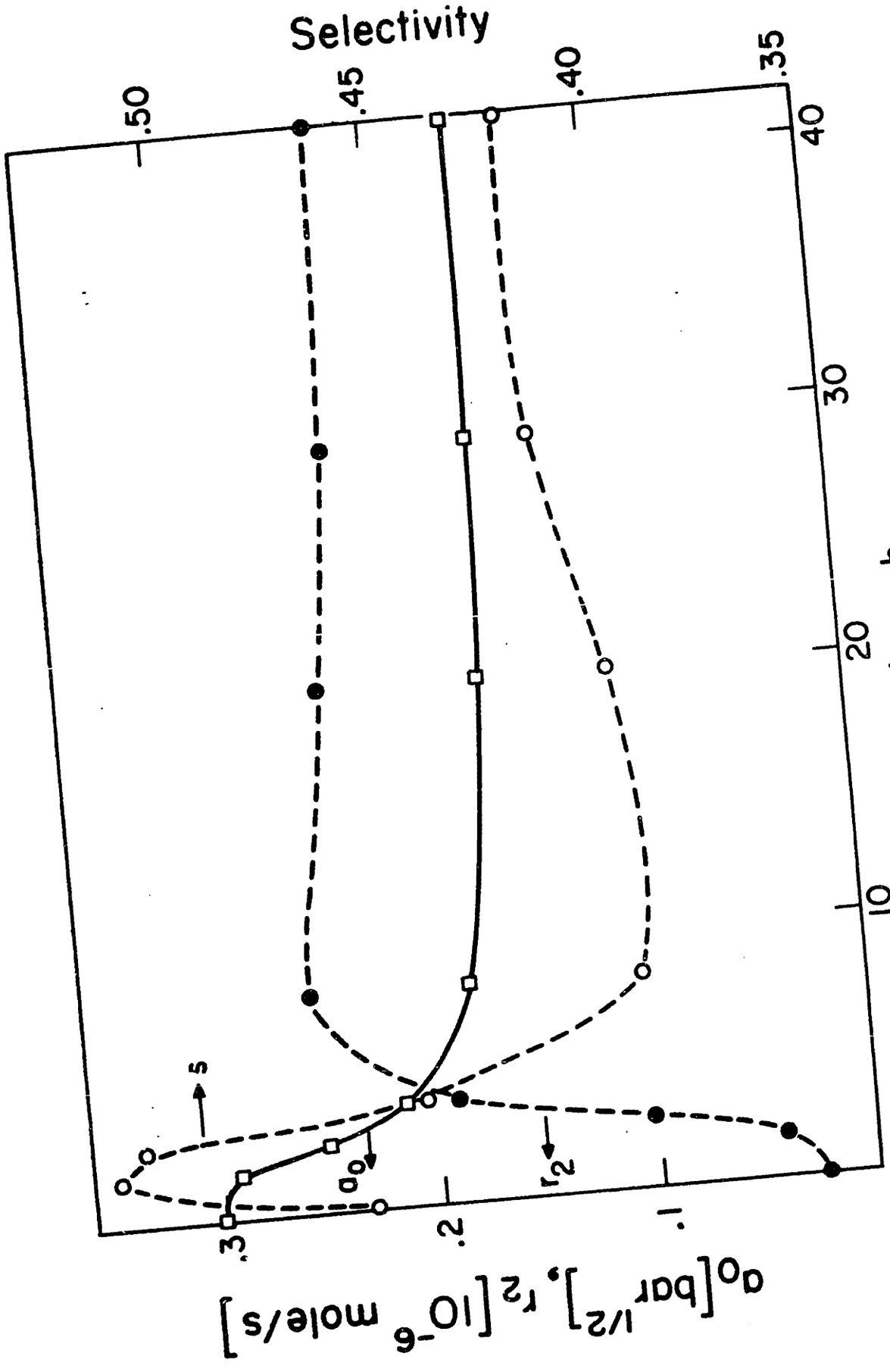

Figure 9: Transient catalytic activity, selectivity and surface oxygen activity of a freshly calcined silver catalyst during the first 40 h on stream. Catalyst is exposed to reactive gas mixture at t = 0.

practically constant over periods of several weeks. All the experiments reported here were performed after the silver catalysts had reached steady state.

The surface of the catalyst used in our open circuit kinetic and potentiometric studies (C2,C3,C5,C6) could absorb approximately $2.0\ (\pm.8)\cdot10^{-6}$ mol O_2. This was estimated as follows. Oxygen was allowed to chemisorb on the catalyst for at least 10 minutes at temperatures above 250°C. The reactor was then purged with ultrapure N_2 for a time t at least eight times longer than the residence time of the CSTR ($\sim$6s) and then flushed with ethylene. The ir CO_2 analyzer was used to monitor continuously the O_2 concentration in the reactor effluent and thus determine the total number of CO_2 molecules formed by integrating the area of the very sharp peak obtained (peak width 5-8 s). The sharpness of the peak verified what was observed with independent steady-state ethylene oxidation experiments, i.e., that the kinetics of the ethylene oxidation to CO_2 are almost two orders of magnitude faster than the oxygen desorption kinetics. Since the ethylene oxidation selectivity of the catalyst was independently determined and shown to be weakly dependent on residence time and gas-phase composition at given temperature, one may assume that the transient nature of these experiments introduces only small variations in selectivity, and thus estimate the amount of oxygen adsorbed on the catalyst at time t. By varying t one can examine the rate of oxygen desorption. A near-first-ord r dependence on adsorbed oxygen was observed (Fig .10) so that

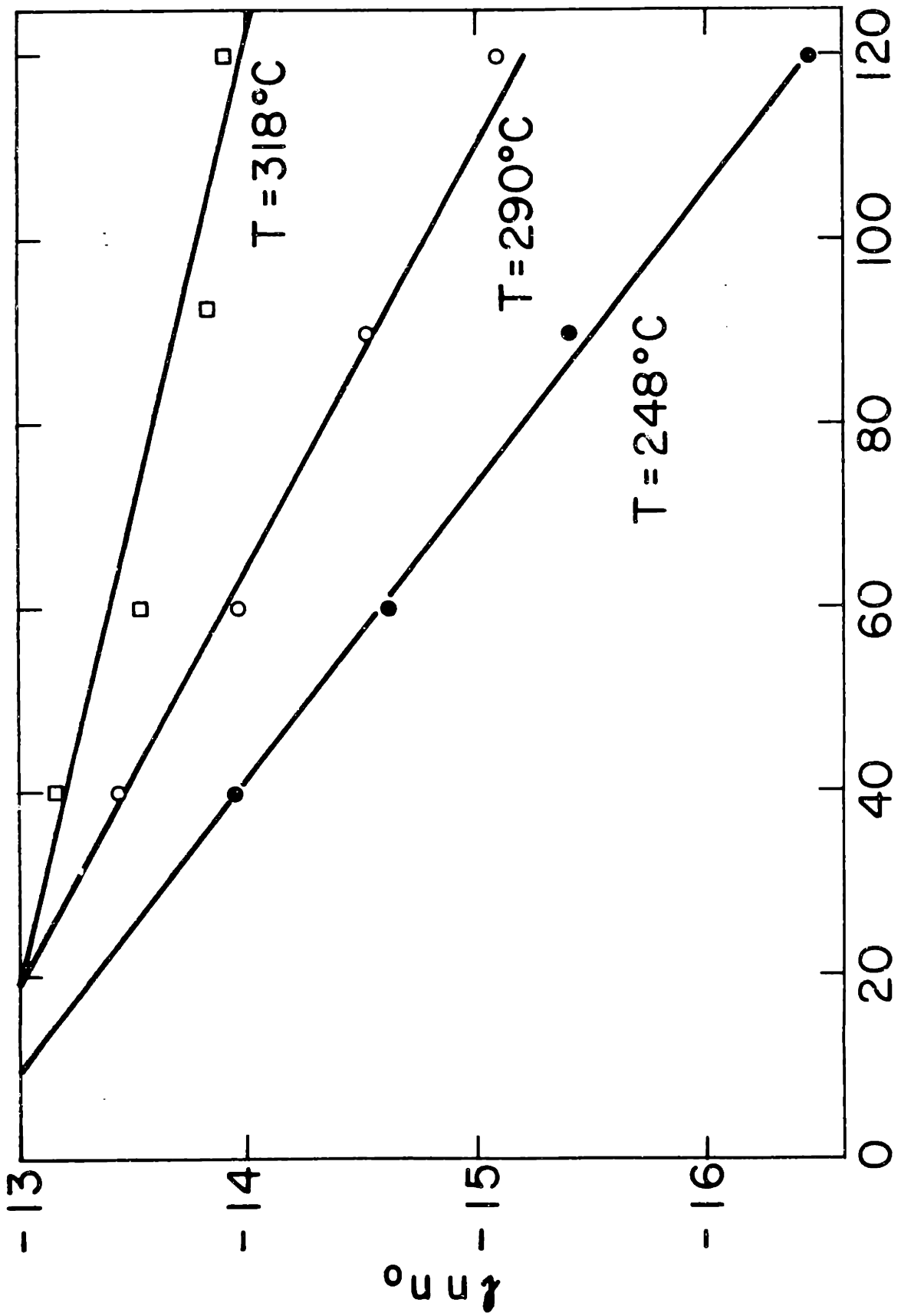

Figure 10: Oxygen desorption experiments. Oxygen mols adsorbed (2x) vs time

the desorption rate R_{des} (moles of O_2 per second) can be expressed as $R_{des} = -K_d\theta_o$. The maximum number of moles of O_2 n_{O_2} adsorbed is found by extrapolating to t = 0. This can be used only as a rough estimate because of the considerable uncertainty introduced by the transient selectivity assumption. The estimated value is $2.0(\pm 0.8)$. 10^{-6} mole O_2 is very weakly dependent on temperature. The values of K_d thus obtained are compared in Table 3 with the rate coefficient K_3.

C2. The oxidation of Ethylene Oxide

Part of the undesired byproduct CO_2 during ethylene oxidation comes from the secondary ehtylene oxide oxidation: $C_2H_4O + \frac{5}{2} O_2 \rightarrow 2CO_2 + 2H_2O$. Therefore we considered it useful to study first separately this particular reaction and combine our results later with the information obtained from ehylene experiments. Experiments were run between 250 and 400°C and atmospheric pressure.

C2.a Kinetic measurements

The rate was calculated from the appropriate mass balance $r = F'(X_{C_2O_4\,(reactants)} - X_{C_2H_4O(products)})$, where F' is the total molar flow rate and x is the mole fraction of ethylene oxide.

The rate is shown in Fig.11 as a function of P_{ETOX} for three different temperatures. It is close to second order with respect to ethylene oxide at the higher temperatures studied, gradually changing to first order and almost zero order at temperatures below 300°C. The relevant kinetic data are given in Table 2. Each point is the average of two measurements.

The role of oxygen was investigated in a separate set of experiements by maintaining P_{ETOX} constant and varying P_{O_2}. The rate is zero order in oxygen as shown in Fig. 12.

A simple first-order rate expression in ethylene oxide can describe the data at intermediate temperatures but is inadequate at the lower and higher temeratures studied. It was found that all the kinetic data could be expressed rather accurately by the rate expression:

Table 2

Kinetic and Potentiometric Results

Temperature °C	Total Flowrate CC STP/min	Reactants		Products		Open Circuit EMF MV
		$100 \cdot X_{ETOX}$	$100 \cdot X_{O_2}$	$100 \cdot X_{ETOX}$	$100 \cdot X_{O_2}$	
400	100	2.27	16.17	1.75	14.86	-8.5
400	124	3.68	13.18	2.95	11.33	-14.5
400	160	5.30	9.74	4.53	7.80	-24.5
400	204	6.54	7.11	5.43	4.34	-37.
400	260	7.40	5.27	6.07	1.93	-45.
360	100	2.25	16.22	1.88	15.3	-10.5
360	124	3.68	13.17	3.16	11.88	-19.
360	160	5.34	6.95	4.73	8.10	-32.
360	204	6.50	7.18	5.90	5.66	-45.5
360	260	7.27	5.55	6.67	4.06	-62.5
320	100	2.27	16.17	2.01	15.50	-19.5
320	124	3.68	13.19	3.51	12.75	-33.5
320	160	5.39	9.55	5.17	9.00	-52.5
320	204	6.50	7.18	6.24	6.54	-66.
320	260	7.23	5.64	7.06	5.22	-80.
290	100	2.18	16.36	2.05	16.04	-29.5
290	124	3.68	13.17	3.59	12.94	-48.
290	160	5.43	9.68	5.26	9.05	-71.5
290	204	6.50	7.18	6.37	6.85	-90.5
290	260	7.27	5.55	7.14	5.22	-107.
260	100	2.31	16.08	2.20	15.80	-51.5
260	124	3.76	13.	3.68	12.80	-75.
260	160	5.43	9.46	5.39	9.36	-102.5

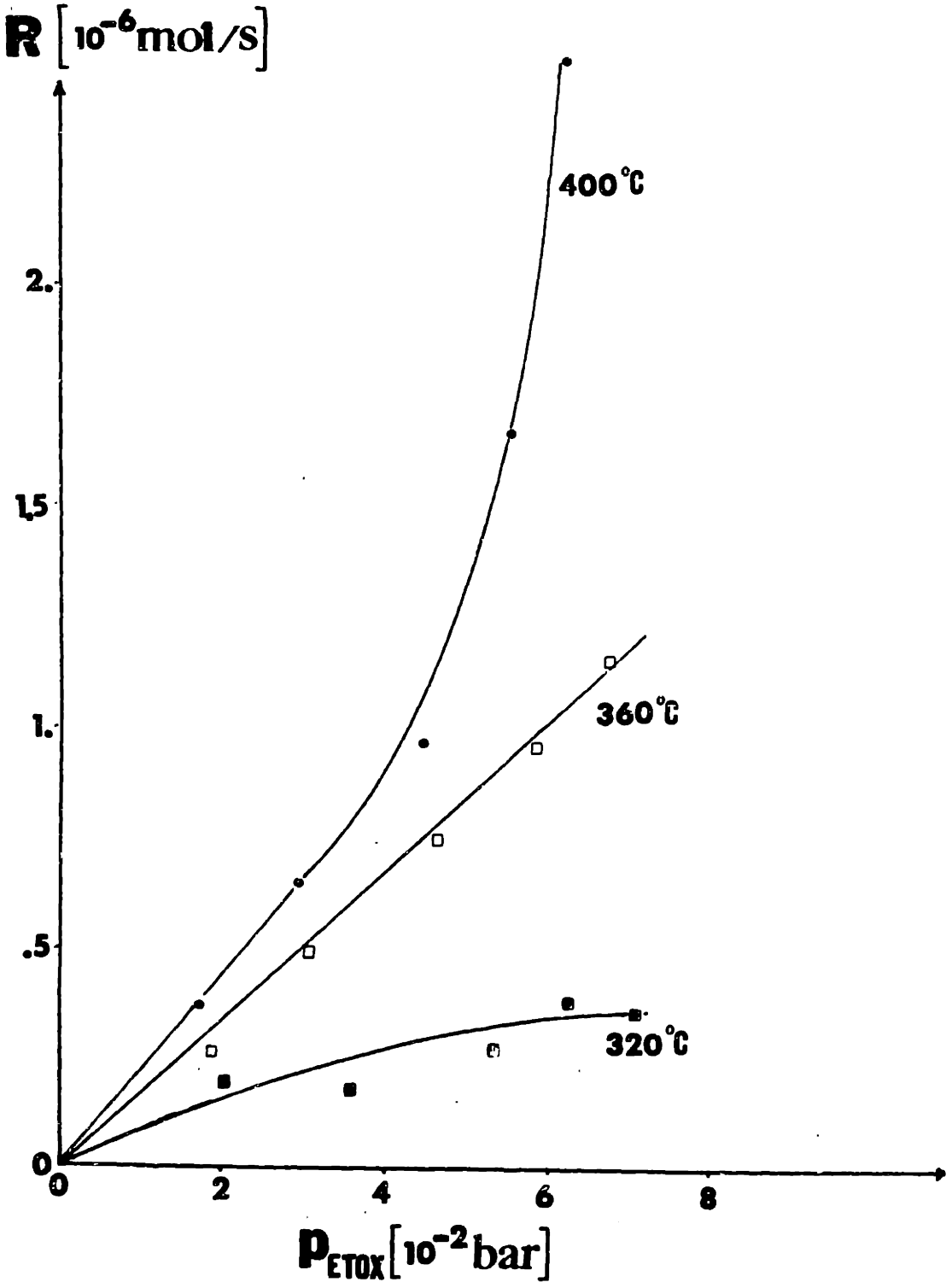

Figure 11: Rate vs P_{ETOX}.

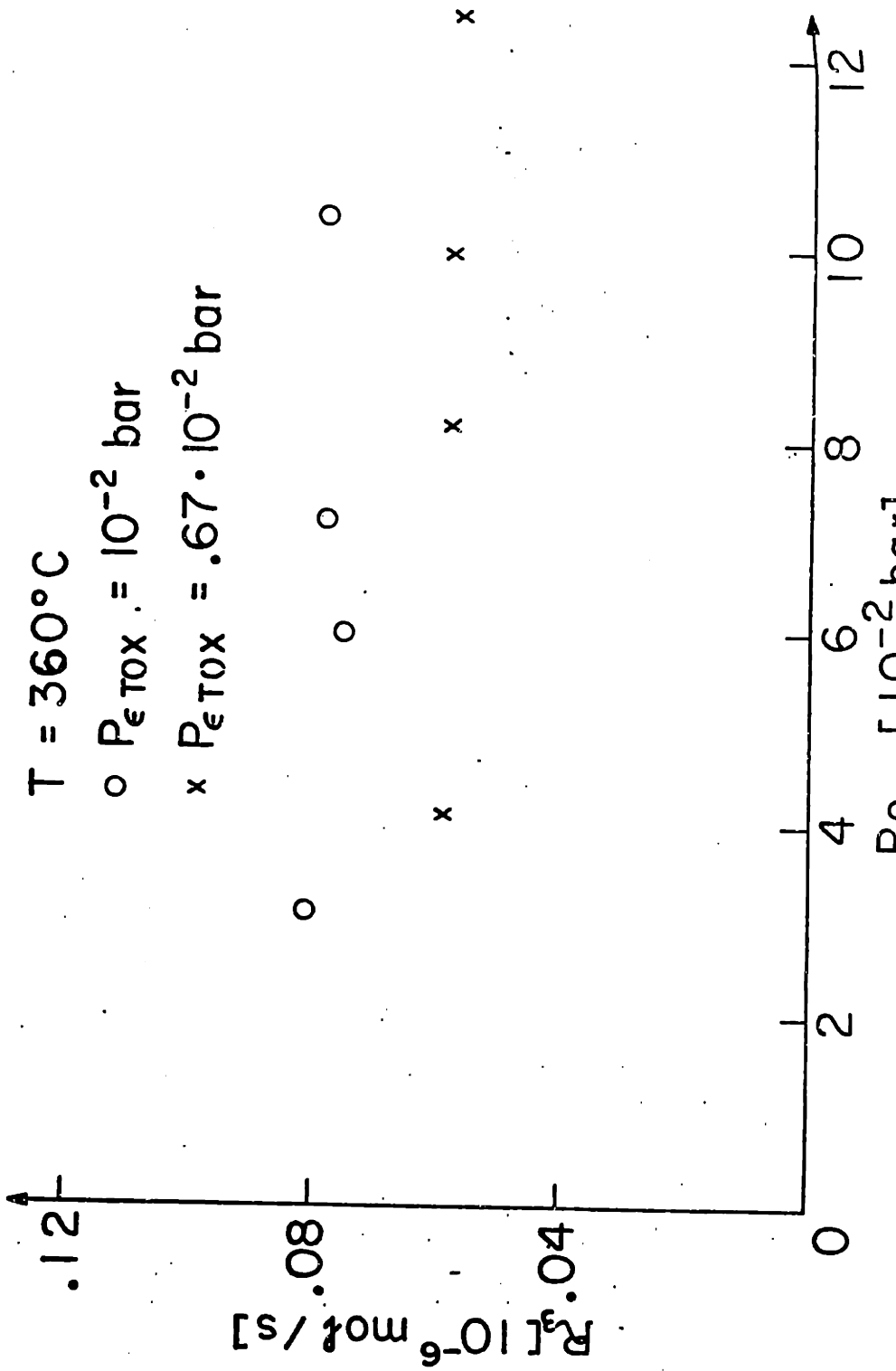

Figure 12: Rate r_3 vs P_{O_2}

$$r = K_3 \frac{K_{ETOX} P^2_{ETOX}}{1 + K_{ETOX} P^2_{ETOX}}, \qquad [C2.1]$$

where

$$K_{ETOX} = 3.3 \cdot \exp\left(\frac{10,600}{T}\right) \text{ bar}^{-2} \qquad [C2.2]$$

and

$$K_3 = 14.4 \exp\left(\frac{-10200}{T}\right) \quad \text{g mol ETOX/s.}$$

In Fig. 11 the close agreement is shown between the rate expression [(C2.1)] and the experimental data.

In a different set of experiments the effect of the CO_2 diluent was studied by replacing CO_2 with N_2 as the diluent and using partial pressures of ethylene oxide below 2%. It was found that the rate could still be fairly well described by Eq. [C2.1] indicating (a) that CO_2 has an almost negligible retarding effect on the rate of the ethylene oxide oxidation and (b) that the rate expression [C2.1] can be safely extrapolated to partial pressures of ethylene oxide well below 0.02 bar, although it was derived by fitting kinetic data obtained with P_{ETOX} varying 0.02 and 0.8 bar.

C.2b. SEP Measurements

The defining equation [A4.4] of the activity a_o of the surface oxygen atoms does not imply that oxygen adsorbs in the form of atoms only. It is fairly well established that several forms of adsorbed oxygen exist on silver (10). To the extent that these various forms of adsorbed oxygen are in thermodynamic equilibrium, i.e., they all have the same steady-state chemical potential, then the emf measurements reflect this common chemical

potential. If, however, such an equilibrium is not established, then the emf reflects the activity of oxygen atoms (62), as they are the fastest ones to equilibrate with the O^{2-} of the stabilized zirconia. This is further discussed below.

As mentioned before, it was observed experimentally that indeed

$$a^2_{O(Ag)} = P_{O_2(g)} \qquad [C2.3]$$

when O_2-inert gas mixtures were introduced in the reactor. However, in the presence of ethylene oxide in the reactor, i.e., under reaction conditions, Eq. [C2.3] is not satisfied anymore and in general

$$a^2_{O(Ag)} < P_{O_2(g)} \qquad [C2.4]$$

although at high temperatures and low partial pressures of ethylene oxide, $a^2_{O(Ag)}$ approaches very closely to P_{O_2}. Several functional forms were examined for the dependence of a_o on gas-phase composition. It was found that the a_o measurements (i.e., the emf data) could be very well correlated in terms of the equation

$$\frac{P_{O_2}^{12}}{a_o} - 1 - K_{ETOX}P^2_{ETOX} \qquad [C2.5]$$

This is shown in Fig.13. It should be noted that

(a) If the left side of Eq. [C2.5] were equal to zero, i.e., $P^{12}_{O_2} = a_o$, that would imply equilibration between surface oxygen and gas-phase oxygen during reaction. This is not true except at very high temperatures and very low values of P_{ETOX}.

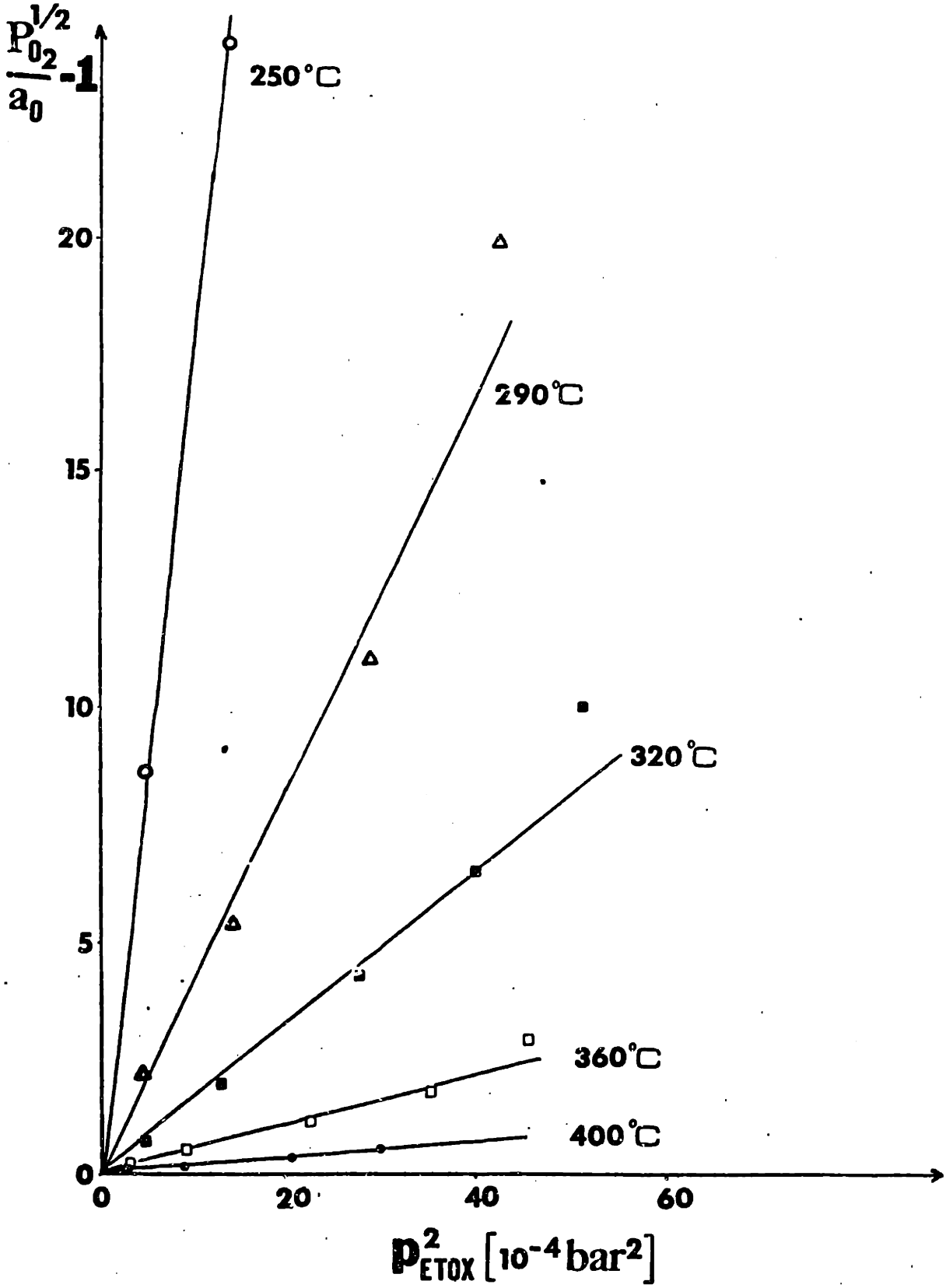

Figure 13: Surface oxygen activity dependence on gas phase composition

(b) The same parameter $K_{ETOX} = 3.3 \cdot 10^{-5} \exp(10,600/T)$ obtained from the kinetic data is the crucial parameter for the description of the surface oxygen activity measurements and corresponds to the slops of the straight lines of Fig.13. The temperature dependence of K_3 and K_{ETOX} is shown in Figs. 14 and 15.

C.2c. Discussion of results

It was proposed by Twigg many years ago (3, 4) that the rate-limiting step of the silver-catalyzed ethylene oxide oxidation is the isomerization of adsorbed ethylene oxide to acetaldehyde which is then rapidly oxidized by surface or gas-phase oxygen to CO_2 and H_2O. This classical picture can now be reexamined in light of in situ surface oxygen measurements.

Any proposed mechanism for the oxidation of ethylene oxide on silver should be able to explain (i) the surface oxygen activity behavior (Eq.C2.5),(ii) the observed rate expression (Eq.C2.1), and (iii) the observation that the same temperature-dependent parameter K_{ETOX} appears both in the rate expression and the oxygen activity equation.

These three requirements decrease the possible mechanisms to a very small number.

First, the inequality

$$a_O^2 < P_{O_2}$$

shows that thermodynamic equilibrium is not established between surface and gas-phase oxygen during reaction. This implies that either oxygen adsorption is rate limiting in the classical sense

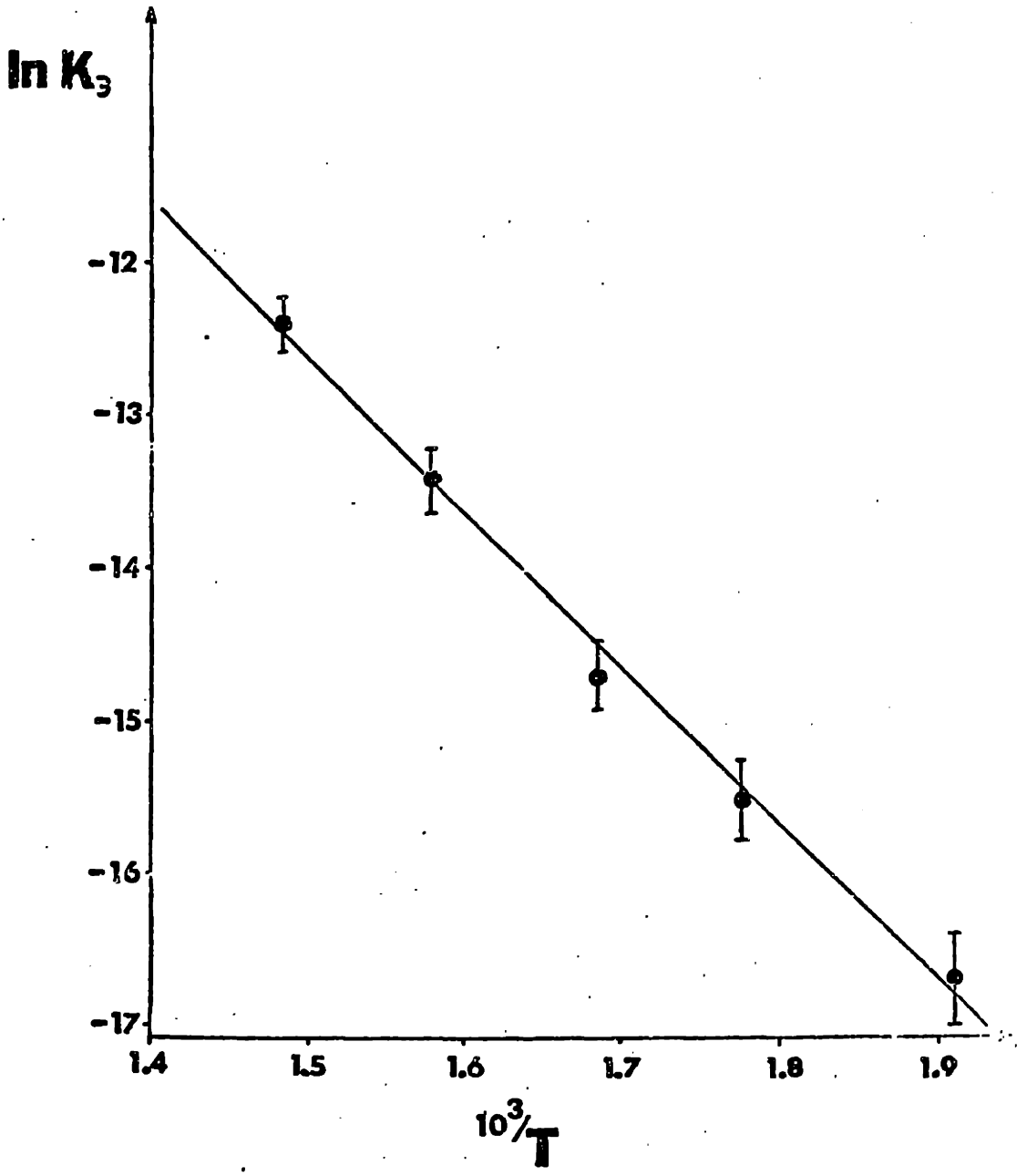

Figure 14: Temperature dependence of K_3

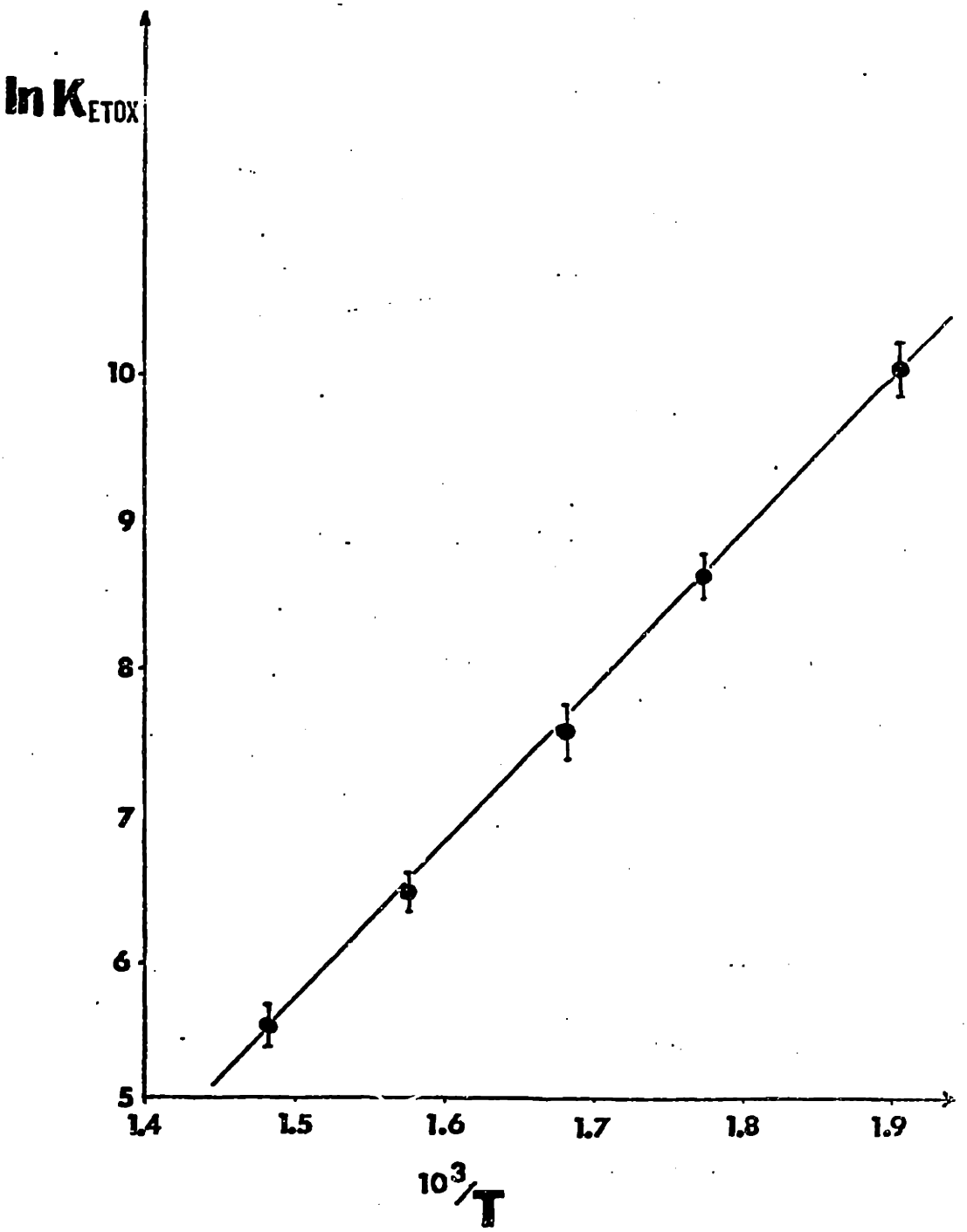

Figure 15.: Temperature dependence of K_{ETOX} obtained from the SEP data.

or that the rate of oxygen adsorption and desorption is comparable with the rate of the oxidation step. The first possibility can be ruled out in light of the rate expression [C2.1] Therefore the reaction rate is of the same order of magnitude with the intrinsic rate of oxygen adsorption on silver.

Both experimental equations [C2.1] and [C2.5] very strongly suggest adsorbed ethylene oxide dimer formation. This is not surprising in view of the previous work of Twigg (3,4) and Force and Bell (8). The rate expression clearly shows that adsorbed ethylene oxide is involved in the oxidation step. Furthermore the fact that $a_O^2 < P_{O_2}$ shows that adsorbed ethylene oxide reacts with adsorbed oxygen rather than gaseous oxygen. Therefore the results are very strongly indicative of a Langmuir-Hinshelwood rather than Rideal-Eley type mechanism.

The question can be addressed of whether the rate-limiting step is the isomerization of adsorbed ethylene oxide dimer to a highly reactive isomer which than reacts with adsorbed oxygen to form CO_2 and H_2O according to Twigg's mechanism. Although the rate expression can thus be account for, we found it impossible to interpret the surface oxygen activity behavior on the basis of such a rate-limiting step. However, we found that the following mechanism could explain all the experimental observations:

$$1/2\{O_2(g) \rightleftarrows 2O^*\}, \qquad (a)$$

$$O^* + S_1 + S_2 \rightarrow O - S_2 + S_1, \qquad (b)$$

$$2C_2H_4O + S_1 \rightarrow C_4H_8O_2 - S_1, \qquad (c)$$

$$O - S_2 + C_4H_8O_2 - S_1 \rightarrow P \xrightarrow{9[O]} 4CO_2 + 4H_2O + S_1 + S_2, \qquad (d)$$

where P stands for a highly reactive intermediate which is rapidly oxidized to CO_2 and H_2O, and O* stands for oxygen in a precursor adsorption state. Postulating this precursor state is necessary in order to account for the a_O behavior (Fig.13) as shown below. The assumption of two different types of surface sites S_1 and S_2 was found necessary in order to account quantitatively for the experimental observations [C2.1] and [C2.5].

On the basis of the above mechanism and with the additional assumption of Langmuir-type adsorption one can explain all the experimental observations in a quantitative manner. This may not be the only possible interpretation, but it is the simplest one we could find.

Since step (c) is in thermodynamic equilibrium one obtains

$$\theta_{ETOX} = \frac{K_{ETOX} P^2_{ETOX}}{1+K_{ETOX} P^2_{ETOX}} \quad , \qquad [C2.6]$$

where θ_{ETOX} is the coverage of surface sites S_1 by ethylene oxide dimer. Therefore K_{ETOX} is the adsorption coefficient of ethylene oxide on silver and one can directly obtain the heat and entropy of chemisorption of ethylene oxide from Eq. [C2.6]

ΔH_{ETOX} = -88,000 J/mol dimer = -44,000 J/mol ETOX

ΔS_{ETOX} = -85.8 J/K · mole dimer = -42.9 J/K·mol ETOX.

At steady state the difference between the rates of oxygen adsorption and desorption equals the rate of reaction and according to steps (a) and (b) one obtains

$$K_a P_{O_2}^{1/2}(1-\theta_{ETOX})(1-\theta_O) - K_d\theta_O(1-\theta_{ETOX}) = K_3\theta_O\theta_{ETOX}, \qquad [C2.7]$$

where K_1 and K_2 are rate coefficients and $K_a/K_d = K_O$ is the

adsorption coefficient of atomic oxygen. In the absence of chemical reaction ($K_3 = 0$) Eq.[C2.7] reduces to the common form of the Langmuir isotherm

$$K_{O_2} P_{O_2}^{1/2} = \frac{\theta_O}{1 - \theta_O}, \qquad [C2.8]$$

Since a_O expresses the square root of the partial pressure of gaseous oxygen that would be in thermodynamic equilibrium with absorbed oxygen at coverage θ_O if such an equilibrium were established, it follows that

$$K_O a_O = \frac{\theta_O}{1 - \theta_O} \qquad [C2.9]$$

even when gaseous-surface oxygen equilbration is not established. Combining Eqs. [C2.6],[C2.7], and [C2.9] one obtains

$$\frac{P_{O_2}^{1/2}}{a_o} - 1 = \frac{K_3}{K_d} K_{ETOX} P_{ETOX}^2 \qquad [C2.10]$$

On the basis of the mechanism (step (b)) desorption of oxygen requires the existence of an adjacent empty site S_1, i.e., the rate-limiting step for oxygen desorption is O migration from an S_2 to an S_1 site. Therefore K_3 is the rate coefficient for this elementary step. If the adjacent S_1 site is occupied by ethylene oxide, reaction occurs. Therefore K_3 is the rate coefficient for the same elementary step of O migration from an S_2 to an S_1 site, so that

$$K_3 = K_d \qquad [C2.11]$$

This is supported by the oxygen desorption experiments from ethylene oxide free silver catalyst (Table 3).

In light of [C2.10],Eq. [C2.11] reduces to the experimental equation

Table 3

Oxygen Desorption and Ethylene Oxide Oxidation Rate Coefficients

Temperature °C	K_d mole/s	K_3 mole/s
248	$5.1 \cdot 10^{-8}$	$4.3 \cdot 10^{-8}$
290	$8.5 \cdot 10^{-8}$	$18 \cdot 10^{-8}$
318	$12.9 \cdot 10^{-8}$	$44.5 \cdot 10^{-8}$

$$\frac{P_{O_2}^{1/2}}{a_O} - 1 = K_{ETOX} P^2_{ETOX} \cdot \qquad [C2.5]$$

The implication of [C2.11] is that the measurable K_3 (Eq.[C2.2]) is in essence the rate coefficient for atomic oxygen desorption, so that the activation energy for atomic oxygen desorption is 85 KJ/g-atom O, $\Delta E^*_{DES\ O}$ = 85 KJ/g-atom O, and $\Delta S^*_{DES\ O} \approx -125$ J/K g-atom O. This activation energy is in reasonable agreement with reported literature values (10).

Finally the rate equation

$$R = K_3 \theta_O \theta_{ETOX} = K_R \frac{K_O a_O}{1+K_O a_O} \cdot \frac{K_{ETOX} P^2_{ETOX}}{1+K_{ETOX} P^2_{ETOX}}$$

reduces to the experimental rate expression [C2.1] if $K_O a_O >> 1$ which implies that most of the S_2 sites are occupied by O atoms during reaction, i.e., $\theta_O \sim 1$ which is quite reasonable under atmospheric pressure conditions. It should be noted that θ_O is insensitive to changes in a_O to the extent that $a_O >> K_O^{-1}$ (Eq.[C2.9]). Practically all the previously reported rate expressions reviewed in (24) can be considered as limiting cases of the rate expression [C2.1]. The activition energy found is in reasonable agreement with previously reported values (4,10). That no second-order dependence of the rate on P_{ETOX} has been reported is readily explained by noticing that all the previous kinetic studies were restricted to operating temperatures below 350°C. The present results should not be taken to imply that atomic oxygen is the only form of oxygen adsorbed on silver. They show, however, that adsorbed atomic oxygen is responsible for the oxidation of ethylene oxide.

C.3 The oxidation of Ethylene

Once the oxidation of ethylene oxide was studied, we proceeded with the study of ethylene oxidation. Kinetic and potentiometric measurements were taken at atmospheric pressure and temperatures between 250°C and 440°C.

C3.a. Kinetic Measurements

The kinetics were studied extensively at temperatures between 250 and 450°C, ethylene partial pressures between 10^{-3} and $2.\cdot10^{-2}$ bar, and oxygen partial pressures between $1.5\cdot10^{-2}$ and $15.\cdot10^{-2}$ bar.

The three independent reactions rates r_1, r_2 (moles C_2H_4/s), and r_3 (moles C_2H_4O/s) defined in the Introduction are calculated as follows from the raw kinetic data of the CSTR: First, we caculated r_3 using the partial pressure of ethylene oxide P_{ETOX} in the products and the rate expression obtained in our previous work for the same catalyst.

$$r_3 = K_3 \cdot K_{ETOX} \cdot P^2_{ETOX} / (1 + K_{ETOX} P^2_{ETOX}) \text{ with}$$

$$K_3 = 14.4 \exp(-10200/T) \text{ mole/s}$$

and

$$K_{ETOX} = 3.3\cdot10^{-5} \exp(10600/T) \text{bar}^{-2}.$$

As it turns out because of the low conversions employed in the present study (<30%), i.e., due to the relatively high P_{ET} and low P_{ETOX}, r_3 is of the order of 1% of r_1 and r_2. This was again verified by introducing ethylene oxide and oxygen in the reactor at the same P_{ETOX} and space velocities employed in the main kinetic study. The rate r_3 is therefore

much smaller than r_1 and r_2 and in most cases small enough to be neglected (<1%). This is also demonstrated by the fact that over the range of space times employed in the present study (3-15 s), selectivity (moles ETOX produced/moles ethylene reacted) was practically space time independent. However it might be anticipated that the presence of ethylene alters the value of r_3 from that obtained in the separate ethylene oxide oxidation study. This effect has been studied separately and found to be small and in the direction of decreasing r_3. Therefore r_3 can be neglected for the purposes of the present investigation, i.e., practically all CO_2 produced comes from direct ethylene oxidation. This has been suggested by previous workers too (3, 4, 7,33).

Thus taking into account that the reactor is a CSTR the reaction rates r_1, r_2 can be calculated from the appropriate mass balances:

$$r_1 - r_3 \approx r_1 = G \cdot X_{ETOX}, \qquad [C3.1]$$

$$r_2 + r_3 \approx r_2 = \frac{1}{2} \cdot G \cdot X_{CO_2}, \qquad [C3.2]$$

where X_{ETOX}, X_{CO_2} are the exit mole fractions of ethylene oxide and CO_2 and G is the total molar flow rate.

The values of r_1 and r_2 thus obtained were also found to satisfy within 1% the mass balance requirement

$$r_1 + r_2 = G[X_{ET,IN} - X_{ET,OUT}]. \qquad [C3.3]$$

Due to the high partial pressure of diluent N_2 (~0.7 bar) and the low conversion, volume changes due to reaction were calculated to be negligible (<0.3%). Each kinetic point

presented here is the average of two measurements usually differing less than 1-2%.

The rate of ethylene oxide production r_1 is plotted in Fig.16 vs. the partial pressure of oxygen at constant T and P_{ET}. The rate of deep ethylene oxidation r_2 is plotted vs. P_{O_2} in Fig.17 . Clearly both r_1 and r_2 are zro order in oxygen over the range of P_{O_2} values investigated.

Figure 18 exhibits the dependence of r_1, r_2 on P_{ET} at 440°C which is the highest temperature studied. Both rates are first order in ethylene.

However at lower temperatures this simple first-order dependence on ethylene disappears as shown in Figs.19 and 20.

It was found that all the kinetic data could be expressed rather accurately by the rate expressions

$$r_1 = K_1 K_{ET} P_{ET} / (1 + K_{ET} P_{ET}), \qquad [C3.4]$$

$$r_2 = K_2 K_{ET} P_{ET} / (1 + K_{ET} P_{ET}) \qquad [C3.5]$$

with

$$K_1 = 0.28 \exp(-7300/T) \text{mole/s}, \qquad [C3.6]$$

$$K_2 = 2. \cdot 10^2 \exp(-11100/T) \text{mole/s}, \qquad [C3.7]$$

$$K_{ET} = 8.7 \cdot 10^{-4} \exp(5800/T) \text{bar}^{-1}. \qquad [C3.8]$$

It should be noted that according to these rate expressions which account for the retarding effect of ethylene, the selectivity depend very little on gas composition at constant temperature, at least over the range of gas-phase compositions investigated. This is shown in Fig.21.

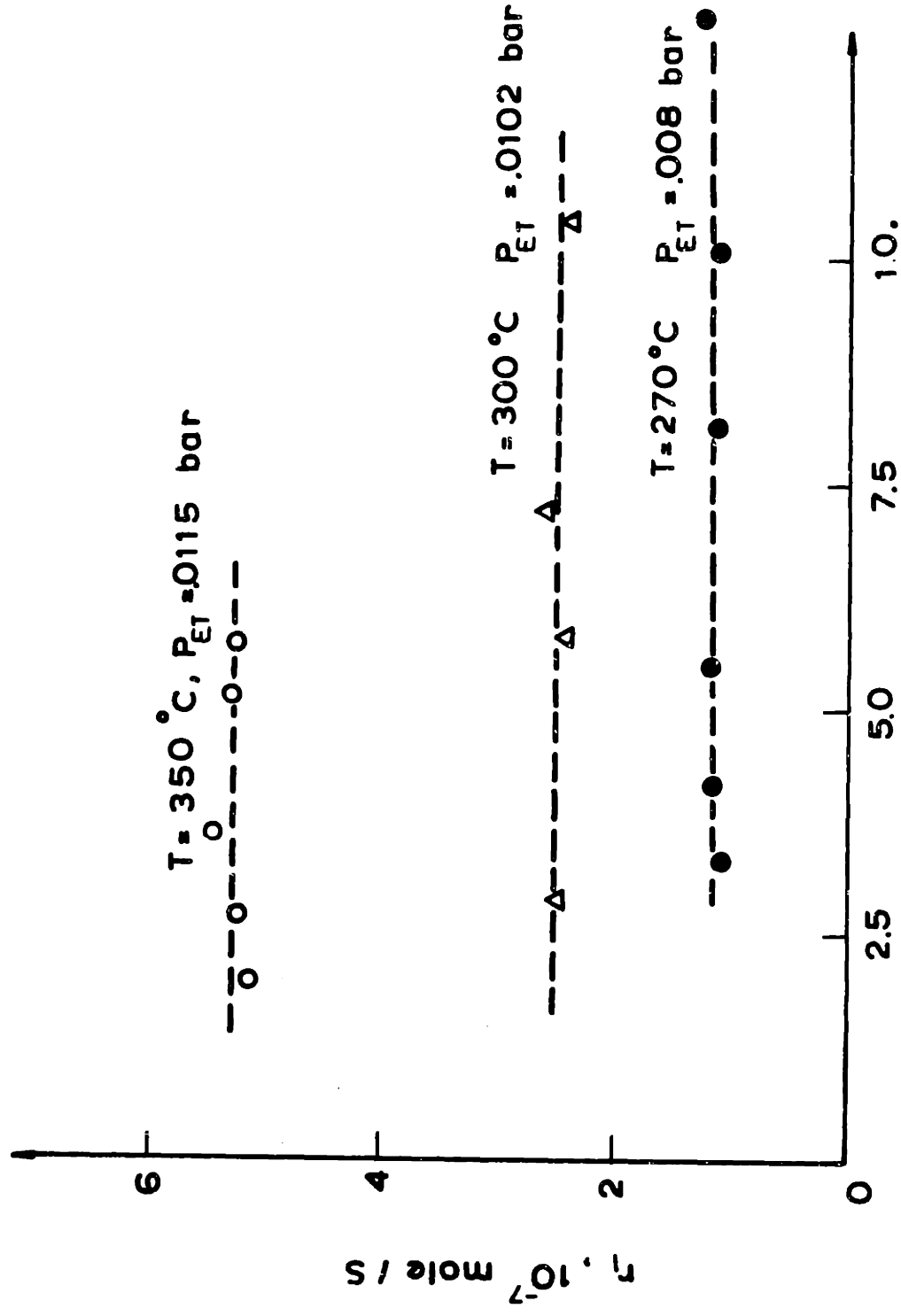

Figure 16: Rate of ethylene epoxidation r_1 vs P_{O_2} at constant P_{ET} and temperature

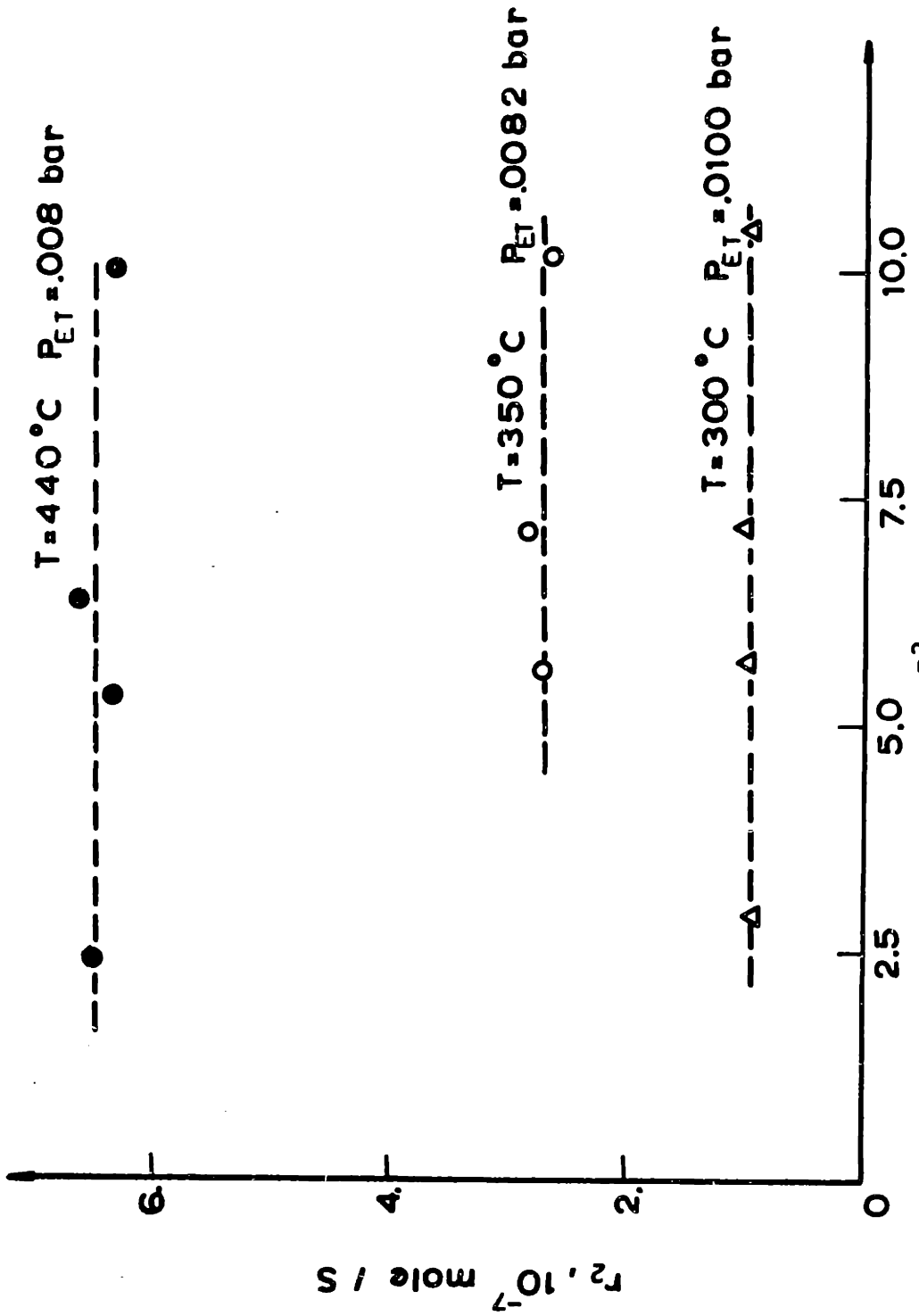

Figure 17: Rate of ethylene oxidation to CO_2 r_2 vs P_{O_2} at constant P_{ET} and temperature

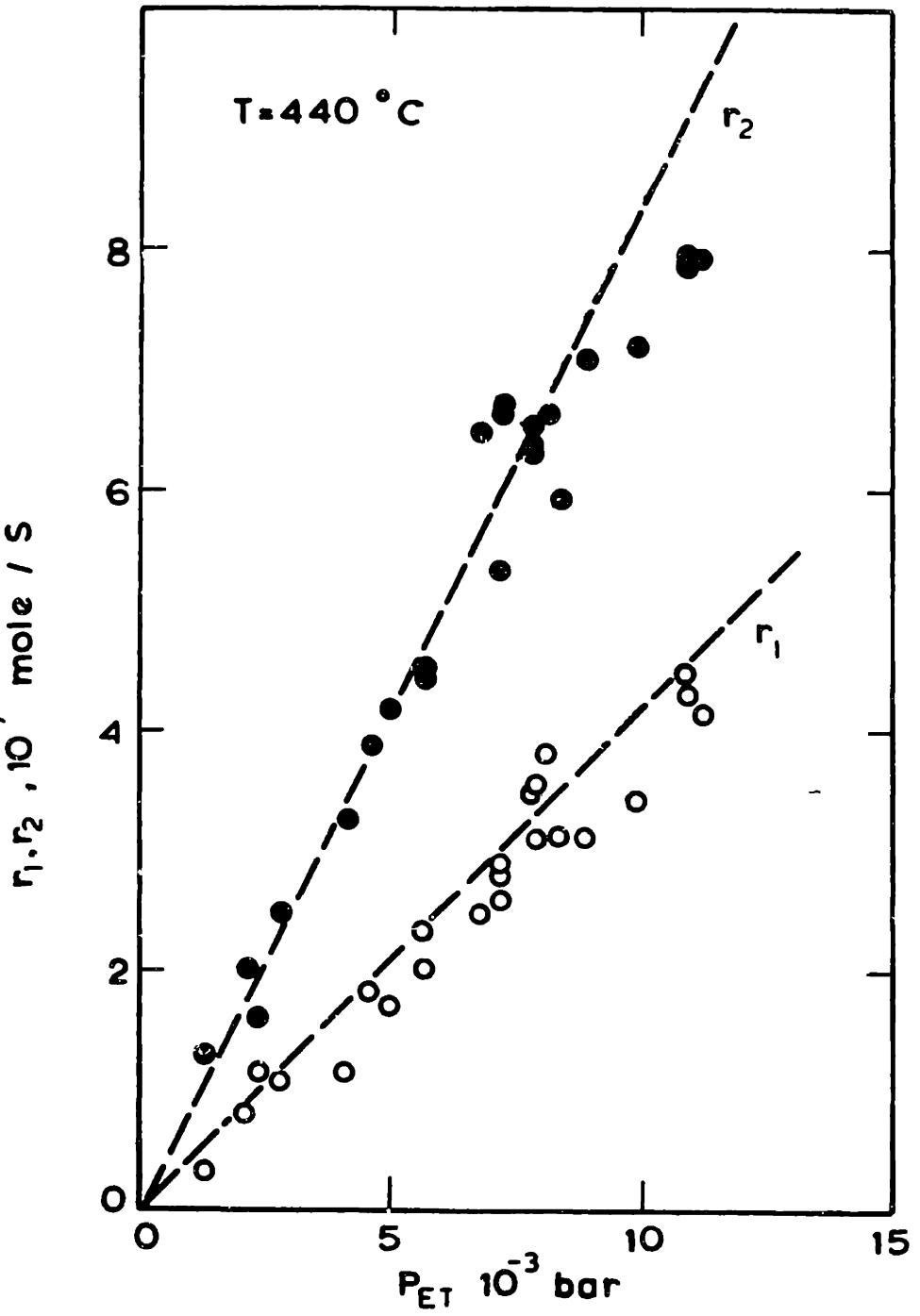

Figure 18: Rates of ethylene epoxidation (r_1) and combustion (r_2) vs P_{ET} at 440°C. The partial pressure of oxygen varies between $1.5 \cdot 10^{-2}$ and $15 \cdot 10^{-2}$ bar.

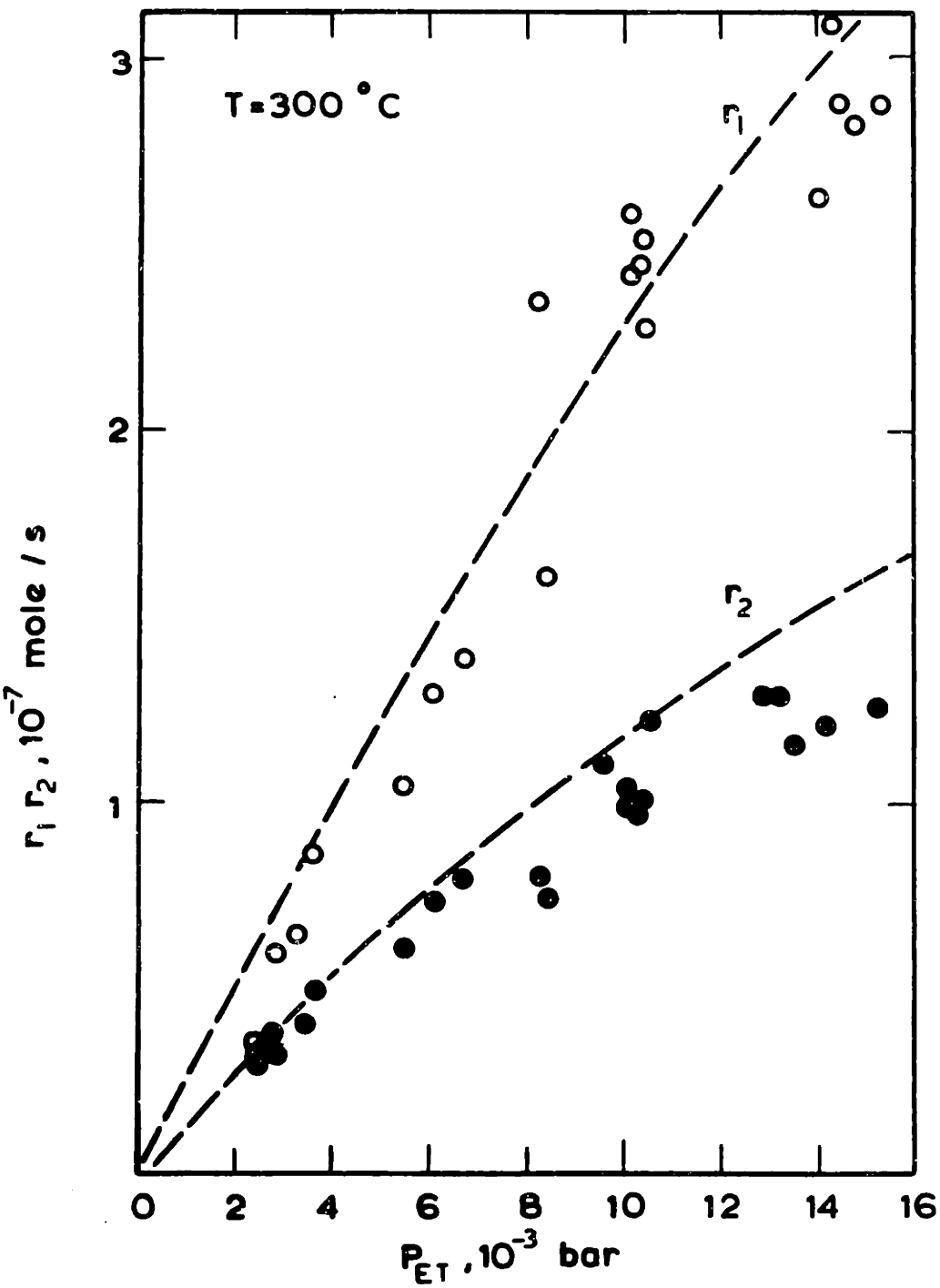

Figure 19: Rates of ethylene epoxidation (r_1) and combustion (r_2) vs P_{ET} at 300°C. Dashed lines from equations

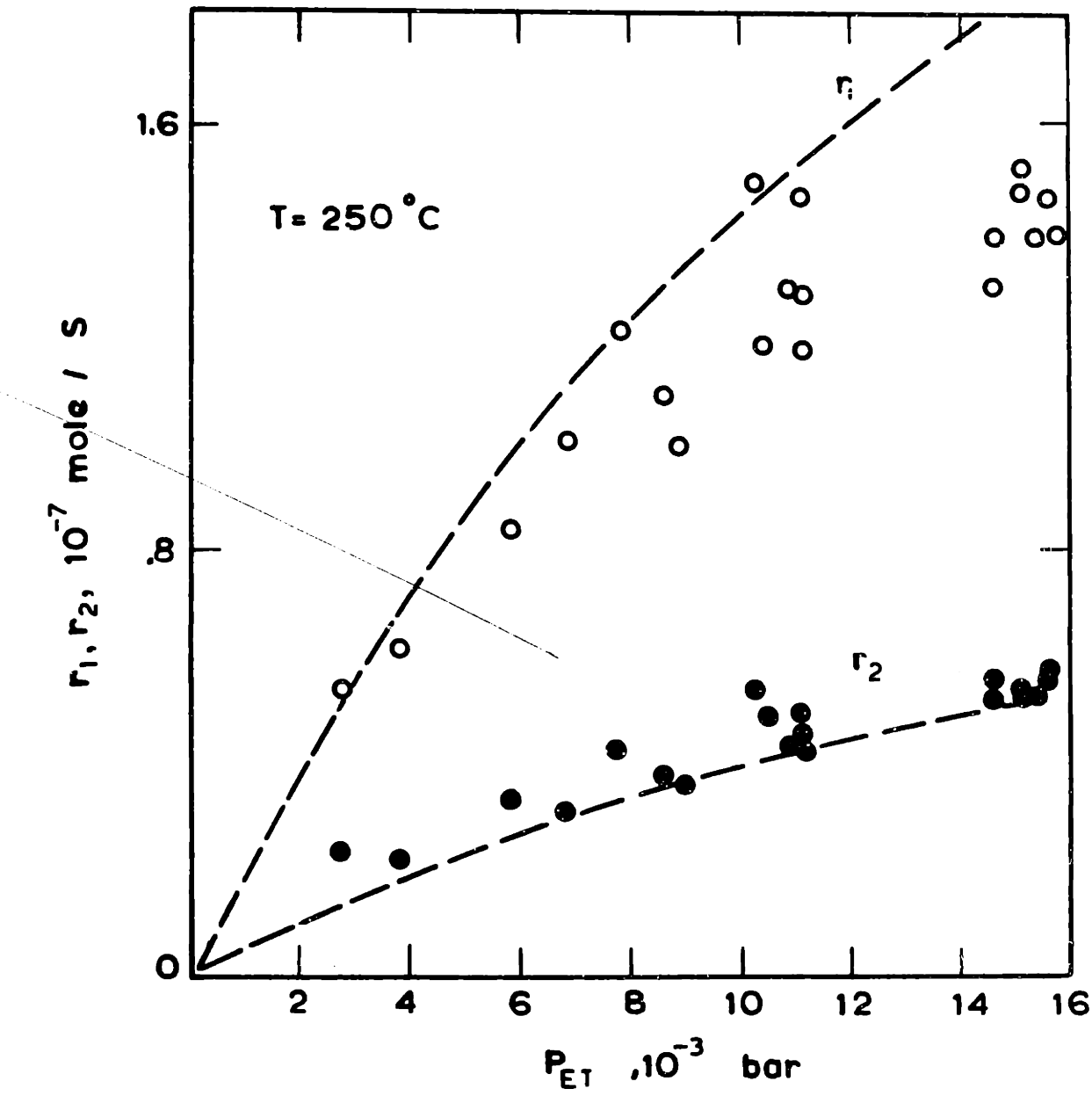

Figure 20: Rates of ethylene epoxidation (r_1) and combustion (r_2) vs P_{ET} at 250°C.

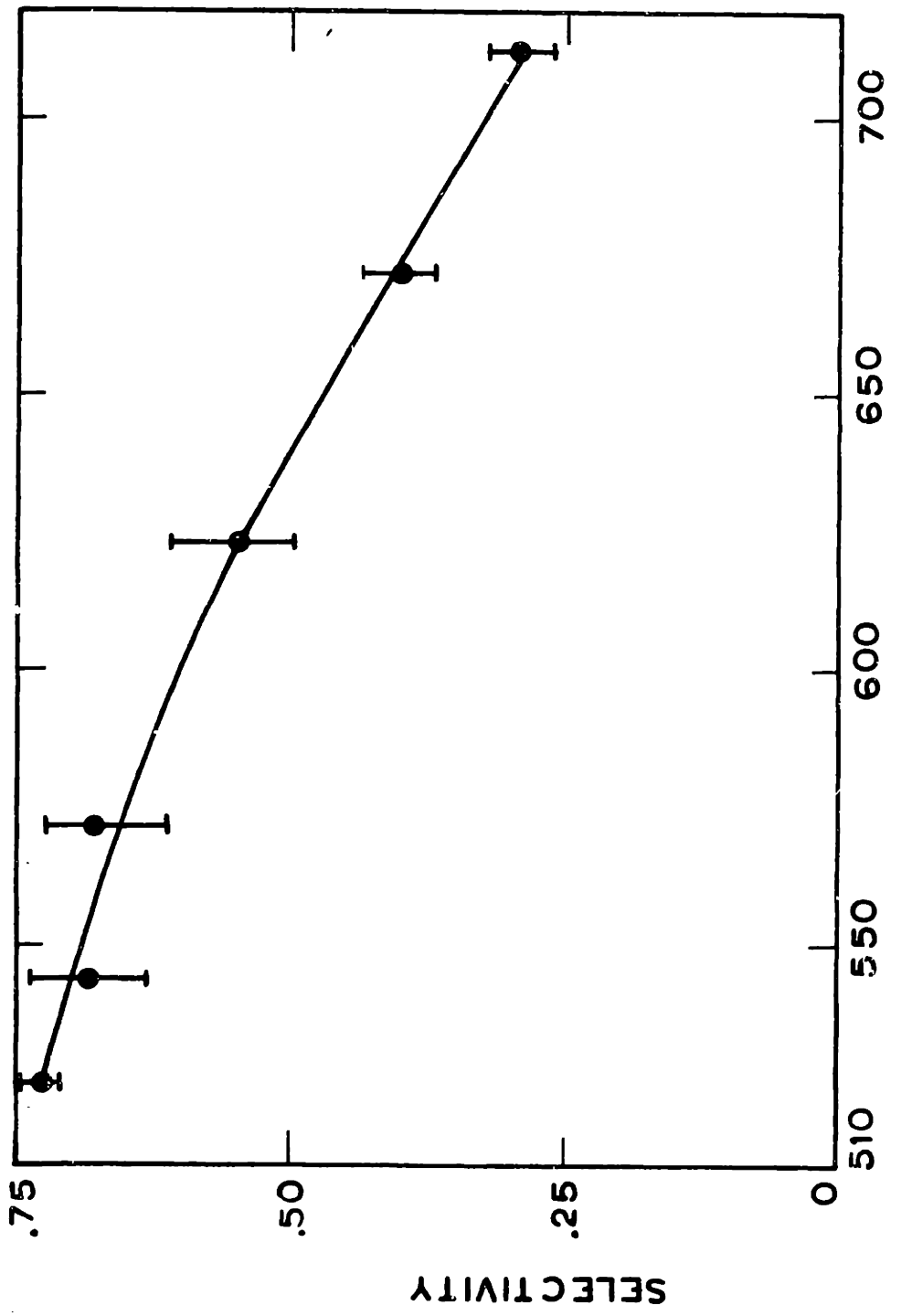

Figure 21: Temperature dependence of the selectivity (moles ethylene oxide produced/moles ethylene reacted).

C.3b. SEP Measurements

With intert-O_2 mixtures present in the reactor the electrochemically measured surface oxygen activity a_O^2 (Eq.[A4.4]) was always found to equal P_{O_2} within 1-2%. However in the presence of ethylene, i.e., during reaction, open-circuit emf values between -20 and -100 mV are obtained and thus, in general, $a_O^2 < P_{O_2}$. This implies that no thermodynamic equilibrium is established between gaseous oxygen and oxygen adsorbed on silver under reaction conditions. It was observed that

a) a_O^2 approaches P_{O_2} with increasing temperature at constant P_{O_2} and P_{ET};

b) a_O^2 increases with increasing P_{O_2} at constant P_{ET};

c) a_O^2 decreases with increasing P_{ET} at constant P_{O_2};

Observation (b) is in agreement with Imre's previous work but observation (c) is not. Imre suggested that the oxygen activity increases with increasing P_{ET}. It should be noted however that his definition of oxygen activity is different from Eq.[A4.2] and that his method of measurement is quite indirect (12).

Several functional forms were examined in order to describe the dependence of a_O on gas-phase composition. It was found that all the a_O measurements could be correlated in a quite satisfactory way by the expression

$$P_{O_2}^{1/2}/a_O = 1 + KP_{ET}/P_{O_2} \qquad [C3.9]$$

with

$$K = 3.4 \cdot 10^{-5} \exp(7800/T). \qquad [C3.10]$$

This is shown in Figs.22 and 23.

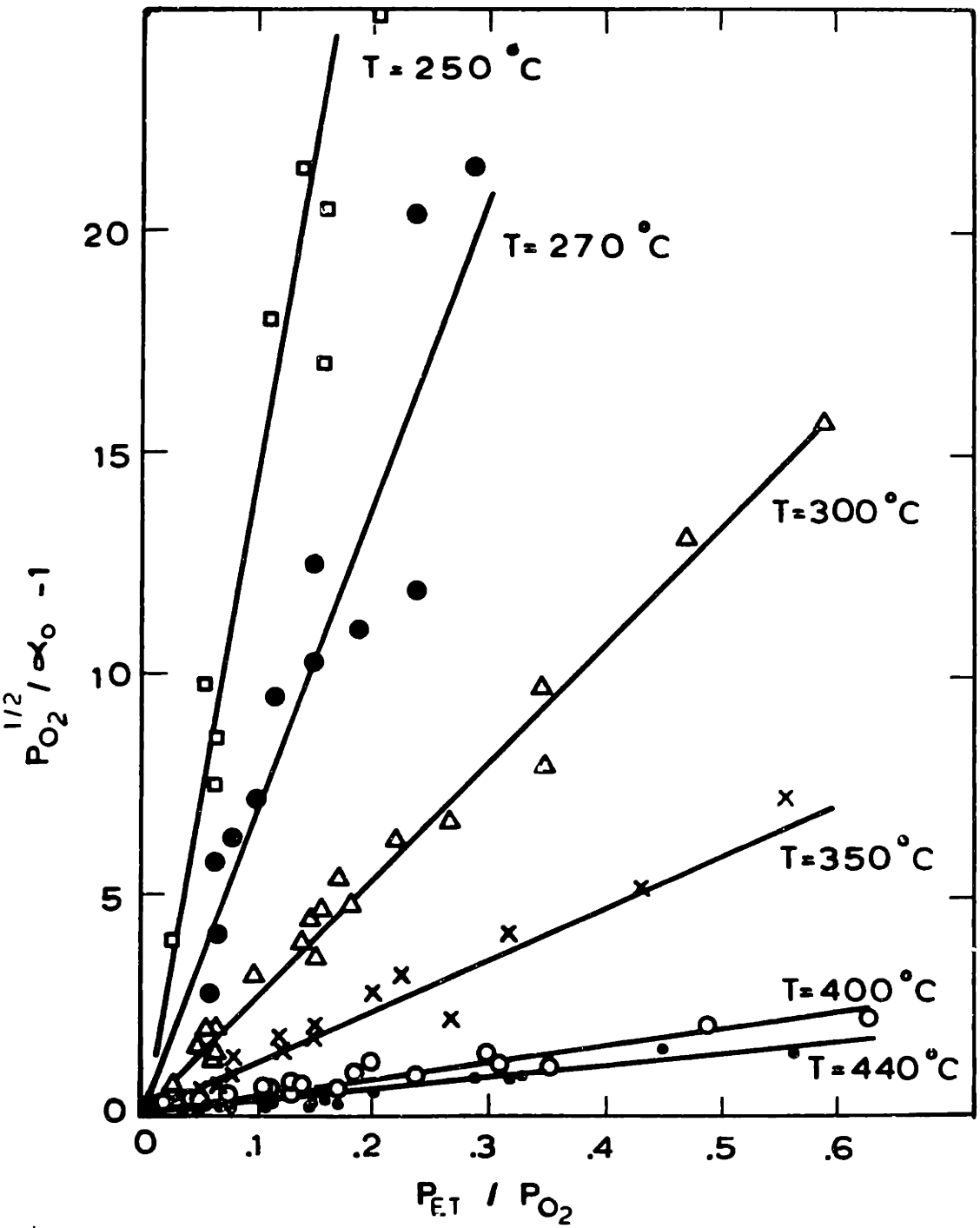

Figure 22: Surface oxygen activity dependence on gas phase composition

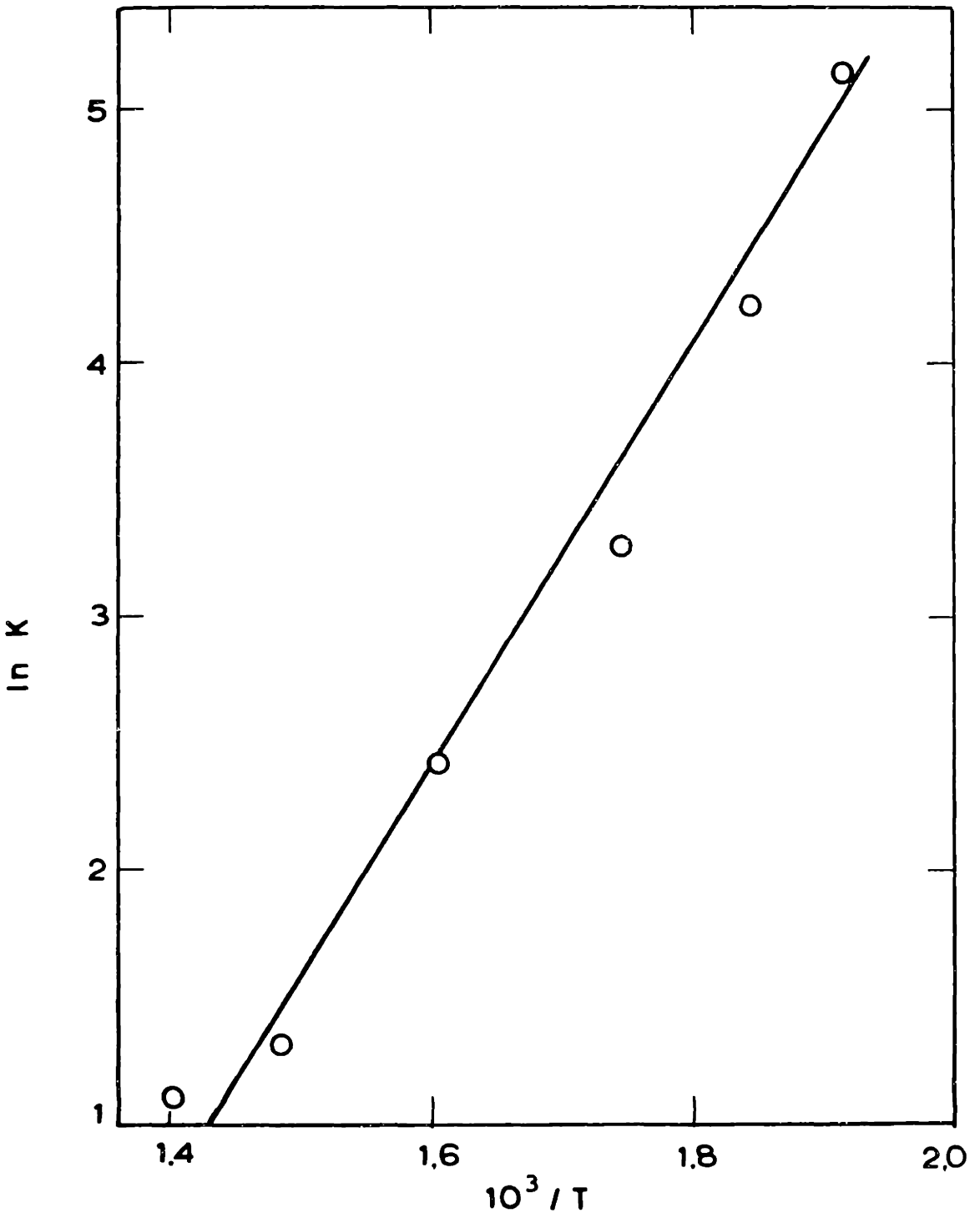

Figure 23: Temperature dependence of the oxygen activity parameter K

The defining Equation [A4.4] of the activity a_O of surface oxygen atoms does not imply that oxygen adsorbs in the form of atoms only. It is well established (7,10,15,16) that several forms of adsorbed oxygen can exist on silver. To the extent that all these forms are in thermodynamic equilibrium, i.e., they all have the same steady-state chemical potential, then the emf E and thus a_O reflect this common chemical potential. If, however, due to fast kinetic processes, such an equilibrium is not established then the emf E reflects the activity of oxygen atoms as they are the fastest ones to equilibrate with the O^{2-} of the solid electrolyte (62). This is further discussed below.

C.3c. Effect of reactants and products on the reaction rates

1. The effect of oxygen and ethylene

Figures 16 and 17 show that both r_1 and r_2 are independent of the partial pressure of oxygen in the gas phase. This is also true for r_3, the secondary ethylene oxide oxidation as shown in fig. 12. It has to be pointed out, however, that all the experimental data were obtained with excess air i.e., $P_{O_2}/P_{ET} > 2$. Obviously we do not expect the reaction rates to be independent of P_{O_2} when $P_{O_2} \to 0$. But at least within the range of gas compositions that were studied r_1, r_2, $r_3 \neq f(P_{O_2})$.

As far as the effect of ethylene may concern equations [C3.4] and [C3.5] show a retarding effect of ethylene on both reaction rates r_1 and r_2 : $r_1 = \frac{K_1 K_{ET} P_{ET}}{1+K_{ET} P_{ET}}$ and $r_2 = \frac{K K_{ET} P_{ET}}{1+K_{ET} P_{ET}}$

Nevertheless the selectivity of the reaction

$S \simeq \frac{r_1}{r_1 + r_2} \simeq \frac{K_1}{K_1 + K_2}$ is essentially independent of P_{ET} as it was mentioned in section C.3a.

2. The Effect of Ethylene Oxide

The effect of ethylene oxide was studied separately. Table 4 contains the experimental kinetic and potentiometric data for 5 different temperatures examined. In these experiments the partial pressure of ethylene and oxygen were kept constant and the effect of ethylene oxide was studied by replacing N_2 by ETO in the feed stream. The term r_{3e} in the table indicates the rate of ETO oxidation as calculated by eqn. [C2.1]: r_2 is the rate of CO_2 production when no excess ETO is introducted in the reactor; r_{tot} is the rate of CO_2 production when both ethylene and ethylene oxide are present in the feed stream; r_{tote} is the sum of r_2 and r_{3e}. From table 4 one can observe that in general $r_{tote} = r_2 + r_{3e} \gg r_{tot}$

The above experiments indicate two things:

a) Indeed the rate of ethylene oxide oxidation is much smaller than that of ethylene oxidation, in agreement with what was mentioned before in this work and also in agreement with previous studies (33).

b) Ethylene and ethylene oxide compete for the same sites on the catalyst surface.

If ethylene and ethylene oxide were adsorbing on different catalyst sites r_{tote} should be approximately equal to the sum of r_2 and r_{3e}. This is not true as shown in table 4. And this cannot be attributed to experimental errors because there is a clear trend of the difference $(r_2 + r_{3e} - r_{tote})$ to increase as P_{ETO} increases.

Table 4

The Effect of Ethylene Oxide

T (°C)	P_{ET} (x10^3bar)	P_{ETO} (x10^3bar)	a_o	$r_2 \cdot 10^3$ (cm^3/min)	$r_{3e} \cdot 10^3$ (cm^3/min)	$r_{toi} \cdot 10^3$ (cm^3/min)	$r_{tote} \cdot 10^3$ (cm^3/min)
440	3.8	.48	.184	435	1.5	435	436
440	3.9	1.8	.178	445	65	515	510
440	3.9	2.72	.173	445	90	555	535
440	3.6	5.74	.157	420	220	628	640
440	3.8	9.72	.149	435	400	774	835
400	6.0	.79	.083	435	2.3	437	437
400	5.9	2.11	.079	428	50	464	478
400	6.0	3.05	.076	435	85	500	520
400	5.65	5.9	.065	410	150	528	560
400	5.6	10.2	.056	406	260	600	666
350	3.8	.466	.111	200	0	200	200
350	3.9	2.04	.105	205	25	218	230
350	4.1	2.72	.105	216	30	236	245
350	3.9	6.1	.091	210	55	245	265
350	3.85	10.2	.081	205	115	291	320
300	3.7	.42	.047	95	1	96	96
300	3.6	1.8	.044	92	8	100	100
300	3.7	2.8	.042	95	10	109	105
300	3.5	6.4	.034	90	30	109	120
300	3.5	10.5	.028	90	55	120	145
250	5.7	.34	.0054	62	1	62	63
250	6.5	1.66	.0035	70	4	64	74
250	6.8	2.63	.003	74	5	67	79
250	6.6	5.83	.0016	71	6	64	77
250	6.8	10.25	.001	74	10	66	84

Nevertheless the effect of ethylene oxide on the reaction rates is negigible as long as $P_{ETO} << P_{ET}$ which is true for low conversions of ethylene. If however P_{ETO} becomes large enough ($P_{ETO} >> P_{ET}$) then the rate expression for r_1 and r_2 [eqns [C3.4] and [C3.5] should be replaced with the following:

$$r_1 = K_1 \frac{K_{ET}P_{ET}}{1+K_{ET}P_{ET}+K_{ETO}P_{ETO}^2} \qquad [C3.11]$$

and

$$r_2 = K_2 \frac{K_{ET}P_{ET}}{1+K_{ET}P_{ET}+K_{ETO}P^2_{ETO}} \qquad [C3.12]$$

which account for the retarding effect of ethylene oxide.

3. The effect of H_2O

No separate experiments were run in order to study a possible effect of H_2O on the reaction rates. Previous workers have suggested that the addition of water vapor to the feed gas has no effect on the production of either ethylene oxide or carbon dioxide (22). Metcalf and Harriott, however, observed that by adding water in the reactor feed r_1 declines in proportion to the -.25 power of P_{H_2O} and r_2 falls off with the -.20 power of P_{H_2O} (19).

Nevertheless, since this occurs for considerably high P_{H_2O} we can conclude that within the range of gas compositions used in our study the effect of water vapor on both reaction rates is negigible.

4. The effect of CO_2

The effect of CO_2 on the rate of ethylene epoxidation and combustion as well as on the surface oxygen activity a_O was studied at temperatures between 250 and 400°C and partial pres-

sures of CO_2 between 0.5 bar and $3 \cdot 10^{-4}$ bar. The partial pressure of ethylene was varied between $0.5 \cdot 10^{-2}$ and $1.6 \cdot 10^{-2}$ bar and that of oxygen between $3. \cdot 10^{-2}$ and $12 \cdot 10^{-2}$ bar.

Figure 24 shows the inhibiting effect of CO_2 and r_1 at $P_{ET} = 1.3 \cdot 10^{-2}$ bar and P_{O_2} between 0.05 and 0.1 bar for the various temperatures examined; r_f is the rate of ethylene epoxidation in the absence of excess CO_2, except that produced by reaction, which corresponds to P_{CO_2} usually less than 10^{-3} bar. Figure 24 shows that CO_2 has a pronounced inhibiting effect on r_1 at temperatures below 330°C.

No single correlation of r_1/r_f with P_{CO_2} was found to hold when P_{O_2} varies. Although over the range of parameters investigated r_1 is zero order in oxygen for low P_{CO_2}, it was found that the rate increases considerably with increasing P_{O_2} at constant ethylene and constant high values of P_{CO_2} (>0.05 bar). Careful examination of the data showed that r_1/r_f could be uniquely related to the ratio P_{CO}/P_{O_2} at constant T:

$$r_f/r_1 = 1 + K'P_{CO_2}/P_{O_2}. \qquad [C3.13]$$

This is shown in Fig. 25, where $(r_f/r_1)-1$ is plotted vs. P_{CO_2}/P_{O_2}. The temperature dependence of the proportionality constant K' is shown in Fig. 26. The parameter K' increases with decreasing temperature since the CO_2 retarding effect on r_1 is significant below 330°C and almost vanishes above 400°C.

Similarly with the ethylene oxidation experiments at low P_{CO_2} values, it was found that the surface oxygen activity a_O is uniquely defined by P_{ET}, P_{O_2}, and T and is totally independent of P_{CO_2}. This is shown in Fig. 27 for various temperatures

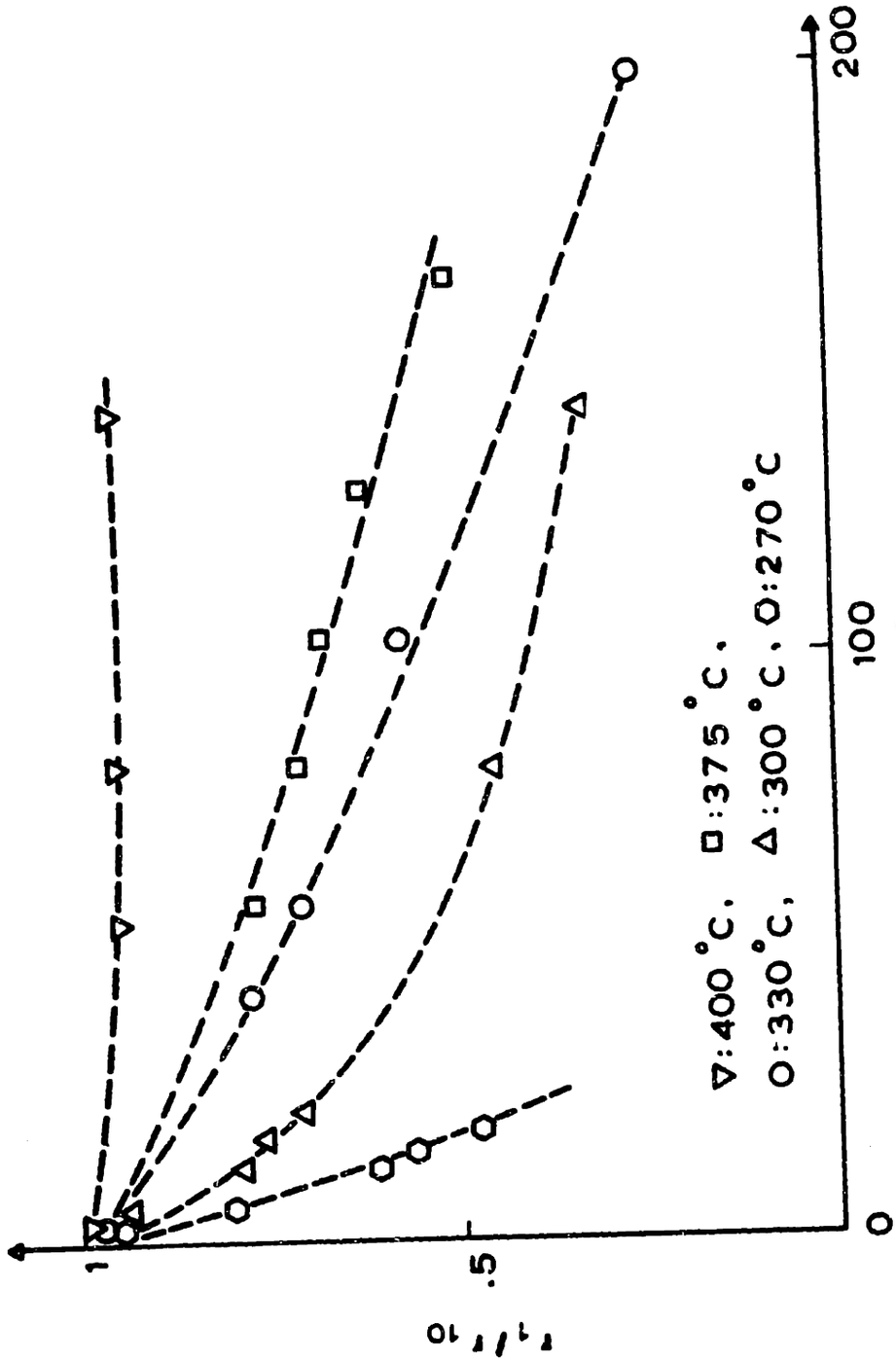

Figure 24: Effect of CO_2 on the rate of ethylene epoxidation r_1.

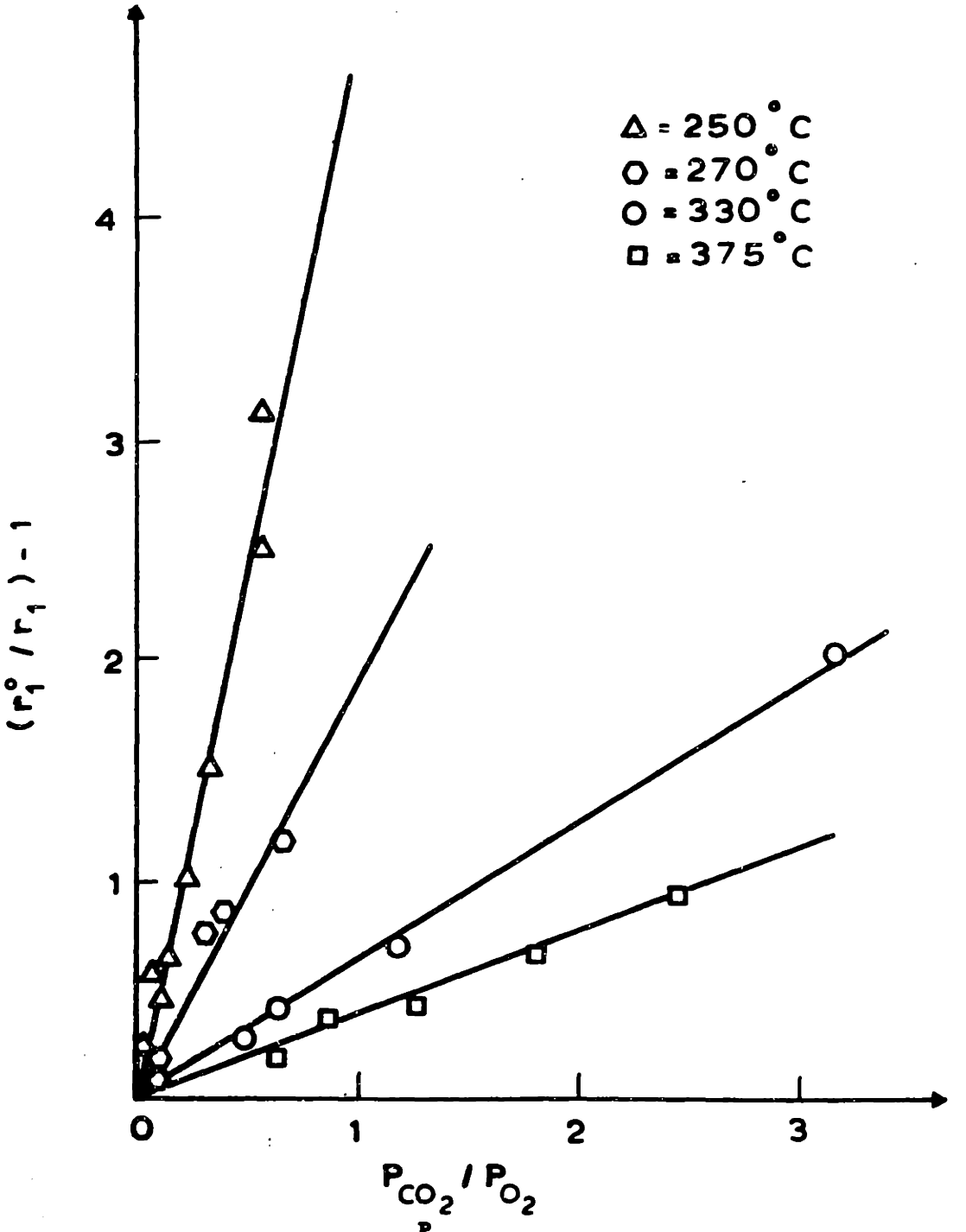

Figure 25: Effect of the $\frac{P_{CO_2}}{P_{O_2}}$ ratio on the rate of ethylene epoxidation r_1.

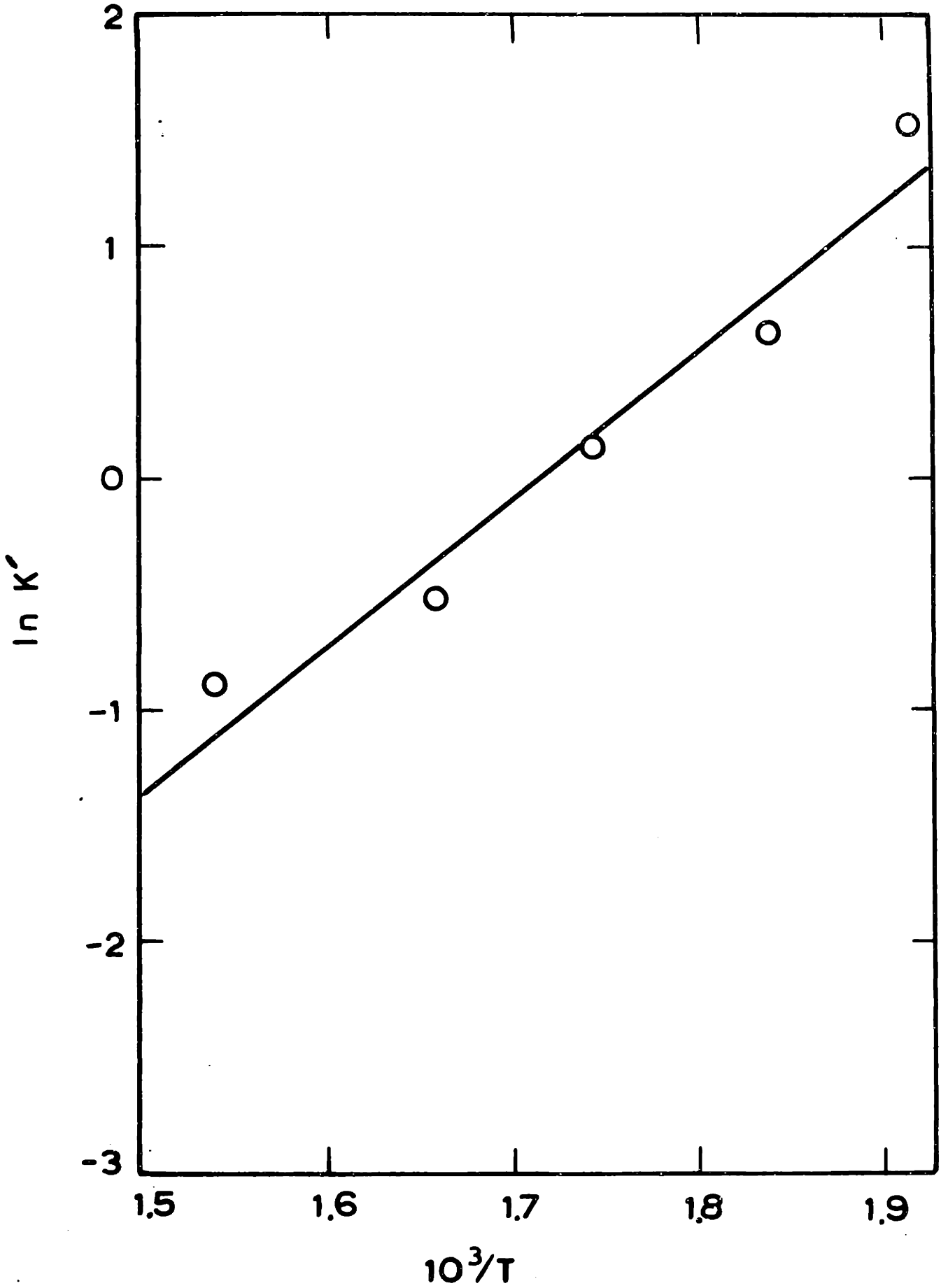

Figure 26: Temperature dependence of K'

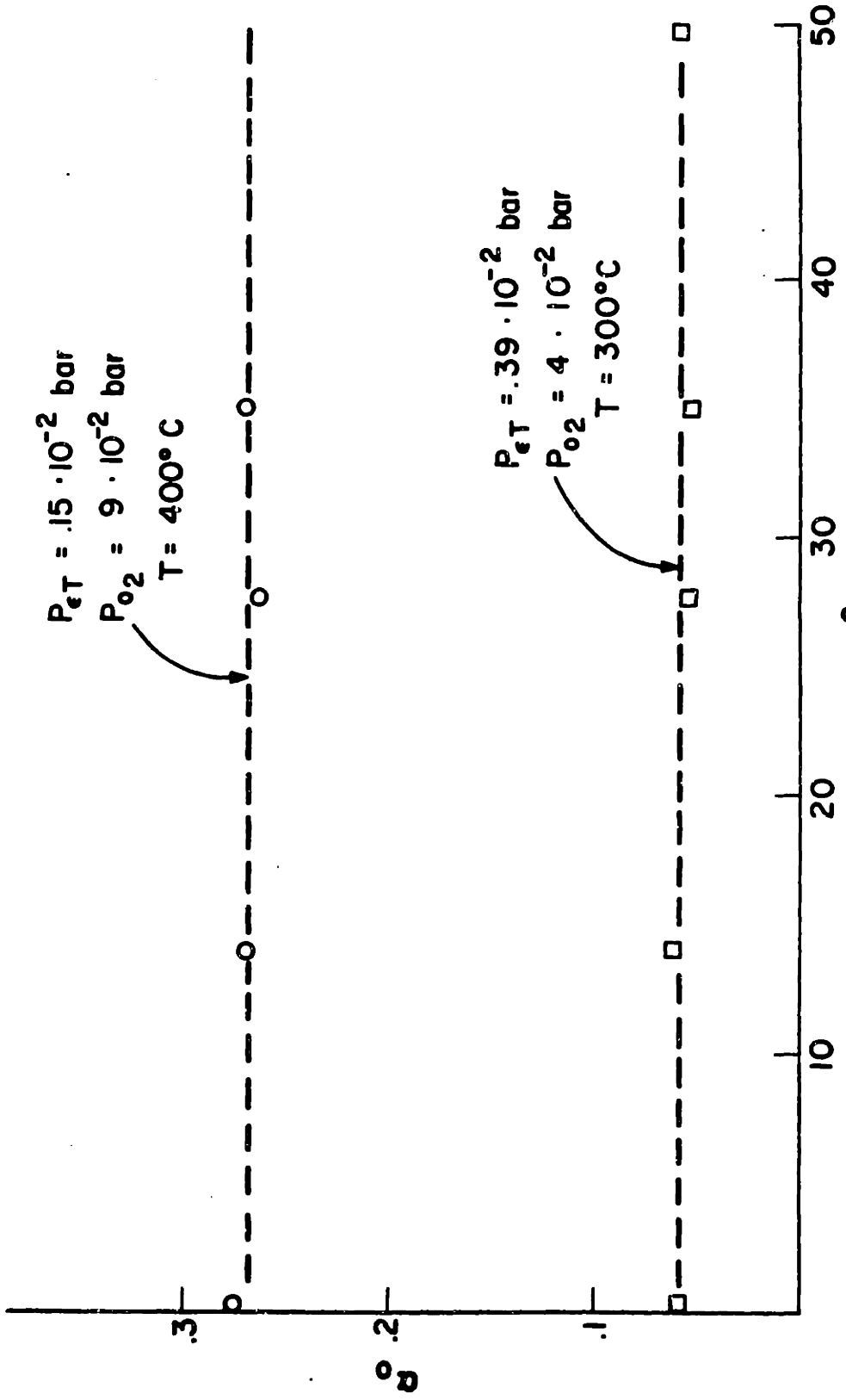

Figure 27: Surface oxygen activity a_O vs P_{CO_2}

and gas-phase compositions. The oxygen activity a_O remains constant within 2% as P_{CO_2} varies more than three orders of magnitude. This is remarkable in view of the fact that at the same time r_1 is decreasing considerably (Fig.24).

Within the accuracy of the experimental measurments the rate of ethylene combustion r_2 remains virtually constant with increasing P_{CO_2}. This is shown in Fig.28 where r_1^0/r_1 and r_2^0/r_2 are compared at constant T, P_{ET}, and P_{O_2}. As shown in the figure the measurement of r_2 is subject to considerable experimental error for high P_{CO_2} values because in this region the ir CO_2 analyzer could not be used and the chromatographic separation of the ethylene peak and the large CO_2 peak was not complete. However, one can definitely conclude that if CO_2 has an effect on r_2 the effect is much smaller than the corresponding one for r_1. This is in agreement with previous work by Hayes (22) and Nault (71) although other workers have reported that CO_2 inhibits r_2 also (19).

C3.d. Discussion of results

Since the early work of Twigg (3, 4) a number of reaction mechanisms have been proposed for ethylene oxidation on Ag. We can discuss now some of these mechanisms on the basis of the reaction network kinetics, previous experimental investigations, and the new information provided by the solid-electrolyte-aided surface oxygen activity measurement.

Twigg basically proposed an Eley-Rideal-type mechanism between gaseous ethylene and atomically adsorbed oxygen (3, 4). According to this early mechanism, reaction of ethylene with one

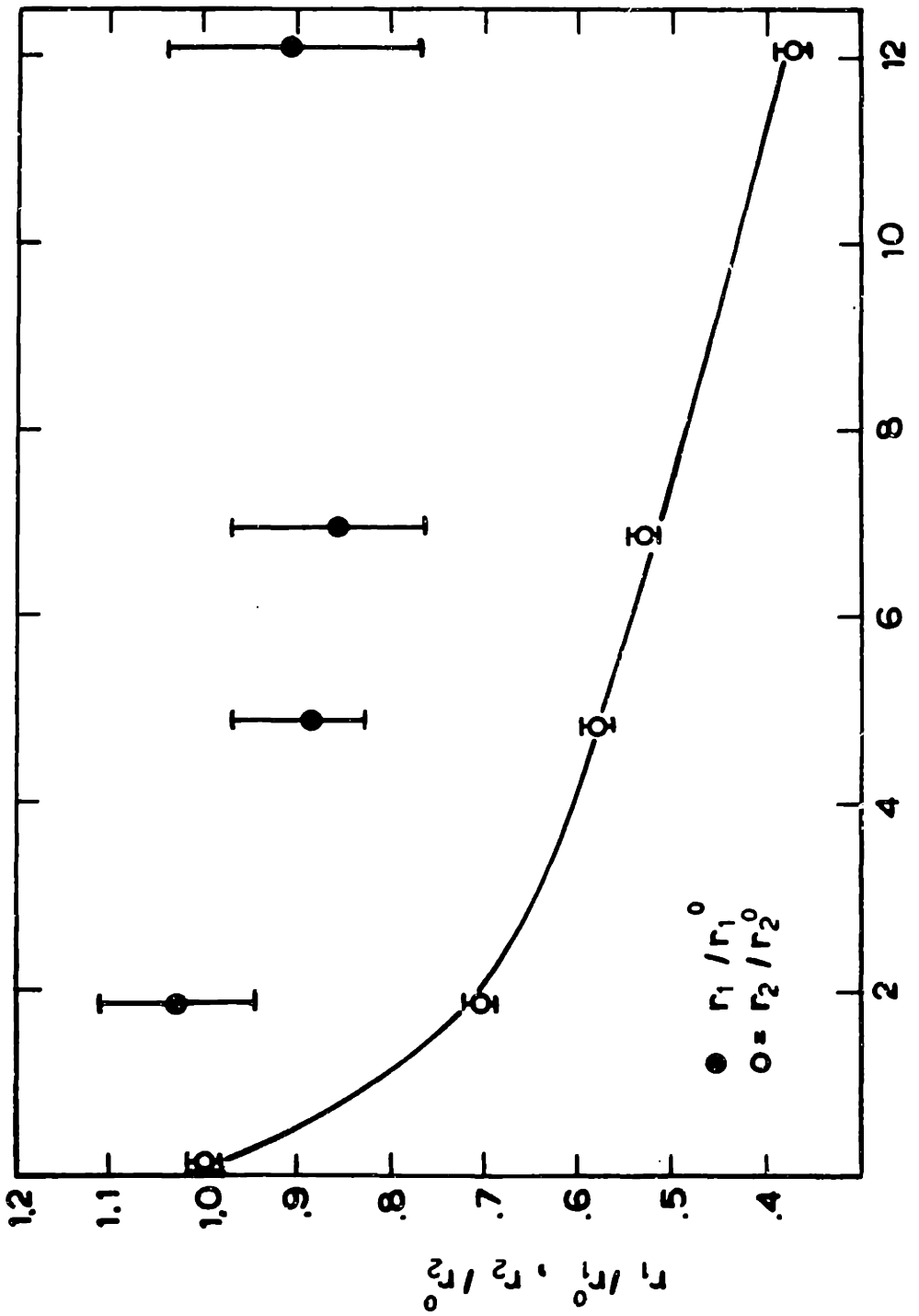

Figure 28: Effect of CO_2 on r_1 and r_2 at constant T, P_{ET} and P_{O_2}

adsorbed oxygen atom gives C_2H_4O, while reaction of C_2H_4 with two oxygen atoms gives CO_2. Since this early work a number of studies have shown that several forms of adsorbed oxygen exist on silver during ethylene oxidation (7,10,11). According to the classical picture of Kilty and Sachtler one of these forms of oxygen, i.e., molecularly adsorbed O_2, gives rise to ethylene oxide while atomically adsorbed oxygen yields CO_2 (10,11). This mechanism can also explain the observed increase in selectivity when trace amounts of chlorinated hydrocarbons are added to the feedstream (11). Furthermore, Twigg's early notions of an Eley-Rideal-type mechanism do not seem to be well accepted by the majority of previous workers (7,34) as recent ir spectroscopic studies have shown several species adsorbed on Ag during ethylene oxidation including at least two forms of oxygen, ethylene, CO_2, and ethylene oxide as well as oligomers of ethylene oxide (8, 9).

The present results including the surface oxygen activity data can be accounted for within the general framework of the Kilty-Sachtler mechanism. In agreement with previous work we found it necessary to postulate the existence of two types of adsorbed oxygen in order to explain the experimental observations presented here. A strong indication of the existence of two types of adsorbed oxygen is the retarding effect of CO_2 (Figs. 27 and 28). Carbon dioxide retards r_1 only and leaves r_2 and the emf almost totally unaffacted. It thus follows that CO_2 competes for the same adsorption sites with the oxygen species responsible for ethylene oxide formation but not with the oxy-

gen species the activity of which is being electrochemically measured and which produces CO_2. Since the emf measurements are expected to reflect the activity of atomic oxygen (62) it would follow that atomic oxygen is responsible for CO_2 formation while a second type of oxygen, presumably molecularly adsorbed, yields ethylene oxide, in excellent agreement with what previous workers have proposed (10,11,12).

A satisfactory mechanism for ethylene oxidation should account not only for the kinetics [C3.4] and [C3.5] but also for the surface oxygen activity behavior (Eq. [C3.9]). Such a mechanism explaining all the experimental observations in a semi-quantitative manner is presented below.

According to the previous discussion we assume two types of surface sites S_2 and S_3 for atomic and molecular oxygen adsorption, respectively. We also assume the existence of a third type of site S_1 for ethylene and ethylene oxide chemisorption. In order to account for the above-mentioned CO_2 effect carbon dioxide must then compete with molecular oxygen for S_3 sites. We assume Langmuir-type adsorption for ethylene on S_1 sites and themodynamic equilibrium between surface and gaseous ethylene during reaction. It thus follows that the coverage θ_{ET} of ethylene on S_1 sites is given by

$$\theta_{ET} = K_{ET}P_{ET}/(1 + K_{ET}P_{ET}), \qquad [C3.14]$$

where K_{ET} is the adsorption coefficient of ethylene, provided P_{ETOX} is small enough (< 0.02 bar) so that $\theta_{ETOX} \approx 0$.

Similarly, assuming Langmuir-type adsorption for molecular

oxygen on S_3 sites and thermodynamic equilibrium between molecularly adsorbed and gaseous O_2 one obtains

$$\theta_{O_2} = K_{O_2}P_{O_2}/(1+K_{O_2}P_{O_2}), \qquad [C3.14]$$

where θ_{O_2} is the O_2 coverage of S_3 sites and K_{O_2} is the molecular adsorption coefficient of oxygen. If P_{CO_2} is high (> 0.05 bar) and the temperature low, then [C3.14] would hsve to be modified in the form

$$\theta_{O_2} = K_{O_2}P_{O_2}/(1+K_{O_2}P_{O_2}+K_{CO_2}P_{CO_2}). \qquad [C3.15]$$

We will also assume Langmuir-type adsorption of atomic oxygen on S_2 sites but will not necessarily assume thermodynamic equilibration between gaseous and atomically adsorbed oxygen. This is possible if the atomic oxygen adsorption-desorption kinetics are relatively slow with respect to the surface reaction. Because of the definition of surface oxygen activity a_O (Eq. [A4.4] and the Langmuir adsorption assumption it follows that

$$\theta_O = K_O a_O/(1+K_O a_O). \qquad [C3.16]$$

Note that this expression relates two intrinsic surface properties and is valid whether or not equilibrium with the gas phase exists. If such an equilibrium exists, then $P_{O_2} = a_O^2$ by definition and [C3.16] reduces to the common form of the Langmuir isotherm for dissociative adsorption.

On the basis of these assumptions it follows that the rate of ethylene oxide formation r_1 is given by

$$r_1 = K_1\theta_{ET}\theta_{O_2} = r_1\frac{K_{ET}P_{ET}}{1+K_{ET}P_{ET}}\cdot\frac{K_{O_2}P_{O_2}}{1+K_{O_2}P_{O_2}} \qquad [C3.17]$$

which reduces to the experimental rate expression [C3.4] if $K_{O_2} P_{O_2} >> 1$. This is quite reasonable since all the experiments were performed with $P_{O_2} > 1.5 \cdot 10^{-2}$ bar. It is reasonable to expect that for very low values of P_{O_2} the rate r_1 will become first order in oxygen.

Similarly, the rate of ethylene deep oxidation r_2 is given by

$$r_2 = K_2 \cdot \theta_{ET} \cdot \theta_O = K \frac{K_{ET} P_{ET}}{1+K_{ET} P_{ET}} \cdot \frac{K_O a_O}{1+K_O a_O} \qquad [C3.18]$$

which reduces to the experimental expression [C3.5] if $K_O a_O >> 1$. It should be noted that $\theta_O \approx 1$ is not inconsistent with the experimental observation $a_O^2 < P_{O_2}$ to the extent that $K_O a_O >> 1$. SEP measurements are quite sensitive to changes in the activity of oxygen at near surface saturation because of the experimental dependence of a_O on the measured emf (Eq. [A4.4]. Thus a_O can change by orders of magnitude while θ_O remains close to unity as long as $K_O a_O >> 1$ as is the case here. From [C3.16] and [C3.17] it follows that the experimentally determined parameter K_{ET} (Fig. 29) is the adsorption coefficient of ethylene on silver. According to Eq. [C3.8] it follows that the enthalpy and entropy of adsorption of ethylene on silver are $\Delta H_{ET} = -11.5$ kcal/mole and $\Delta S_{ET} = -14$ cal/mole·K. Both values are quite reasonable and in good agreement with those reported by Dettwiller (34).

The difference in activation energies of K_2 and K_1 (22. - 14.5 = 7.5 kcal/mole) explains well the monotonic drop in selectivity with increasing temperature (Fig. 21).

The surface oxygen activity dependence on temperature and gas-phase composition can be explained now by considering

a steady-state mass balance for adsorbed atomic oxygen:

$$0 = K_{ad} \cdot P_{O_2}^{1/2} \cdot (1-\theta_O)(1-\theta_{ET}) - K_d \cdot \theta_O (1-\theta_{ET}) - \gamma \cdot K_2 \theta_{ET} \theta_O + K_1 \theta_{ET} \theta_{O_2} \quad [C3.19]$$

The first term corresponds to the atomic oxygen adsorption step using the same assumptions made in the ethylene oxide study i.e., that atomic oxygen adsorption on a S_1 site requires an empty adjacent S_2 site. The second term corresponds to oxygen desorption under the same assumptions. Note that in the absence of ethylene ($\theta_{ET} = 0$) the last two terms vanish and Eq. [C3.19]reduces to the common form of the Langmuir isotherm with $K_O = K_{ad}/K_d$. The third term refers to atomic oxygen reacting with ethylene to form CO_2. The coefficient γ would equal 6 if all oxygen contained in CO_2 is originally atomically adsorbed. However since some of that oxygen may originate from the gas phase once an activated complex between adsorbed ethylene and adsorbed atomic oxygen is formed we will leave γ unspecified and treat it as an adjustable parameter. The last term accounts for atomic oxygen formed from molecular oxygen. We assume that whenever ethylene reacts with molecularly adsorbed oxygen to form ethylene oxide, the oxygen atom thus formed migrates to an atomic oxygen adsorption site S_1.

Taking into account Eqs. [C3.14] and [C3.16] and dividing [C3.19] by $K_{ad}(1 - \theta_O)(1 - \theta_{ET})a_O$ one obtains

$$\frac{P_O^{1/2}}{a_O} - 1 \quad \theta_O = \frac{K_1}{K_d} \cdot K_{ET} \cdot P_{ET} \cdot \left[\frac{\gamma K_2}{K_1} \theta_O - \theta_{O_2} \right] \qquad [C3.20]$$

and taking into account that $\theta_O \approx 1$ according to the kinetics (Eq. [C3.5]):

$$P_O^{1/2}/a_O = 1 + \frac{K_1 K_{ET}}{K_a} P_{ET} \left[\frac{\gamma K_2}{K_1} - \theta_{O_2}\right] . \qquad [C3.21]$$

The ratio K_2/K_1 is of order 1. It varies from roughly 2 at 440°C to 0.5 at 250°C. Agreement with experiment becomes quantitative if $\gamma K_2/K_1 \simeq 1$. This assumption is not unreasonable but cannot be justified independently. With this assumption and according to Eq. [C3.14] it follows that

$$1 - \theta_{O_2} = 1/K_{O_2} P_{O_2} \qquad [C3.22]$$

and Eq. [C3.22] reduces to the experimental expression

$$P_{O_2}^{1/2}/a_O = 1 + KP_{ET}/P_{O_2} \qquad [C3.23]$$

which describes the surface oxygen activity behavior, with

$$K = K_{ET} K_1 / K_{O_2} K_d$$

Figure 23 shows the temperature dependence of K which corresponds to Eq. [C3.23]. The temperature dependence of K_{ET} and K_1 is described by Eqs. [C3.8] and [C3.7], respectively. One could thus estimate ΔH_{O_2}, the heat of oxygen molecular adsorption, from K_{O_2} if the activation energy of K_d were known. By using an average literature value of ~28 kcal/mole (10,72) for the rate coefficient of atomic oxygen desorption one estimates ΔH_{O_2} = -9.5 kcal/mole, in agreement with the calorimetric data of Ostrovskii et al. at high oxygen coverages (73).

In the above analysis which explains the experimental observations [C3.4], [C3.5], and [C3.9] the effect of CO_2 on r_1 has been neglected.

Since CO_2 competes with molecular oxygen only, the rate of ethylene combustion r_1 given by [C3.4] should remain unchanged

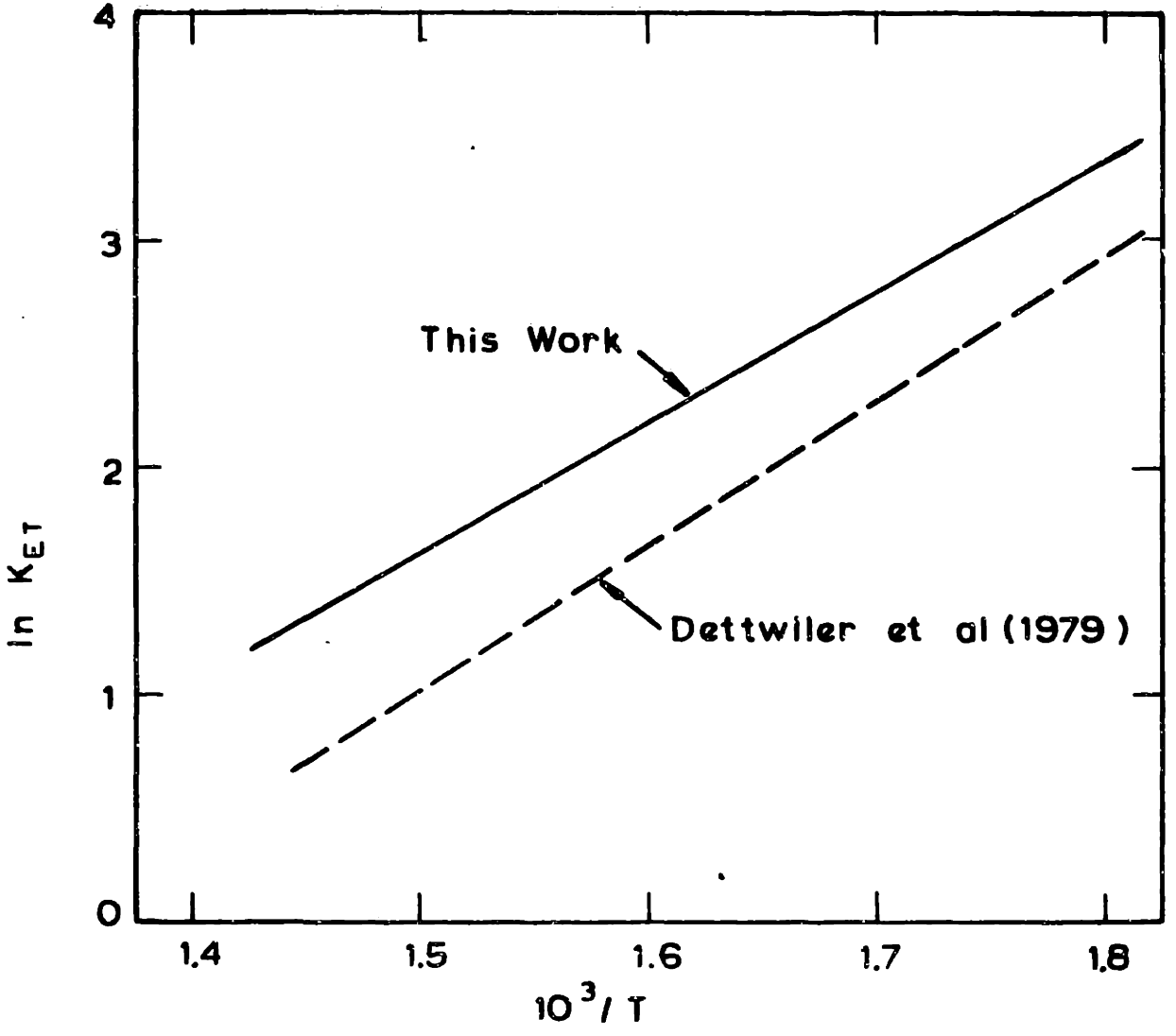

Figure 29: Temperature dependence of ethylene adsorption coefficient K_{ET}.

in agreement with experiment. However, the coverage of O_2 on molecular oxygen and carbon dioxide adsorption sites becomes

$$\theta_{O_2} = \frac{K_{O_2}P_{O_2}}{1+K_{O_2}P_{O_2}+K_{CO_2}P_{O_2}} \quad \frac{K_{O_2}P_{O_2}}{K_{O_2}P_{O_2} + K_{CO_2}P_{CO_2}} \qquad [C3.25]$$

where K_{CO} is the adsorption coefficient of CO_2. That last equation is valid as long as $K_{O_2}P_{O_2} >> 1$. It thus follows from [C3.4] that

$$r_1^\circ/r_1 = 1 + \frac{K_{CO_2}}{K_{O_2}} \frac{P_{CO_2}}{P_{O_2}} \qquad [C3.26]$$

provided r_1 and r_1° are measured at the same P_{ET}. This is the experimentally obtained relation [C3.13] if $K' = K_{CO_2}/K_{O_2}$. Thus the parameter $K' = 1.2 \cdot 10^{-5} \cdot \exp(6600/T)$ can be interpreted as a ratio of two adsorption coefficients.

This would imply $\Delta H_{CO_2} - \Delta H_{O_2} \simeq -13.1$ kcal/mole, where ΔH_{CO_2} and ΔH_{O_2} are the heats of adsorption of CO_2 and molecular O_2, respectively. If $\Delta H_{O_2} \simeq -10$ kcal/mole ( ) one obtains $\Delta H_{CO_2} \simeq -23$ kcal/mole. The difference $\Delta H_{CO_2} - 1/2\Delta H_{O_2}$ of the two heats of adsorption is -18 kcal/mole, quite close to the $\Delta H°$ of the reaction

$$Ag_2O + CO_2 \rightarrow Ag_2CO_2 \qquad [C3.27]$$

which is -18.5 kcal/mole at 298 K. Although this may be coincidental it does suggest the possibility of CO_2 forming surface carbonate by adsorbing on oxygen atoms trapped in molecular oxygen adsorption sites after reaction of molecular oxygen with ethylene to form ethylene oxide. This is supported by the results of Force and Bell's study (8 , 9) who observed sur-

face carbonate formation upon chemisorption of CO_2 on Ag in the presence of O_2, as well as by those of Czanderna who reports that CO_2 adsorbs on silver only when the surface is partially oxidized (72).

C4. The Effect of electrochemical oxygen pumping during Ethylene oxidation

C4.a. Qualitative description

Several different zirconia reactor cells were used in the course of the experiments. The cells differed in zirconia thickness and in the surface area S of the silver catalyst electrode. The electrolyte thickness varies roughly between 150 and 300 μm. The surface areas of the reactor cells are shown in table 5.

The effect of electrochemical oxygen pumping on the rates of ethylene epoxidation r_1 and deep oxidation r_2 is shown in figure 30. At time t<o the circuit is open and the catalyst is at a steady state characterized by $r_{10} = 7.6 \cdot 10^{-8}$ mole/s and $r_{20} = 8.9 \cdot 10^{-8}$ mole/s. At t = o a constant current of +25 mA is applied to the cell and $O^{2-} = i/2F = 1.3 \cdot 10^{-3}$. As figure 30 shows $\Delta r_1/r_{10} = .2$, i.e. Δr_1 is two orders of magnitude larger than G_o^{2-}, indicating a dramatic change in the properties of the Ag catalyst. During the transient as well as at steady state the ratio $\Delta r_1/\Delta r_2$ remains practically constant at 1.7. At time t = 90 min the circuit is opened and the catalyst returns to its initial state indicating the reversibility of the phenomenon. At t = 180 min a constant current of -25 μA is applied through the cell so that oxygen is pumped from the catalyst. The rates r_1, r_2 as well as the selectivity drop. When the circuit is opened again the rates return to the original steady state values r_{10} and r_{20}.

Figure 31 shows the effect of applying a constant current

Table 5

Catalyst-electrode surface areas

Reactor-cell #	Reactive oxygen uptake a (moles O_2)
RC2	$2.3 \cdot 10^{-7}$
RC3	$.4 \cdot 10^{-7}$
RC4	$2.5 \cdot 10^{-7}$
RC5	$20 \cdot 10^{-7}$
RC6	$6.5 \cdot 10^{-7}$
RC7	$9.4 \cdot 10^{-7}$
RC8	$5.2 \cdot 10^{-7}$
RC9	$.4 \cdot 10^{-7}$
RC10	$10 \cdot 10^{-7}$
RC11	$2.6 \cdot 10^{-7}$

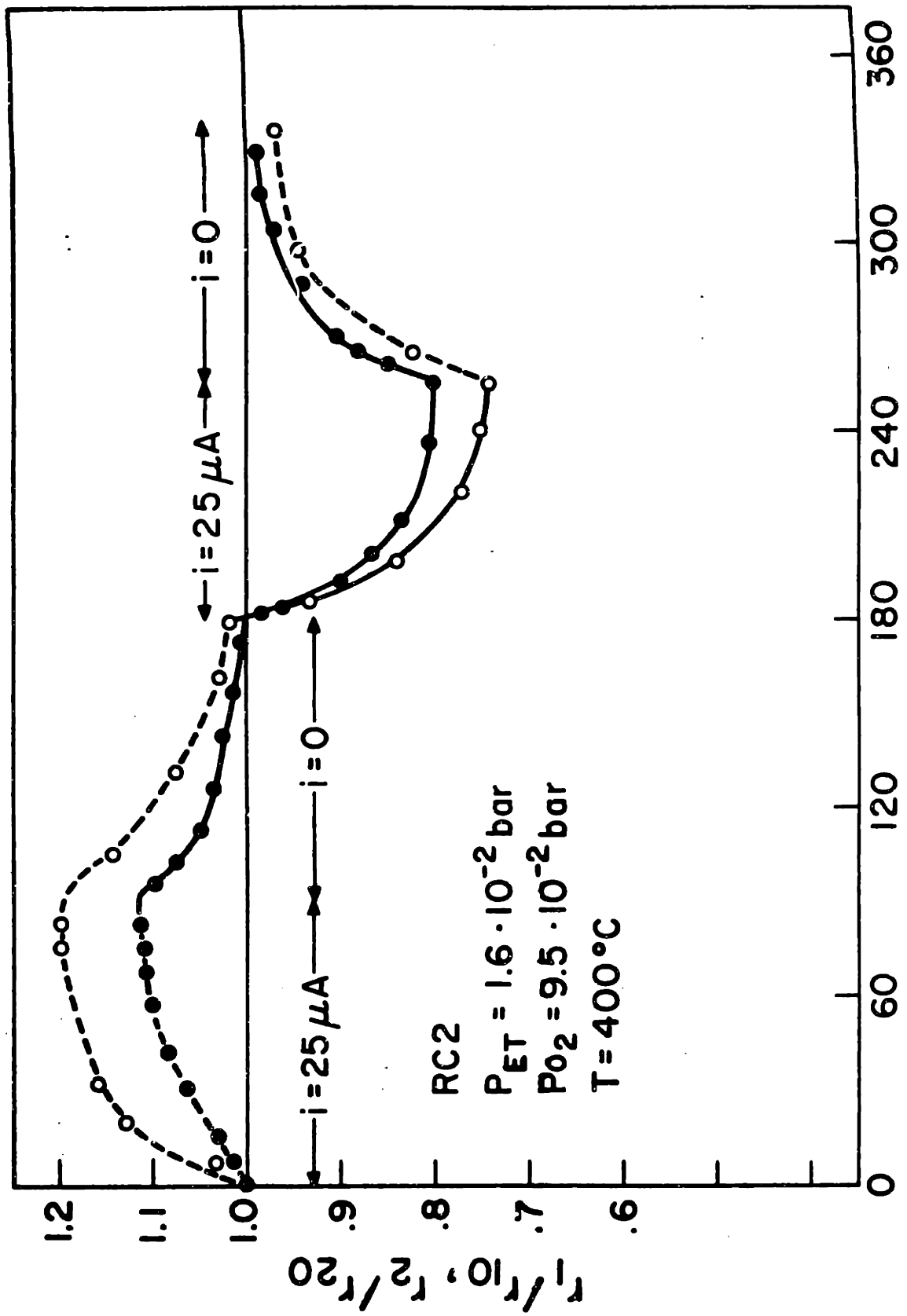

Figure 30: Transient effect of electrochemical oxygen pumping

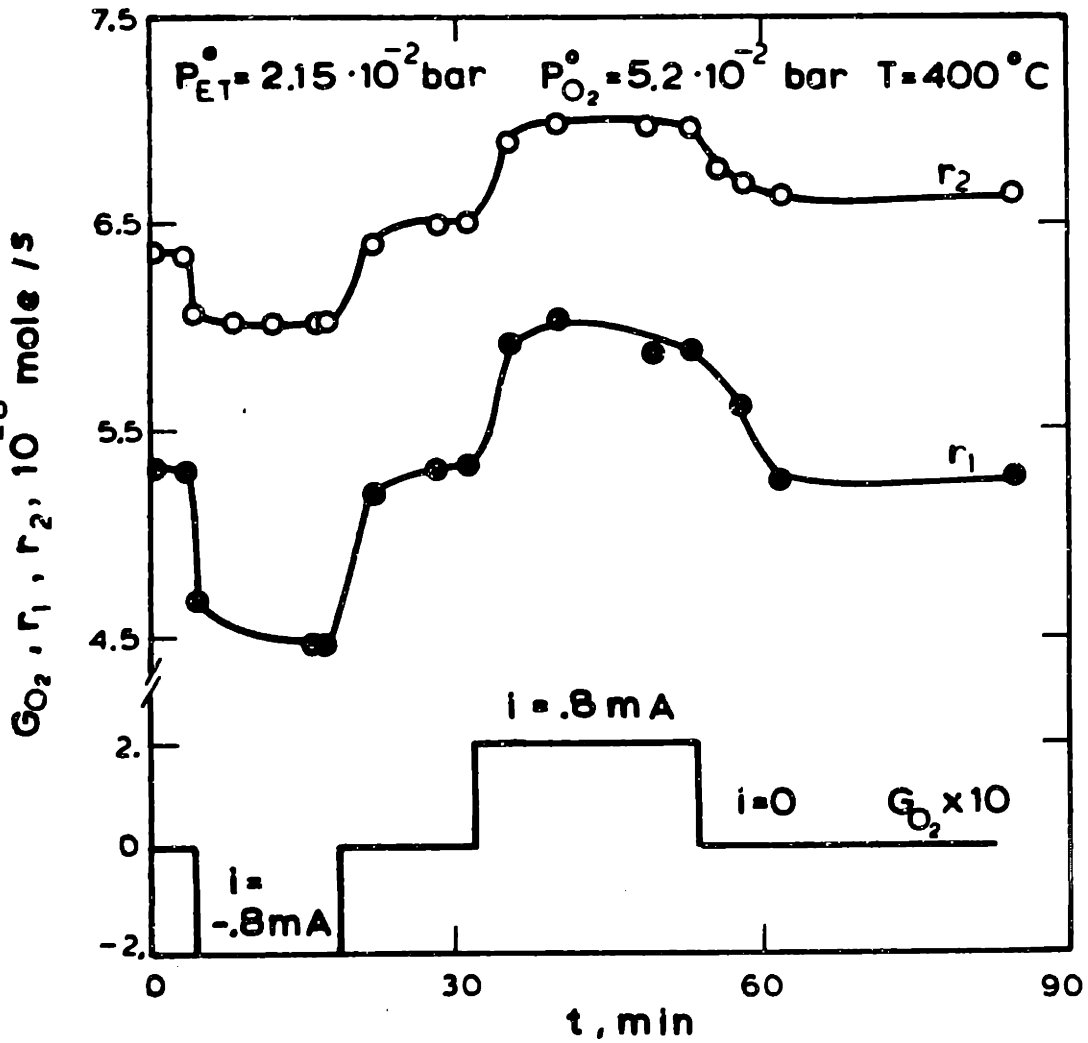

Figure 31: Effect of electrochemical oxygen pumping on the rate of ethylene epoxidation r_1 and deep oxidation r_2. Comparison with the rate of oxygen transport through the electrolyte G_{O_2} = i/4F.

$i = \pm 800$ A to cell reactor 1, while monitoring the rate of ethylene epoxidation, r_1, and the rate of ethylene oxidation to CO_2, r_2, at a residence time of 6.5s. At the start of the experiment the circuit is open and the catalyst is at steady-state activity and selectivity. The reactive oxygen uptake Q of the silver catalyst electrode of cell reactor 1 is 1.4×10^{-7} moles O_2. At time t = 0 the galvanostat is used to apply a current i = -800 A with a corresponding rate of oxygen removal from the catalyst $G_{O_2} = i/4F = 2 \times 10^{-9}$ moles O_2/s. This causes a decrease in r_1 and r_2. The decrease in the total rate of oxygen consumption, i.e., $0.5\Delta r_1 + 3\Delta r_2$, is approximately 7 times greater than G_{O_2}. The decrease in r_1 is larger than the corresponding decrease in r_2, thus selectivity drops. At the same time the voltage V of the cell gradually changes from $V = E = -65$ mV to a steady-state value $V \simeq -2V$, with a relaxation time constant approximately equal to that of r_1 and r_2. Subsequently the circuit is opened and r_1, r_2, and V are restored to their intrinsic values within 3-4 min. The galvanostat polarity is then reversed and a current i=- 800 μA is applied to the cell with a corresponding rate of oxygen transport to the catalyst $G_{O_2} \simeq 2 \times 10^{-9}$ mole/s. This causes an increase in r_1 and r_2, which is considerably larger than G_{O_2}. Since the increase in r_1 is greater, selectivity increases. At the same time the cell voltage gradually reaches a steady-state value $V \simeq 2$ Volts. Finally the circuit is opened again and the catalyst activity and selectivity as well as the open-circuit is emf relax to their initial values within a few minutes. Thus the phenomenon is reversible and

no permanent change of the silver catalyst has taken place.

C4.b. Overvoltage effects

Figure 32 shows a typical transient cell voltage response when a constant current i is imposed to the cell at time t = 0. AT t<o the cell voltage equals the open circuit emf E given by [A4.4].The initial rapid rise at t = 0 is caused by the ohmic drop iR_c, where R is the ohmic resistance of the cell which is primarily due to the zirconia electrolyte resistance. The subsequent gradual increase ΔV to a final asymptotic value, corresponds to charging of the electrode-electrolyte double layers and formation of surface intermediates on the silver electrode (74). These surface intermediates must be adsorbed oxygen species, possibly surface silver oxide. The increase ΔV is the cell overpotential; ΔV as well as the relaxation time constant τ_o, defined as the time required for ΔV to reach 63% of its final steady state value (74) were both found to be strongly dependent on gas phase composition. They both vanish as P_{O_2}/P_{ET} approaches zero. It can thus be concluded that double layer charging of the electrode-electolyte interface happens quite fastly and has a negligible contribution to the ΔV transient.

Within the accuracy of the experimental data the galvanostatic transient response of ΔV is identical to the transient rate response Δr_1 and Δr_2, i.e. $\tau_o = \tau_c$ where τ_c is the relaxation time constant for the two rates. This is shown in figure 33 for two different reactors under similar operating conditions and also in figure 34 where the transient and the steady state r_i values for four reactors are plotted vs. the

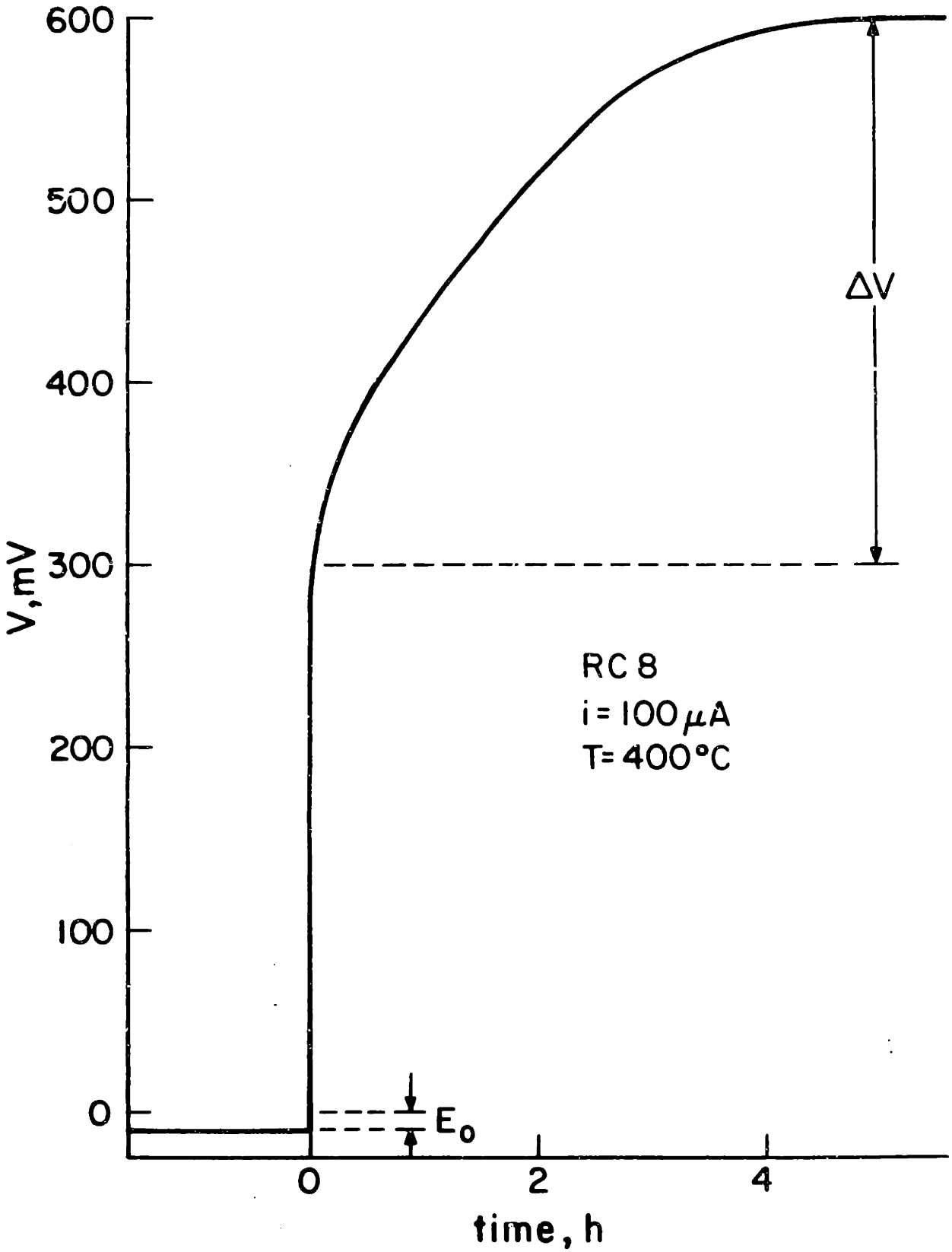

Figure 32: Transient cell voltage response when a constant current i = +100μA is applied at t = 0. P_{O_2} = .140 bar, P_{ET} = .008 bar.

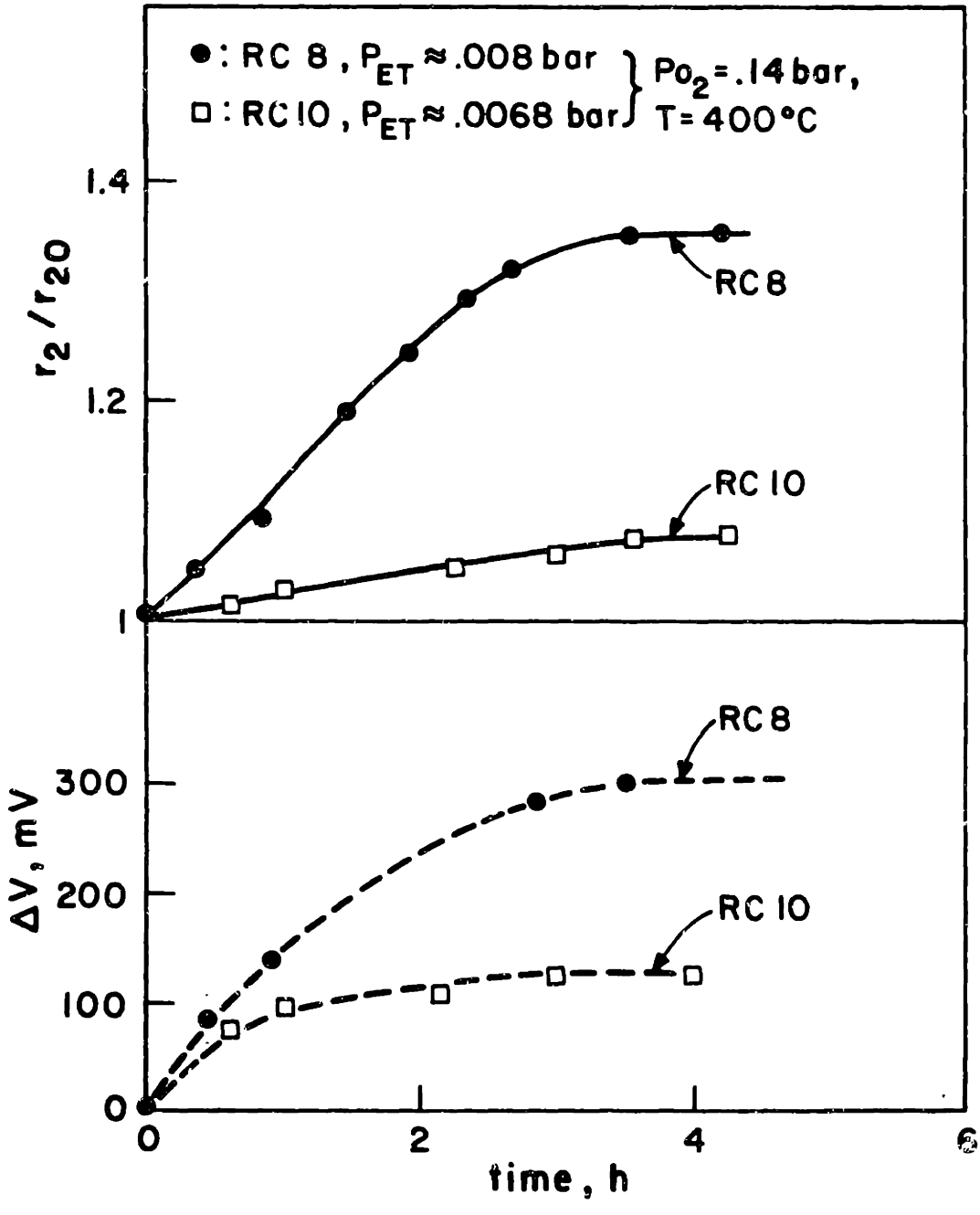

Figure 39: Galvanostatic transients of the rate of ethylene deep oxidation r_2 and of the cell overvoltage. The rate of epoxidation r_1 parallels r_2. (i = 100 μA)

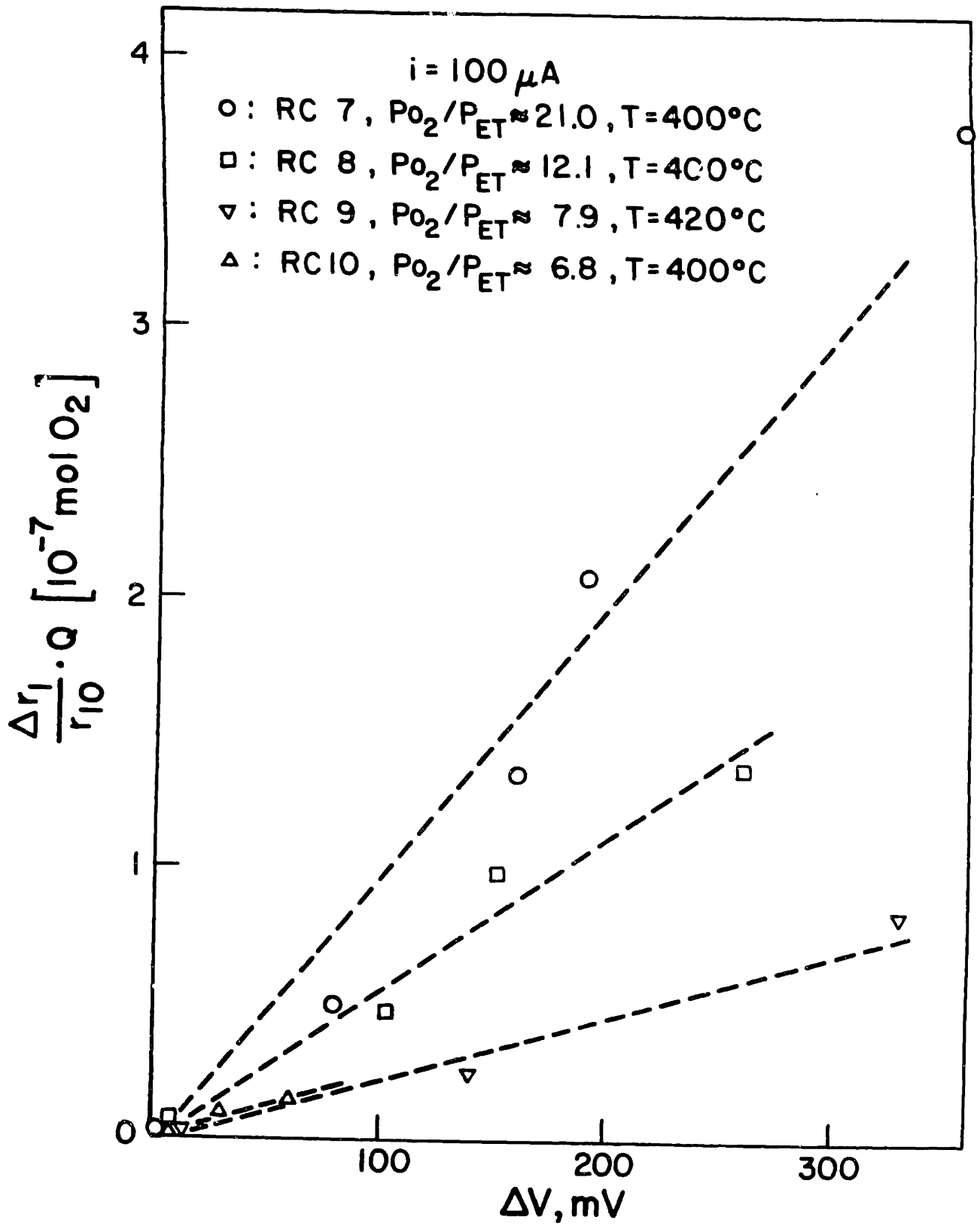

Figure34: Overvoltage effect on the increase in the rate of ethylene epoxidation at constant gas phase composition

cell overvoltage ΔV. In view of the fact that r_{io} is proportional to the surface area Q it follows from figure 34 that for constant gas phase composition

$$\Delta r_i \alpha \Delta V \qquad [C4.1]$$

Equation [C4.1] is valid both during transients as well as at steady state in which case

$$(\Delta r_i)_{max} \alpha \Delta V_{max} \qquad [C4.2]$$

C4.c. Effect of gas phase composition

In Fig.35 the effect of oxygen pumping to the catalyst is shown at lower current densities. Figures 35 through 39 refer to the catalyst of reactor cell 2 (Table 5). Before t = 0 the circuit is open and the catalyst is at steady state with a constant rate of ethylene epoxidation r_{10} ($\simeq 5.0 \times 10^{-6} \cdot P_{ET}$ moles/s). At t = 0, a constant current i = 100 μA is applied to the cell and oxygen is pumped to the catalyst at a constant rate $G_{O_2} \simeq 2.6 \times 10^{-10}$ moles/s. The rate of epoxidation r_1 increases considerably.

The bottom horizontal line $(G_{O_2}/r_{10})_{max} \simeq 2.5 \times 10^{-3}$ corresponds to $P_{ET} \simeq 2 \times 10^{-2}$ ($r_{10} = 1.02 \times 10^{-7}$ mole/s) and shows the anticipated maximum relative increase in r_1 on the basis of the rate of oxygen transport to the catalyst through the electrolyte. Stated differently, if the nature of the catalyst were no changing during oxygen pumping and each O^{2-} ion pumped to the catalyst produced one ethylene oxide molecule, then the increase in r_1 would be smaller or equal ($P_{ET} \simeq 2 \times 10^{-2}$

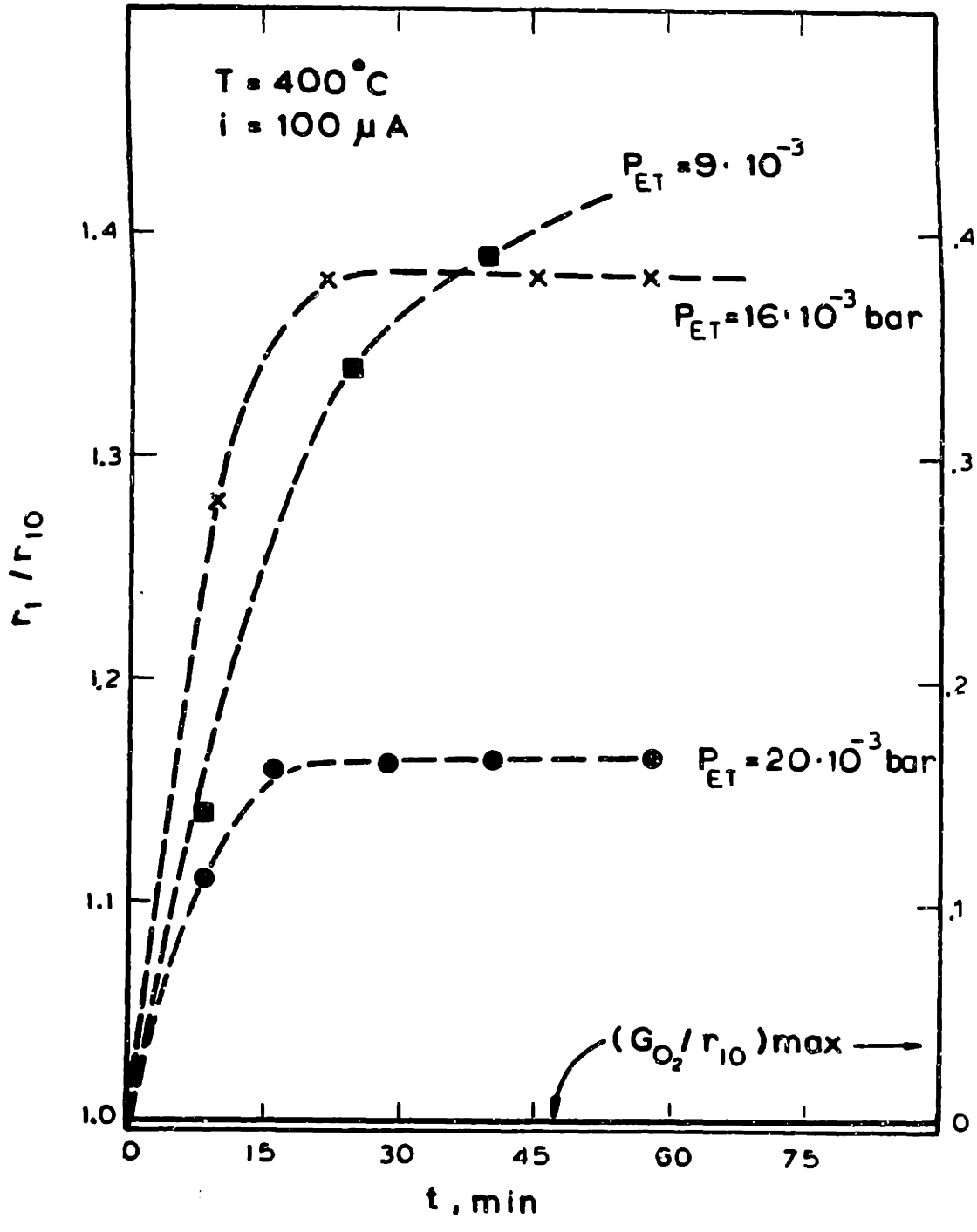

Figure 35: Transient behavior of the rate of ethylene oxidation r_1 when a constant current i = 100 µA is applied at t = 0.

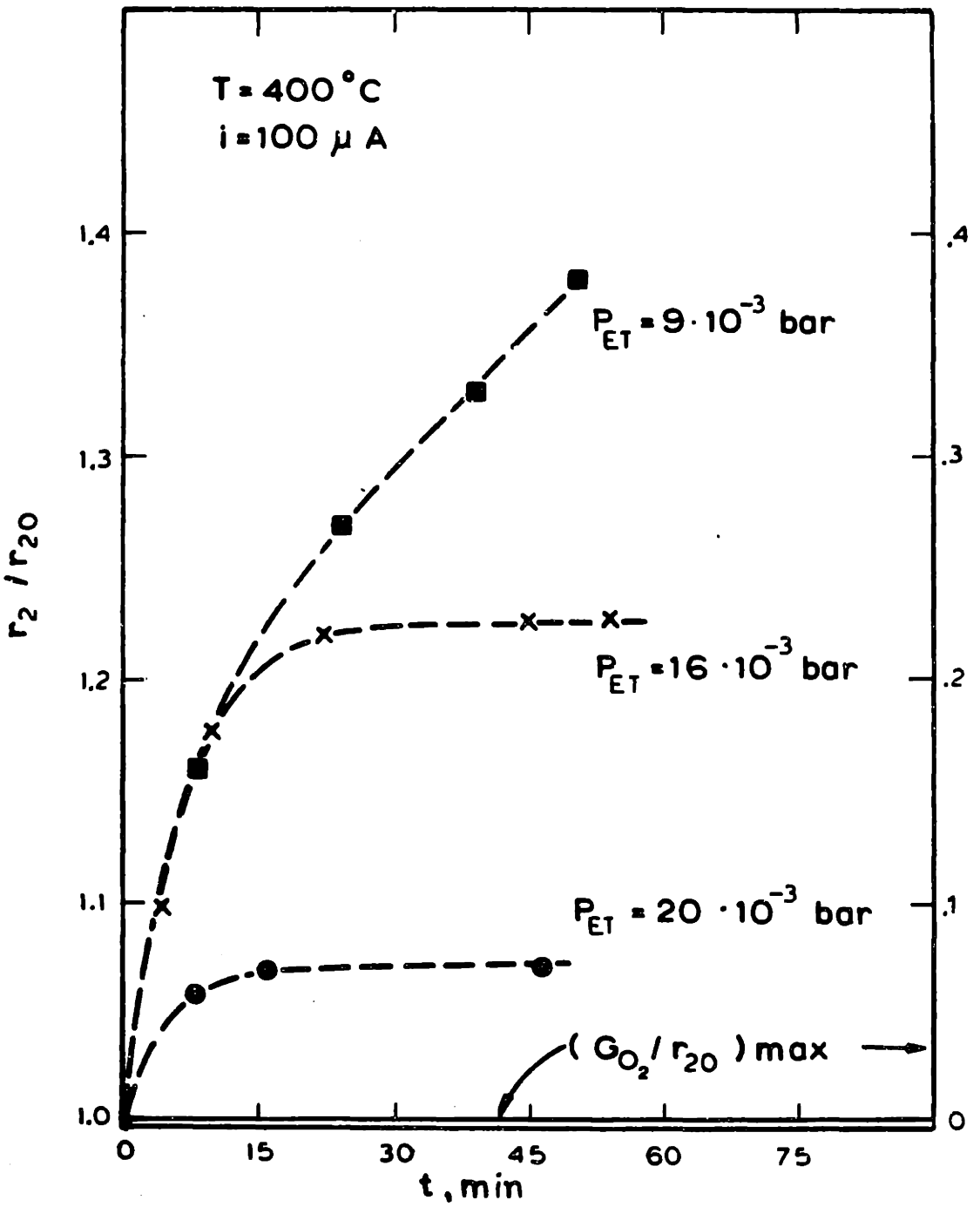

Figure 36: Transient behavior of the rate of ethylene deep oxidation r_2 when a constant current i = 100 μA is applied at t = 0.

bar) to $(G_{O_2}/r_{10})_{max}$. Thus the increase in r_1 is here 160 and 360 times greater than the increase corresponding to the rate of electrochemical oxygen pumping, for $P_{ET} = 2 \times 10^{-2}$ and 9×10^{-3} bar respectively.

The corresponding transient effect on the rate of CO_2 production r_2 is shown in Fig.36. The increase in r_2 is two orders of magnitude larger than G_{O_2} but smaller than the increase in r_1, thus selectivity to ethylene oxide increase. An interesting feature of Figs. 35 and 36 is the decrease in the relaxation time constant of the system with increasing P_{ET}. The relaxation time τ_c is defined as the time required to reach 63% of the final steady-state rate increase.

As shown in figure 34 the increase in the rate r_i depends on both overvoltage ΔV and gas phase composition. A series of runs performed at constant P_{ET} showed that $\Delta r_i/r_{io}$ is proportional to P_{O_2}. It was then established that $\Delta r_i/r_{io}$ is proportional to the P_O/P_{ET} ratio. It was also found that all the data transient and steady state, obtained with ten different reactors, each having different electrode surface area can be correlated in terms of one surprisingly simple equation,

$$\frac{\Delta r_i}{r_{io}} \cdot Q \cdot \frac{P_{ET}}{P_{O_2}} = \alpha_i \Delta V \qquad [C4.3]$$

where α_1, α_2 (i=1,2) are constant with a ratio $\alpha_1/\alpha_2 = 1.65 \pm .3$. This is shown in figure 37. Equation [C4.3] contains as a limiting case equation [C4.1] which is valid for constant gas phase composition.

It should be noted that at temperatures above 350°C r_{io}

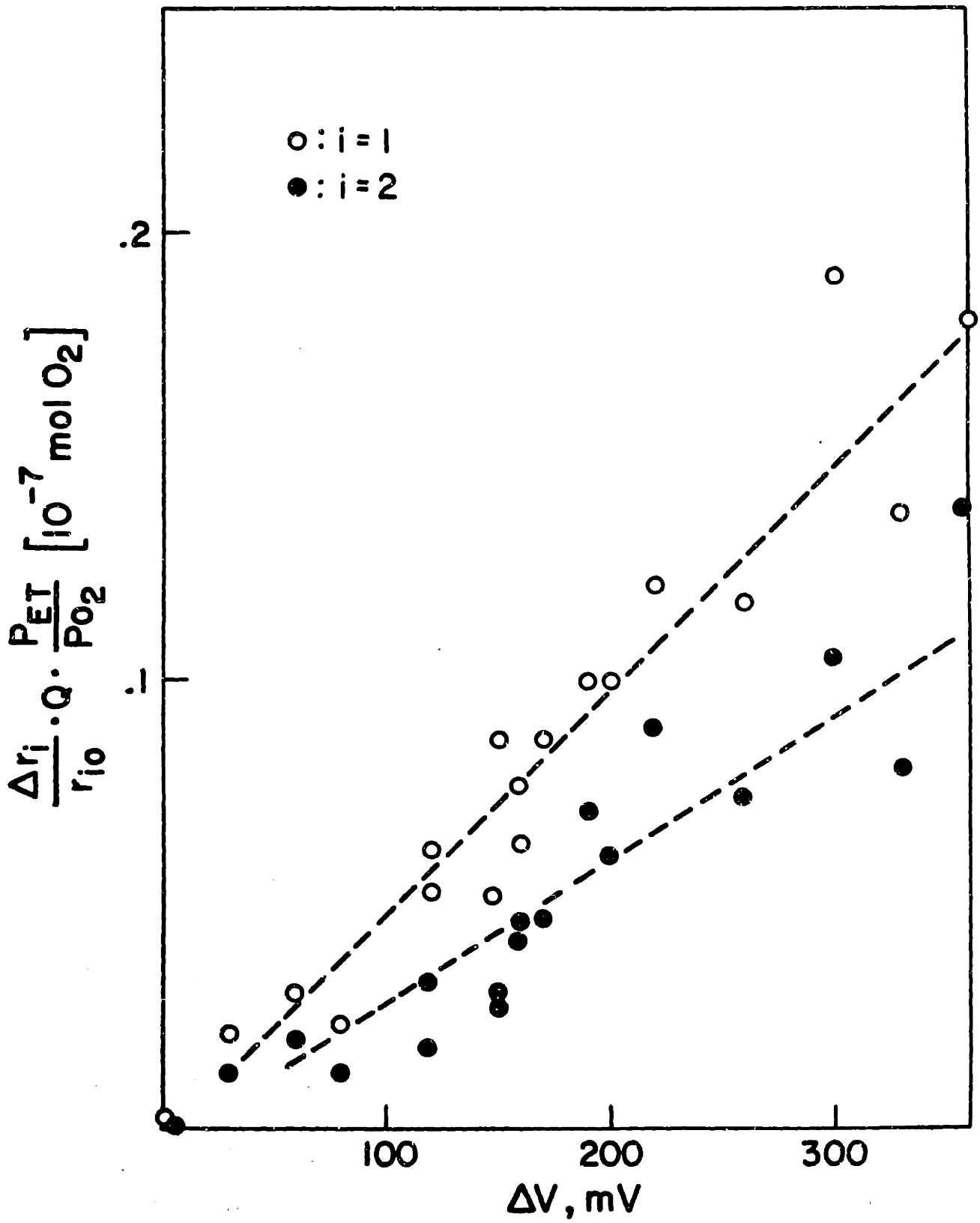

Figure 39. Overvoltage effect on the rates of ethylene epoxidation (i=1) and deep oxidation (i=2). At constant overvoltage the relative rate increases are proportional to P_{O_2}/P_{ET}. Temperature = 400°C.

is first order in ethylene and zero order in oxygen, i.e.

$$r_{io} = k_{io} \cdot Q \cdot P_{ET} \qquad [C4.4]$$

It follows that equation [C4.3] can be written as

$$\Delta r_i = k_{io} \cdot \alpha_i \cdot P_O \cdot \Delta V \qquad [C4.5]$$

which contains as a limiting case the observation that Δr_i vanishes when $P_{O_2} \rightarrow 0$, i.e. when the reactor is run as a fuel cell

Equations [C4.3],[C4.4] and [C4.5] are also valid both during transients and at steady state.

Most galvanostatic transients followed a first order response with reasonable accuracy, in agreement with [C4.3]

$$\Delta V = \Delta V_{max}(1-e^{-t/\tau_o}) \qquad [C4.6]$$

Table 7 shows the dependence of τ_o on gas phase composition. For constant surface area and current the time constant τ_o is roughly proportional to $\Delta V_{max} \cdot P_{O_2}/P_{ET}$. It is also shown that τ_o is proportional to $\Delta r_i/r_{io}$ in agreement with equation [C4.3]

C4.d. Effect of the imposed current i

The effect of varying the imposed current at constant gas phase composition is shown in Figs.38 and 39. At times before t = 0 the circuit is open and the catalyst is at steady state which a constant rate of ethylene epoxidation $r_{10} = 0.89 \times 10^{-7}$ moles/s. At time t = 0, a constant current is applied and the transient increase in r_1 and r_2 is monitored. It can be seen that the relaxation time constant of the system decreases slightly with increasing current. It is also clear that in-

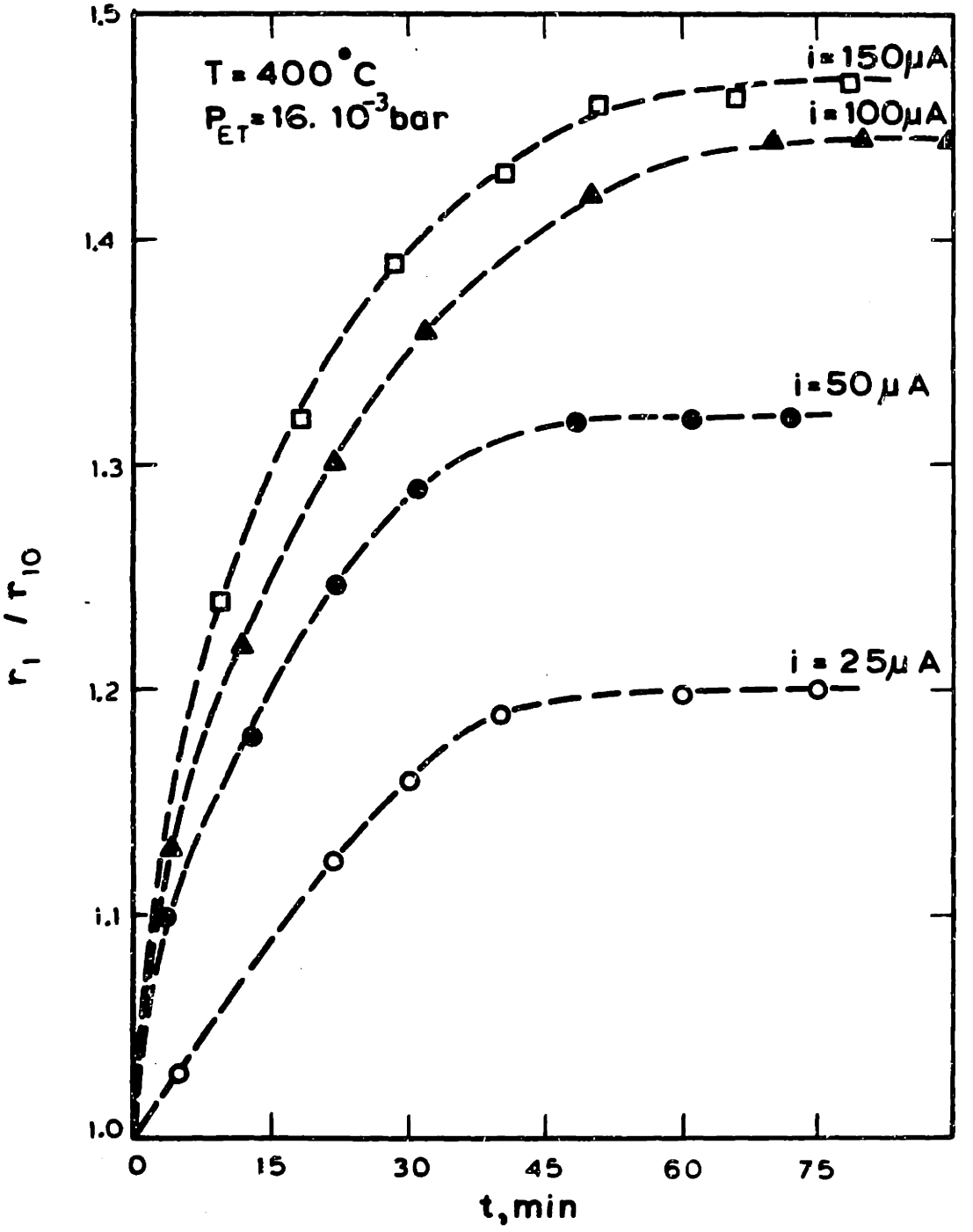

Figure 38: Transient effect of r_1 when different currents are applied at t = 0.

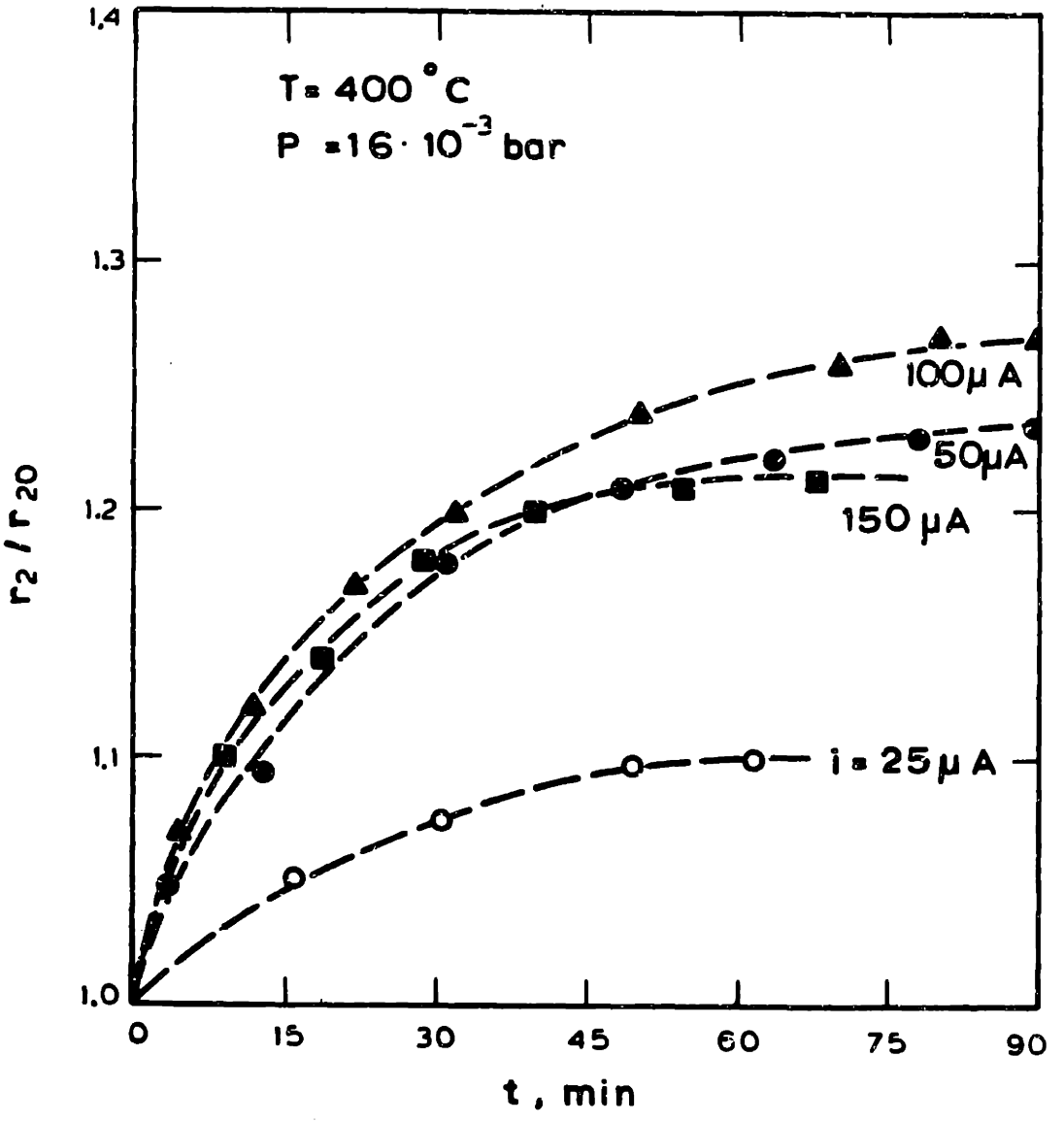

Figure 39: Transient effect on r_2 when different currents are applied at t = 0.

Table 6

Effect of Electrode Surface Area on the Experimental Relaxation Time Constant τ and Comparison with 4FQ/i

Reactor Cell#	Q=Oxygen uptake (moles $O_2 \times 10^{-7}$)	τ_c (min)	4FQ/i (min)
RC3	.45	13.5	5.8
RC2	2.3	22.5	29.6
RC4	2.5	25	32.2
RC5	20	>100	257

Table 7

Gas phase composition effect on the relaxation time constant τ_o for i = 100 μA

Reactor cell#	Q moles O_2	P_{O_2}/P_{ET}	V_{max} (mV)	$\Delta r_1/r_{10}$	$\Delta r_2/r_{20}$	τ_o (min)
RC8	$5.2 \cdot 10^{-7}$	17.5	300	.64	.35	150
RC8	$5.2 \cdot 10^{-7}$	12.1	250	.27	.17	75
RC8	$5.2 \cdot 10^{-7}$	7.9	180	.15	.09	35
RC10	$10 \cdot 10^{-7}$	6.9	60	.02	.015	20
RC10	$10 \cdot 10^{-7}$	20.5	160	.16	.085	130

creasing the imposed current in excess of 100 A does not produce any additional increase in r_1 and r_2. This is shown in Fig.40, where the steady-state increases Δr_1 and Δr_2 in the rates of ethylene epoxidation and combustion are plotted vs. imposed current. Since the increase in r_1 is considerably higher than that in r_2, the selectivity increases. The bottom line in Fig.40 corresponds to the ratio of the rate of oxygen pumping to the catalyst over the intrinsic rate of oxygen consumption, taking into account that the intrinsic selectivity is of order 0.5. If the specific rate on the catalyst were no changing due to oxygen pumping then $\Delta r_1/r_{10}$ and $\Delta r_2/r_{20}$ would collapse into the bottom line $G_{O_2}/(r_{10}/2 + 3r_{20})$. Because Δr_1 and Δr_2 doe not increase with current for i > 100 μA, it be comes clear why Δr_1 and Δr_2 are only 7 times larger than G_{O_2} for i = 800 μA (Fig.31).

C4.e. Catalyst-Electrode Surface Area Effects

At constant temperature, gas phase composition and current, therefore constant overvoltage, the relative increase in the reaction rates $\Delta r_i/r_{io}$ is inversely proportional to the electrode surface area. This is a consequence of equation [C4.4] and is shown in figure 41 for five different reactors. Thus in order to maximize the relative increase one should minimize the electrode surface area, i.e. minimize the porous silver film thickness without causing a major decrease in its conductivity. A decrease in the electrode surface area also causes a moderate decrease in the relaxation time constant τ_c. This is shown in figure 42 which contains data from 5 reactors obtained at $P_{O_2}/P_{ET} \simeq 7$ and T = 400°C and shows that $1/\tau_o$ is a

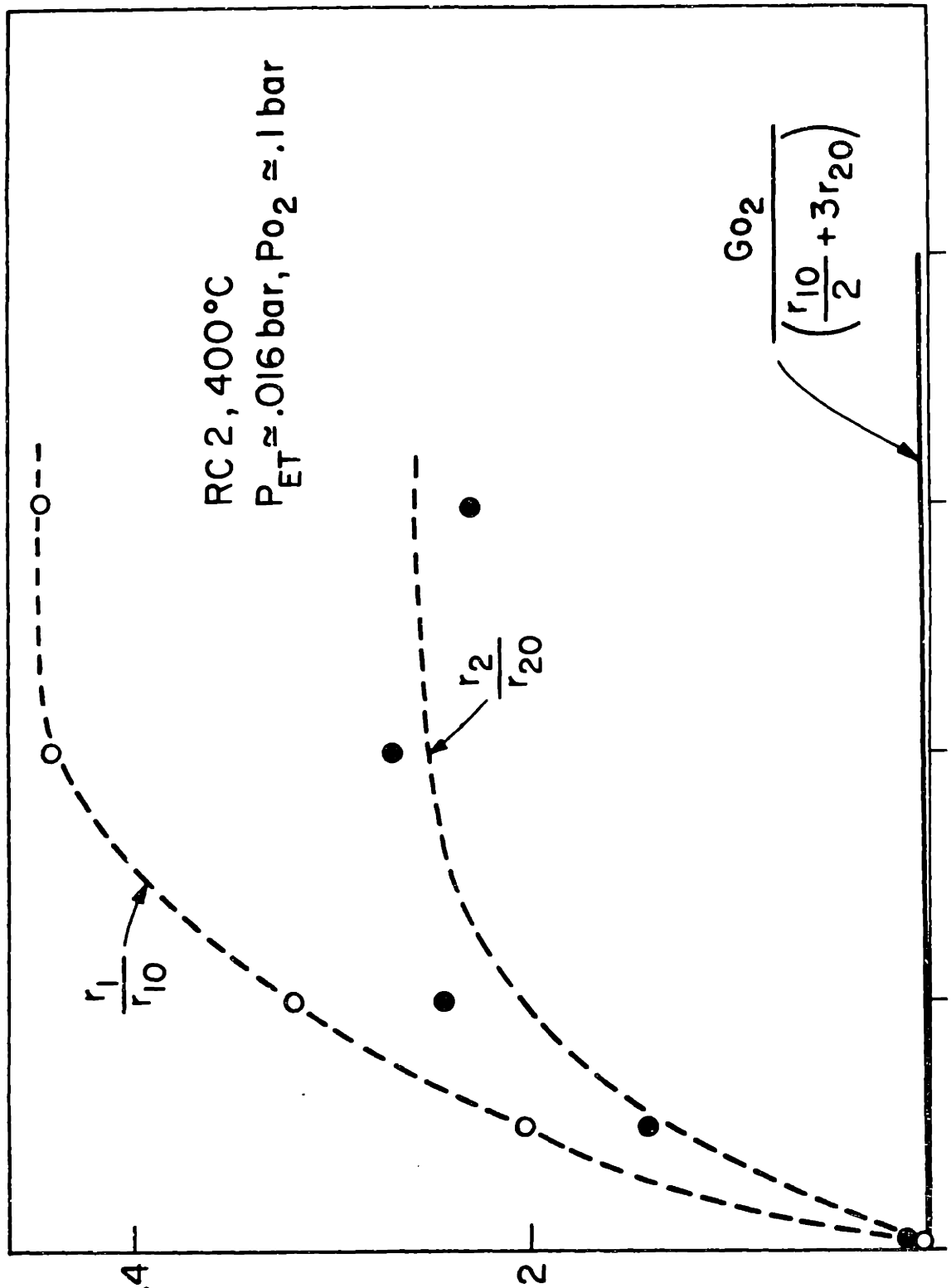

Figure 40: Effect of current on the steady state increase in the rate of ethylene epoxidation and combustion. Comparison with rate of oxygen pumping to the catalyst. Intrinsic (i=0) selectivity ~.5.

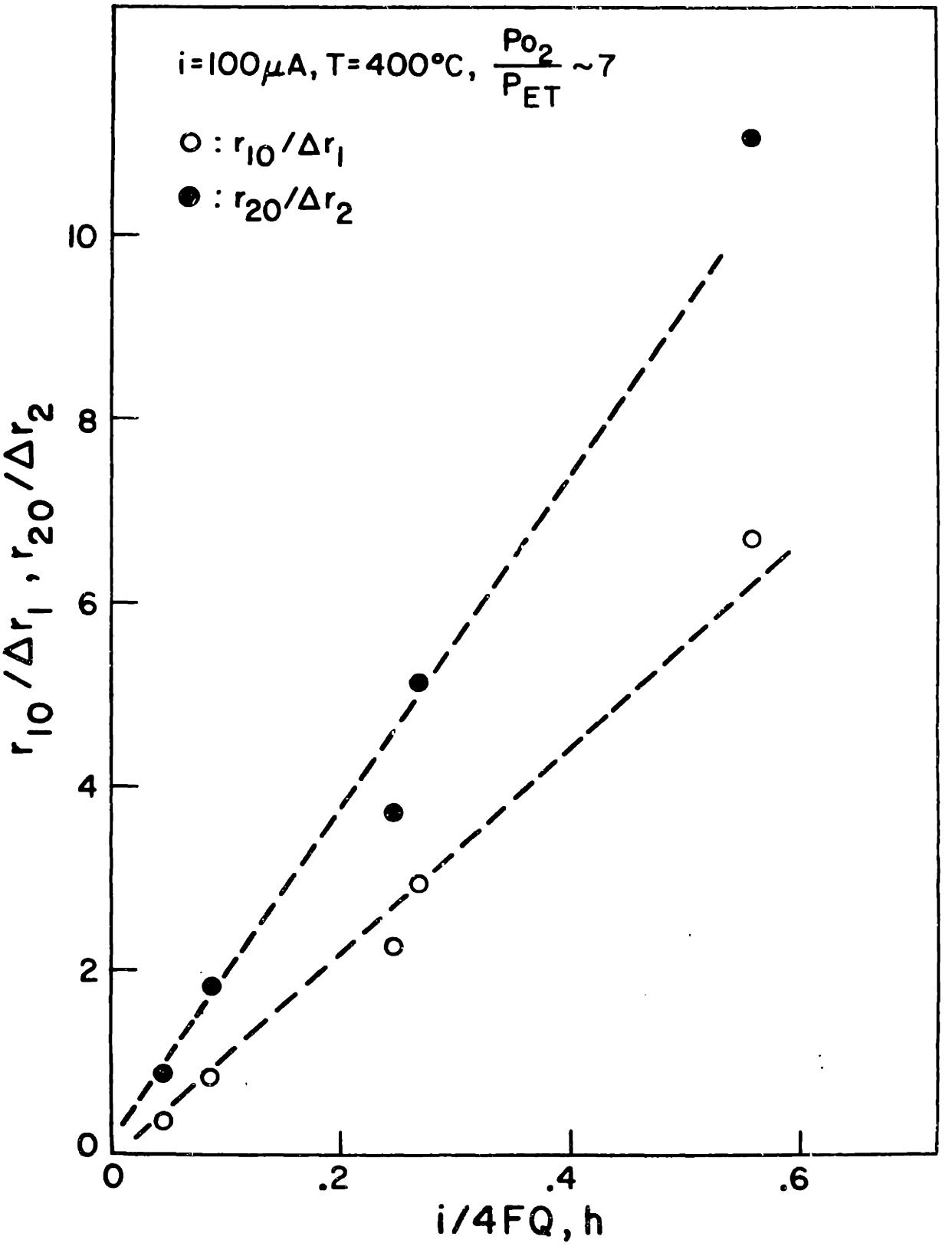

Figure 41: Effect of silver catalyst-electrode surface area Q on the relative steady state increase in the rates of epoxidation r_1 and deep oxidation r_2

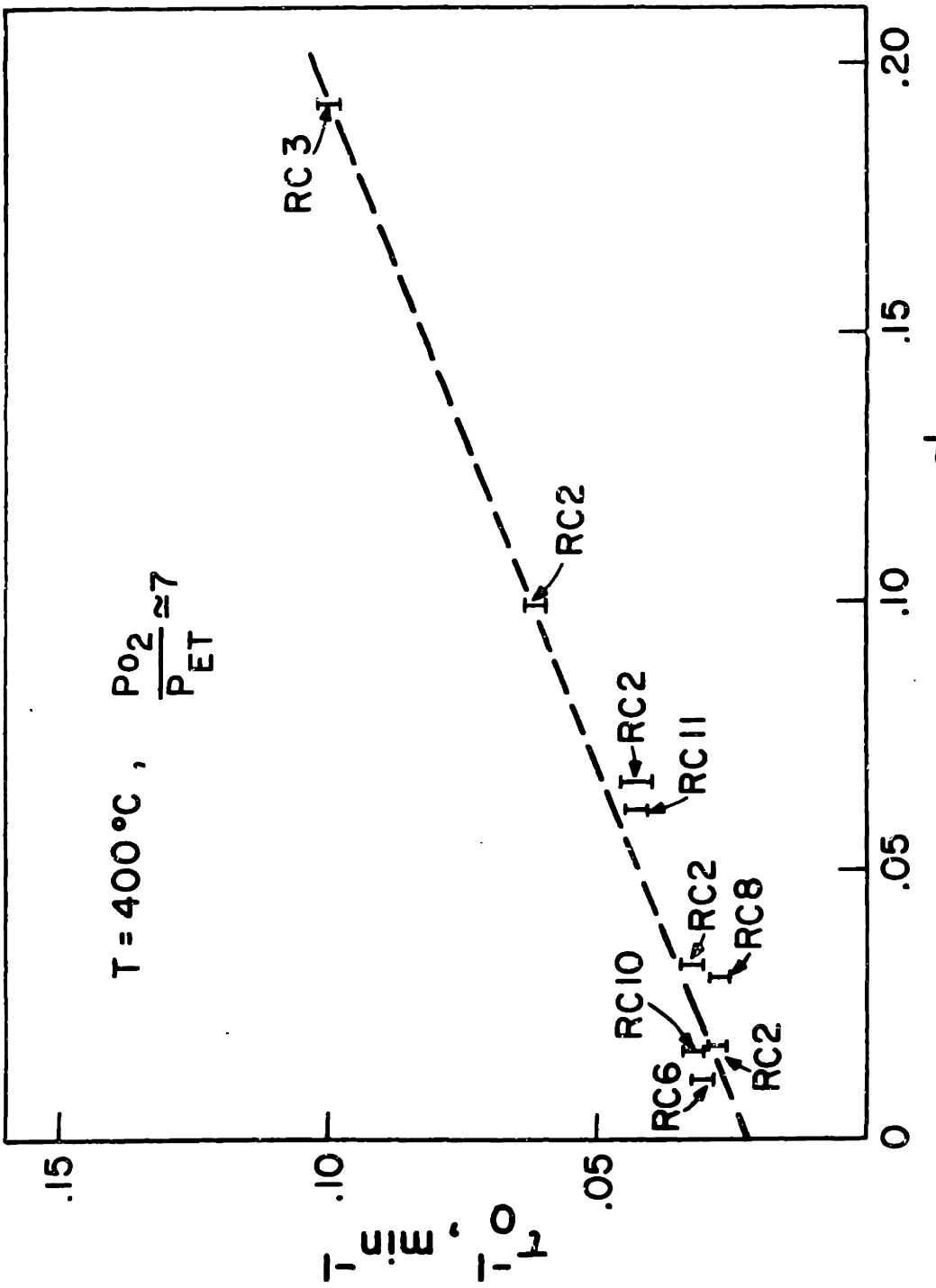

Figure 44: Effect of silver catalyst-electrode surface area Q on the cell relaxation time constant.

linear increasing function of i/4FQ. An explanation for these observations is given in the discussion section.

Figure 43 demonstrates a problem frequently encountered during the oxygen pumping experiments. The galvanostatic transient was obtained with reactor RC9 which had the lowest electrode surface area Q(Table), therefore exhibited the largest relative effect $\Delta r_i/r_{io}$, i.e. a threefold increase in ethylene oxide yield and a 210% increase in CO_2 production with a corresponding 20% increasing in selectivity. As shown on the figure the constant current i = 100 μA was applied at t=o. At t=40 min and long before the reactor would reach steady state the cell resistance suddenly dropped from a few KΩ to 1-2 Ohms indicating electrolysis of the zirconia eletrolyte and metallic zirconium formation. This is possible since the total cell voltage ($\Delta V+iR_c$) at t=40 min had reached approximately 2.5 V. As shown on the figure subsequently to the electrolyte breakdown both r_1 and r_2 slowly return towards their intrinsic values r_{10} and r_{20} since electronic rather than ionic conduction is now occuring across the cell. The cell cannot function as an oxygen concentration cell anymore since the electrolyte has been destroyed; the open circuit emf E always remains equal to zero regardless of the reactor gas composition. It was thus concluded that total voltages in excess of 2.5 V should not be applied to the cell at these relatively low temperatures.

C4.f. Temperature effects

At constant current and gas composition, temperature has an interesting effect on the steady state rate increases Δr_1

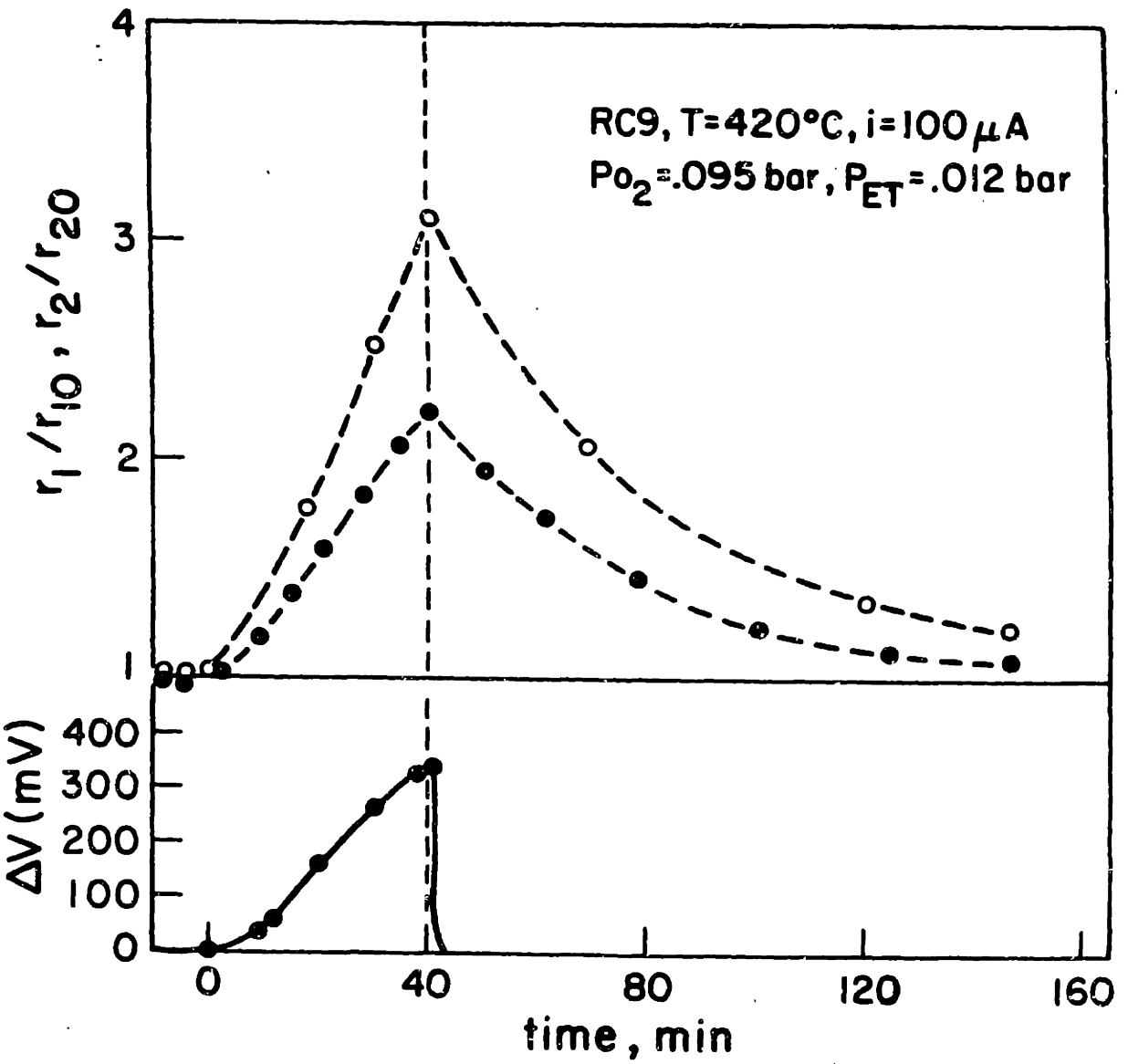

Figure 43: Transient galvanostatic response of the rates of ethylene oxidation r_1 (O) and deep oxidation r_2 (●) and of the cell overvoltage ΔV for reactor RC9. Electrolyte breakdown occured at t = 40 min.

and Δr_2 (Fig.44). At temperatures below 350°C both Δr_1 and Δr_2 increase rapidly with an activation energy E*=33±3 Kcal/mole. However at temperatures above 350°C Δr_1 and Δr_2 decrease with an apparent negative activation energy E** = 19 ± 2 Kcal/mole. The overvoltage ΔV decreased monotonically from 90 mV at 320°C to 3-5 mV at 400°C. It thus appears that the behavior of ΔV parallels the behavior of Δr_1 and Δr_2 at high T but not at temperatures below 350°C. A possible explanation is given in the discussion section. Figure 44 also shows that within the accuracy of the experimental data the ratio $\Delta r_1/\Delta r_2$ remains practically constant at 1.75±.25 which corresponds to .64±.04 selectivity on the oxide.

C4.g. Effect on Yield and Selectivity

Figures 45 and 46 show the transient effect of oxygen pumping on the selectivity and ethylene oxide yield of reactor cell 3. Here the intrinsic selectivity and yield (moles ethylene oxide produced per mole of ethylene fed to the reactor) are 0.52 and 2.2×10^{-2} respectively at $P_{ET} = 1.5 \times 10^{-2}$ bar and $P_{O_2} = 0.1$ bar.

The magnitude of Δr_1 and Δr_2 was found to increase with increasing P_{O_2}/P_{ET} ratio and to be only weakly dependent on the electrode surface area. Since the intrinsic rates r_{10} and r_{20} are proportional to the elctrode surface area the relative rate changes $\Delta r_1/r_{10}$, $\Delta r_2/r_{20}$ as well as the change in selectivity become more pronounced when the catalyst electrode has small surface area, e.g., reactor cell 3 (Table 5 and Figs. 45 and 46).

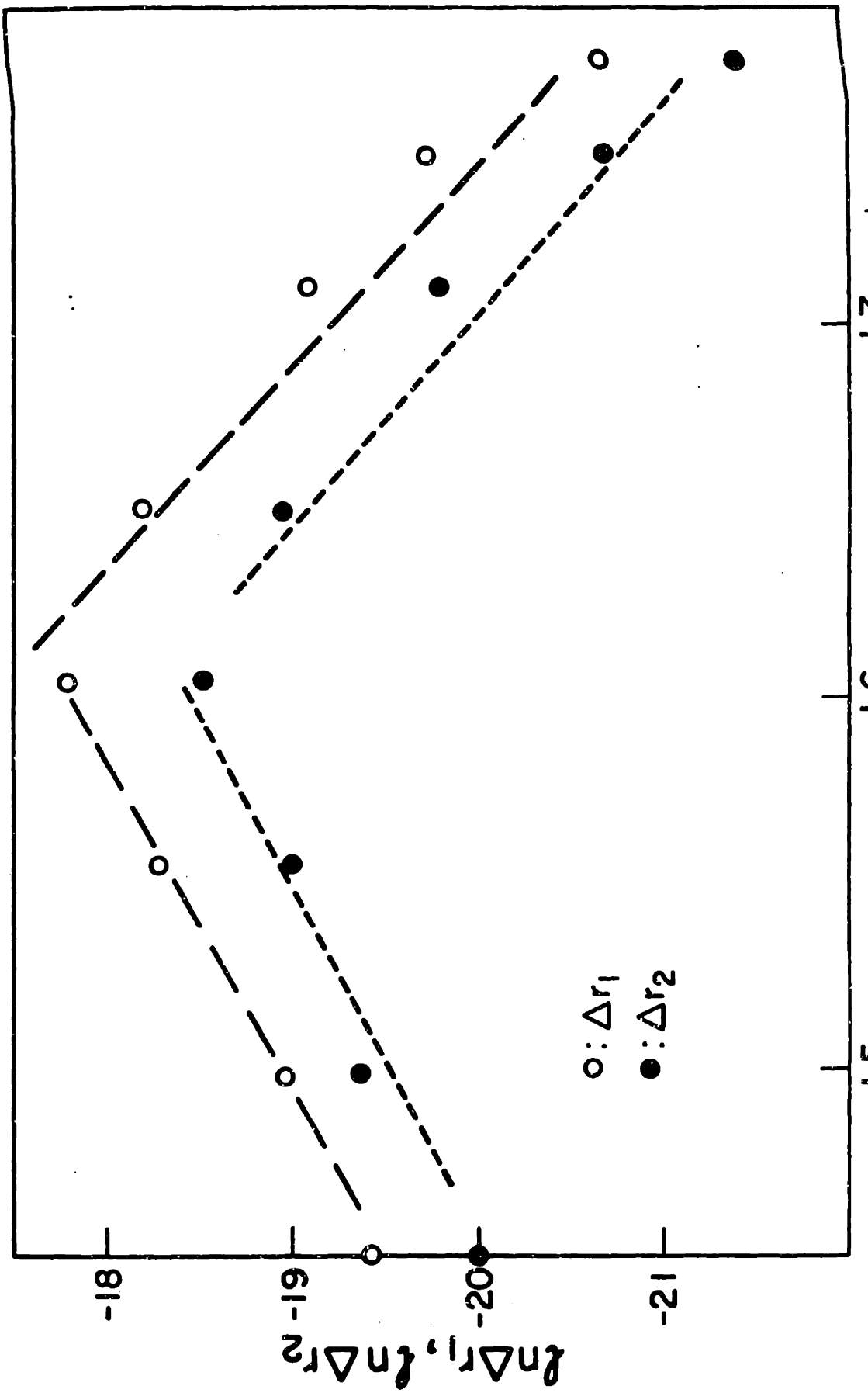

Figure 44: Temperature effect on the steady state rate increase in r_1 and r_2 at constant current i = 50 μA and gas composition (P_{O_2} = .10 bar, P_{H_2} = .015 bar)

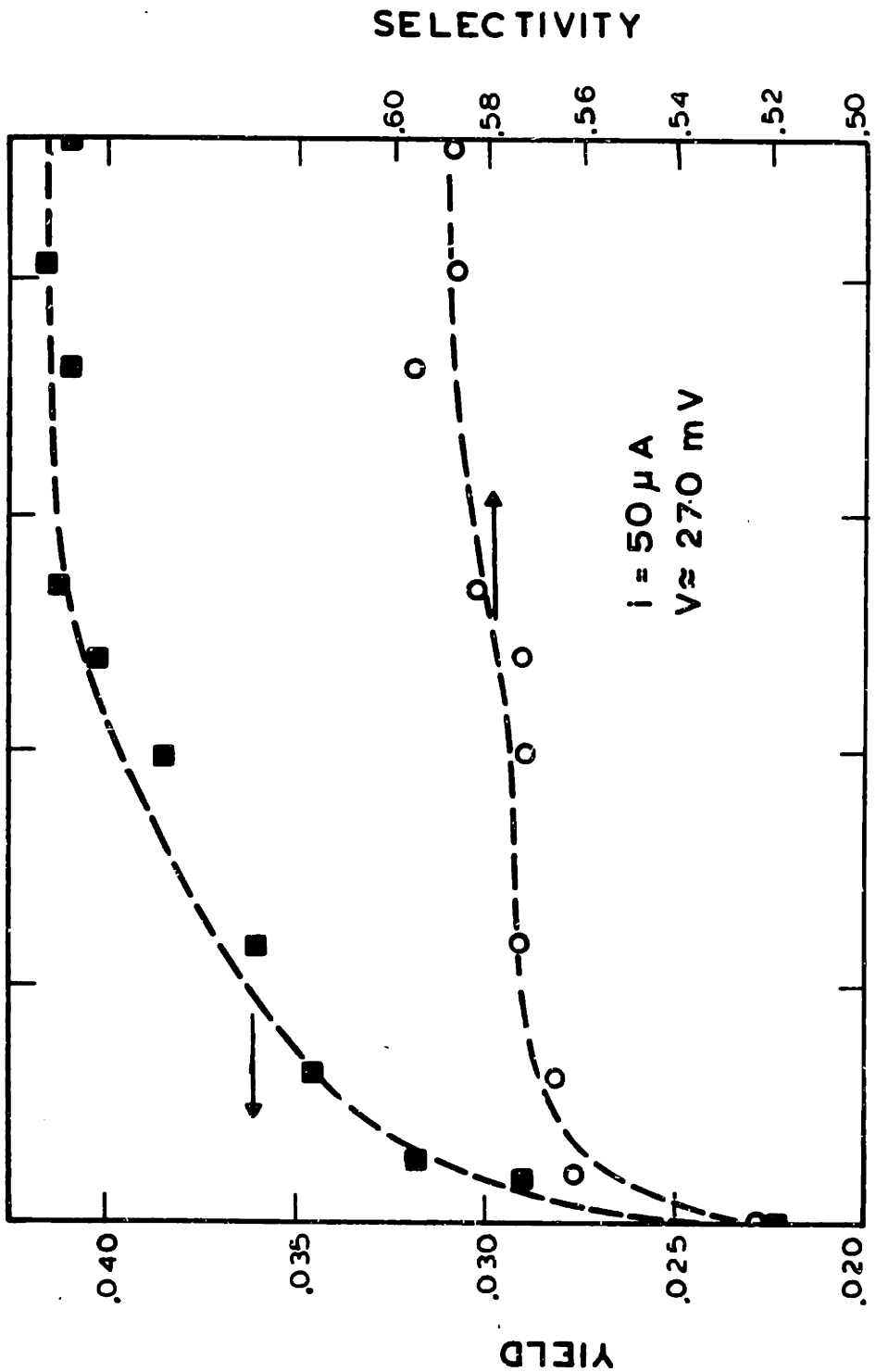

Figure 45: Transient effect of oxygen pumping to the catalyst on selectivity and yield of ethylene oxide (reactor RC2). Current applied at t = 0. Temperature: 400°C.

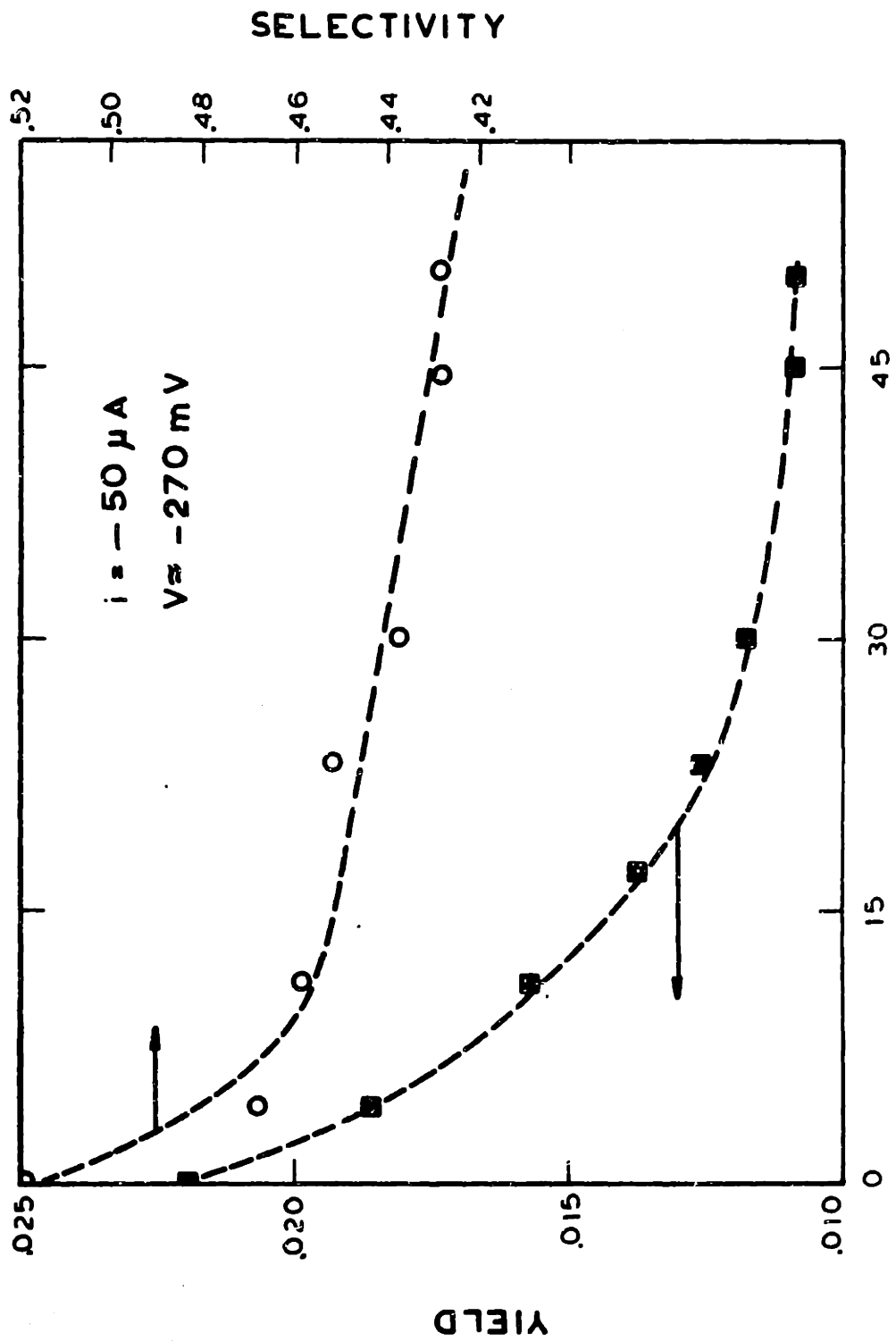

Figure 46: Transient effect of electrochemical oxygen removal from the catalyst on selectivity and yield on selectivity and yield of ethylene oxide

Oxygen pumping to the catalyst (Fig.45) causes the selectivity to increase to 0.59 while the yield almost doubles. Oyxgen pumping from the catalyst (Fig.46) reduces the selectivity to 0.42 and the yield to 1.1×10^{-2}. Thus the selectivity changes from 0.42 to 0.59 and the yield from 1.1×10^{-2} to 4.4×10^{-2} by simply applying a current of ± 50 μA to the cell.

C4.h. Discussion of results

The nature of the silver catalyst is clearly altered significantly during electrochemical oxygen pumping. The increase or decrease in the rates of ethylene epoxidation and combustion is more than two orders of magnitude higher than the rate of oxygen transport through the electrolyte. The selectivity also changes considerably. It can be easily shown that the electrolyte temperature cannot rise locally more than 2 K at most, due to I^2R heat generated during oxygen pumping. This was also shown by measuring the temperature of the electrolyte at a distance of 1 mm from the two electrodes and observing no measurable temperature rise during pumping. The absence of local catalyst heating due to oxygen pumping is also demonstrated by the fact that upon reversing the direction of pumping both r_1 and r_2 decrease (Fig.30).

Internal gas phase diffusional limitation inside the porous silver film are totally absent under the conditions of these experiments (C1.b). External concentration gradients have also been shown to be negligible (C1.b). Thus it can be safely concluded that it is the intrinsic properties of the

silver catalyst that change during electrochemical oxygen pumping.

When oxygen is pumped to the catalyst the thermodynamic activity of oxygen on the silver catalyst electrode increases considerably because of the external voltage applied. It thus becomes possible to at least partly oxidize the silver catalyst electrode. The experimentally observed relaxation time constants of the system show conclusively that this process must involve surface rather than bulk oxidation of the silver crystallites. The polycrystalline Ag films used could adsorb typically $Q = 2 \times 10^{-7}$ moles O_2. Typical currents employed in the present study were of order 100 μA corresponding to 2.6×10^{-10} moles O_2/s transported through the electrolyte. Thus the time required to fully cover the silver surface with surface oxide is of order 12 min in good agreement with the experimental relexation time (Table 6).

If, on the other hand, oxygen pumping caused bulk oxidation of the silver catalyst this would require approximately 2×10^{-4} moles O_2. With currents of order 100 μA this would correspond to time constants of about 50 h. It therefore follows that the observed phenomenon is due to surface oxidation of the silver crystallites. The phenomenon may be related to that observed during anodic oxidation of ethylene on a silver electrode in a low-temperature aqueous solution electrochemical cell (75) despite the significant differences in temperature and electrolyte material.

One can only speculate about the nature of the surface silver oxide formed during oxygen pumping to the catalyst and

about its relation to the various forms of chemisorbed oxygen found on silver (10). Infrared spectroscopic studies of the catalyst during pumping should prove useful for elucidating the nature of the surface specie which is reponsible for the observed phenomenon. It seems however that this chemisorbed oxygen species or surface oxide preexists on silver before pumping. Otherwise it is difficult to explain the dramatic decrease in r_1 and r_2 upon pumping oxygen away from the catalyst (Figs. 31 and 46).

Furthermore, the observation that the transient rate change behavior parallels the transient overvoltage behavior (Figures 33,34 and equations C4.3, C4.5 and C4.6) proves undoubtedly that the increase or decrease in the surface concentration of an adsorbed oxygen species or surface silver oxide. There is previous evidence in the literature for the existence of surface silver oxides including the work of Seo and Sato (29) who observed a continuous exoelectron emission from silver catalysts during ethylene epoxidation and explained their results in terms of formation of surface silver oxide Ag_2O with molecular oxygen ion O_2^- adsorbed on it (29). This picture seems to be in excellent agreemtn with the present results, i.e. with equation [C4.5]

$$r_i = k_{io} \cdot \alpha_i \cdot V \cdot P_{O_2}$$

if the change in the amount of surface oxide is proportional to ΔV and the coverage of molecular oxygen adsorbed on the

oxide is proportional to P_{O_2}, or at least if the rates of epoxidation and combustion on the silver oxide are first order in oxygen.

Equations [C4.3],[C4.5] and [C4.6] which describes the dependence of Δr_i on the overvoltage are extremely simple but deserve some special attention. They all indicate that Δr_i is proportional to ΔV but independent of the surface area of silver electrode. This is why the relative increase in the rates $\Delta r_i/r_{io}$ is highest for reactors with small surface area (Fig.43) and becomes insignificant for reactors with large surface area. It thus appears that although ΔV is an intensive variable it is nevertheless a measure of the change $S\cdot\Delta c$ in the mole number of silver oxide and not of the concentration change Δc. This is because all the reactors used had the same electrolyte area $A = 2cm^2$ as explained in detail below: Neglecting the double layer capacitance of the electrode electrolyte interface the constant current i imposed during the transient can be split in two parts (74):

$$i = C_{ad}\,\frac{d(\Delta V)}{dt} + i_{CTR} \qquad [C4.7]$$

where i_{CTR} is the current corresponding to the charge transfer reactions, i.e.

$$O^{2-} + C_2H_4 \rightarrow \text{Products} + 2e^- \qquad [C4.8]$$

$$O^{2-} \rightarrow 1/2\ O_2(g) + 2e^- \qquad [C4.9]$$

and C_{ad} is the adsorption pseudo capacitance of the oxide which by definition equals (74):

$$C_{ad} = \frac{dq}{dV} = \lambda\cdot F\cdot\frac{d(Sc)}{V} \qquad [C4.10]$$

where q is the charge stored in the oxide and is a constant. If one assumes that Sc varies linearly with V, i.e. that the oxide pseudo capacitance is constant one obtains

$$C_{ad} = \lambda \cdot F \frac{\Delta(Sc)}{\Delta V} \qquad [C4.11]$$

The capaciatance C_{ad} depends on the gas-electrode-electrolyte interline "area" S´ but not on the total electrode surface area S. If the porosity of all the elctrode catalysts used is the same, which is a reasonable assumption since they were all prepared by the same calcination procedure, it follows that the interline "area" S´is proportional to the flat electrolyte surface area A, i.e. the constant λ equals $\lambda_o A$, where λ_o is another constant which does not depend on any macroscopic dimension.

$$C_{ad} = \lambda_o \cdot A \cdot F \cdot \frac{\Delta(Sc)}{\Delta V} \qquad [C4.12]$$

Since all reactors used in the present study had the same electrolyte surface area A, it then becomes clear that they all had the same adsorption pseudo capcitance C_{ad}, therefore ΔV is proportional to $\Delta(Sc)$ as previously stated.

Although the exact nature of the surface silver-oxygen species or surface oxide formed and destroyed during electrochemical O^{2-} pumping to and from the silver catalyst respectively is not known, it was found that a simple kinetic model could explain almost all the macroscopic features of the oxygen pumping effect in a semi-quantitative manner. This model represents a first attempt to understand the new phenomenon and could be refined and/or modified as more information becomes available about the silver-oxygen species created and

destroyed during oxygen pumping.

The model is based on the hypothesis that oxygen pumping to the catalyst causes an increase in the surface concentration of active silver oxide. The activity and selectivity on the surface of this silver oxide, denoted by AgO_2^*, is assumed higher than that on reduced silver. In order to account for the experimentally observed increase in the relaxation time constant with increasing P_{O_2}/P_{ET} ratio it becomes necessary to postulate that AgO_2^* forms on sites adjacent to chemisorbed oxygen. We first consider a mass balance for O_2^*:

$$S\cdot\theta_{O_2}\cdot\frac{dc}{dt} = \frac{i}{4F}\left(1-\frac{c}{c_M}\right) + K_1\cdot S\cdot\theta_{O_2}(c_M-c) - K_2\cdot S\cdot P_{ET}\cdot c, \quad [C4.13]$$

where $S(cm^2)$ is the surface area of the silver catalyst electrode, θ_{O_2} is the surface coverage of molecularly adsorbed oxygen on the reduced silver surface, c (moles O_2/cm^2) is the surface concentration of AgO_2^*, c_M is the saturation surface concentration of AgO_2^* corresponding to full coverage of sites available for oxide formation, and $K_2(s^{-1}cm^{-2})$ and $K_2(bar^{-1}\cdot s^{-1}\cdot cm^{-2})$ are specific rate constants for O_2^* formation and destruction from molecularly adsorbed oxygen and gaseous ethylene, respectively. The first term on the right side of Eq. [C4.13] corresponds to O_2^* formation due to electrochemical oxygen pumping. We assumed that no multiple layers of surface oxide can form.

It follows from [C4.13] that the steady-state concentration c of AgO_2^* is

$$\frac{c}{c_M} = \frac{(i/4FSc_M) + K_1\theta_{O_2}}{(i/4FSc_M) + K_1\theta_{O_2} + K_2\cdot P_{ET}} \quad [C4.14]$$

According to [C4.14], if no current is applied to the cell the oxide coverage c_O is given by

$$c_O/c_M = K_1\theta_{O_2}/(K_1\theta_{O_2} + K_2P_{ET}). \qquad [C4.15]$$

Therefore the steady-state increase $\Delta c = c - c_O$ in the concentration of AgO_2* is

$$\Delta c/c_M = (i/4FSc_M)\cdot K_2P_{ET}/\{[(i/4FSc_M) +$$

$$+ K_1\theta_{O_2} + K_2P_{ET}][K_1\theta_{O_2} + K_2P_{ET}] . \qquad [C4.15']$$

At temperatures above 350°C the rates of ethylene epoxidation and combustion on polycrystalline silver have been found to be first order in ethylene and near zero order in oxygen (Section C3)

$$r_{jo} = k_{jo}\cdot S\cdot P_{ET}. \qquad [C4.16]$$

In view of Eq. [C4.15'] and in order to account for the observed increase in Δr_j with increasing P_{O_2}/P_{ET} ratio one must assume that the rates of epoxidation (j = 1) and combustion (j = 2) on the silver oxide AgO_2* are first order in gaseous oxygen

$$\Delta r_j = k_j\cdot S\cdot P_{O_2}\cdot \Delta c, \qquad [C4.17]$$

where k_j ($s^{-1}bar^{-1}$) are rate constants for ethylene epoxidation (j = 1) and combustion (j = 2) on the oxide. Combining with Eq. [C4.15'] one obtains

$$\Delta r_j = (i/4F)\cdot k_j \cdot K_2 \cdot P_{O_2} \cdot P_{ET} / \{[(i/4Fsc_M) +$$

$$+ K_1\theta_{O_2} + K_2P_{ET}][K_1\theta_{O_2} + K_2P_{ET}]\} \qquad [C4.18]$$

and according to [C4.17] one obtains

$$\Delta r_j/r_{jo} = \frac{k_j \cdot K_2 \cdot (i/4F) \cdot P_{O_2}}{k_{jo} \cdot S} \Big/$$

$$\{[(i/4FSc_M) + K_1\theta_{O_2} + K_2P_{ET}][K_1\theta_{O_2} + K_2P_{ET}] \; . \qquad [C4\ 19]$$

With $\theta_{O_2} \approx 1$ the steady-state [C4.19] expalins the steady-state observations and it also explains two additional observations; i.e., that Δr_j vanishes when $P_{O_2} = 0$ an that the relative rate increases $\delta r_j/r_{jo}$ is large for reactors with small electrode surface area S.

The experimental relations [C4.3] through [C4.6] which express the dependence of Δr_i and $\Delta r_i/r_{io}$ on ΔV and gas phase composition can now be explained in a quantitative manner, taking into account that the change in the moles of silver oxide (Sc) caused by electrochemical oxygen pumping is directly measurable and proportional to the overvoltage ΔV. Assuming that the changes Δr_i in the rates of ethylene epoxidation r_1 and combustion r_2 are proportional to the change in the moles of AgO_2^* and that both reactions on the AgO_2^* surface area are first order in oxygen one obtains

$$\Delta r_i = k_i \cdot P_{O_2} \cdot \Delta(Sc) \qquad [C4.20]$$

Using equation [C4.12] one obtains

$$\Delta r_i = k_i \cdot \lambda_o \cdot A \cdot F \cdot (\Delta V) \cdot P_{O_2} \qquad [C4.21]$$

which coincides with the experimental equation [C4.5] with $k_{io}\alpha_i = k_i \cdot \lambda_o \cdot A \cdot F$. It should be noted that according to [C4.21] Δr_i is proportional to the electrolyte surface area A but does not depend on the electrode surface area. The experimental relation

$$\Delta r_i \propto \Delta V \qquad [C4.1]$$

valid for constant gas phase composition is obviously a special case of [C4.21]. Finally to explain the dependence of $\Delta r_i / r_{io}$ on ΔV and gas phase composition one must assume that oxide forms on silver sties which are inactive for reaction before the oxide forms and take into account that at temperatures above 350°C and under open-circuit conditions both r_{10} and r_{20} are first order in ethylene and zero order in oxygen.

$$r_{io} = k_{io} \cdot Q \cdot P_{ET}$$

This last equation is not inconsistent with the hypothesis that the rates on AgO_2^* are first order in oxygen to the extent that the amount of AgO_2^* is small under open circuit conditions.

Combining with equation [C4.21] one obtains the experimental relation

$$\frac{\Delta r_i}{r_{io}} \cdot Q \cdot \frac{P_{ET}}{P_O} = \alpha_i \Delta V \qquad [C4.3]$$

where

$$\alpha_i = \frac{k_i}{k_{io}} \cdot \lambda_o \cdot A \cdot F \qquad [C4.22]$$

According to eq. [C4.13] the relaxation time constant of the system $\tau_c = \tau_o$ is given by

$$\frac{1}{\tau_c} = \frac{4FSC_M}{i}\left(1 + \frac{1}{K_{O_2} P_{O_2}}\right) + K + \frac{K_2 P_{ET}}{K_{O_2} P_{O_2}}\left(1 + K_{O_2} P_{O_2}\right) \qquad [C4.23]$$

The above equation is in excellent agreement with figure

(42) which shows $1/\tau_c$ for 5 different reactors to be a linear increasing function of 4FQ/i with a positive intercept. One of the implications is that the amount of surface oxide at full coverage Sc_M is comparable to the reactive oxygen uptake Q of the catalyst. There are several ways to account for the observed maximum in Δr_i at constant gas composition and imposed current i (Fig.44). Although the behavior shown in the figure is quite reproducible, further epxerimental work is required to examine the effect of gas phase composition and i on the temperature dependence of r_i. One possible explanation for the observed maximum can be obtained by closer examination of equation [C4.7]. The charge transfer current i can be written as $i_{CTR,A} + i_{CTR,B}$ where the former term corresponds to the charge transfer reaction [C4.8] and the latter to the charge transfer reaction [C4.9]. Using the low field (74) one obtains

$$i_{CTR,A} = i_{O,A} \cdot F(\Delta V)RT \qquad [C4.24]$$

$$i_{CTR,B} = i_{O,B} \cdot F(\Delta V)/RT \qquad [C4.25]$$

The exchange current densities $i_{O,A}$ and $i_{O,B}$ are temperature dependent and can be expressed as

$$i_{O,A} = \vec{K}_{O,A} \exp(- \frac{\Delta G_A^{\ddagger}}{RT}) \qquad [C4.26]$$

$$i_{O,B} = \vec{K}_{O,B} \exp(- \frac{\Delta G_B^{\ddagger}}{RT}) \qquad [C4.27]$$

where K_{OA}, $K_{O,B}$ are constants and $\Delta G_A^{\ddagger}$, $\Delta G_B^{\ddagger}$ are the standard Gibbs energies of formation of the activated complex for the

charge transfer reactions [C4.8] and [C4.9].

Thus equation [C4.7] can be written as:

$$C_{ad}\frac{d(\Delta V)}{dt} = i - \frac{F(\Delta V)}{RT}[\vec{k}_{O,A}\exp(-\frac{\Delta G_A^{\ddagger}}{RT}) + \vec{k}_{O,B}\exp(-\frac{\Delta G_B^{\ddagger}}{RT})] \quad [C4.28]$$

At steady state equation [C4.28] gives

$$(\Delta V) = \frac{iRT}{F\cdot\vec{k}_{O,A}\cdot\exp(-\frac{\Delta G_A^{\ddagger}}{RT})\cdot]1 - \frac{\vec{k}_{O,B}}{\vec{k}_{O,A}}\exp\,(-(\frac{G_B^{\ddagger}-\Delta G_A^{\ddagger}}{RT}))} \quad [C4.29]$$

If the activation energies for the epoxidation and combustion reactions on silver oxide equal E*, then the rate coefficients k_i in equation [C4.21] can be expressed as

$$k_i = k_i^o \exp\,(-E^*/RT) \quad [C4.30]$$

Combining equations [C4.21], [C4.29] and [C4.30] one obtains

$$\Delta r_i = \frac{k_i^o\cdot\lambda_o\cdot A\cdot P_{O_2}\cdot i\cdot RT\cdot\exp(\frac{-E^*+\Delta G_A^{\ddagger}}{RT})}{1 + \frac{\vec{k}_{O,B}}{\vec{k}_{O,A}}\exp\,(-\frac{(\Delta G_B^{\ddagger}\ \Delta G_A^{\ddagger}}{RT})} \quad [C4.31]$$

Equation [C4.31] predicts a maximum in r_i for a large number of combinations of E*, $\Delta G_A^{\ddagger}$, $\Delta G_B^{\ddagger}$. As an example the set E* = 43 Kcal/mol, $\Delta G_A^{\ddagger}$ = 10 Kcal/mol and $\Delta G_B^{\ddagger}$ = 62 Kcal/mole yields the correct experimental values for the phenomenological activation energies of Δr_i, i.e. +33 Kcal/mol at low T and =19 Kcal/mole at high T. It should be noticed however that these phenomenological activation energies must be gas phase composition dependent since the quantities $\vec{k}_{O,A}$, $\vec{k}_{O,B}$, $\Delta G_A^{\ddagger}$, $\Delta G_B^{\ddagger}$ which appear in equation [C4.31] will depend on the coverages of ethylene and oxygen at the gas-electrode-electrolyte three phase boundary.

C.5. The oxidation of Propylene oxide

Following the same procedure as in the case of ethylene oxidation the oxidation of propylene oxide to CO_2 and H_2O was studied first separately. Kinetic and potentiometric results of this study are given and discussed below.

C5.a. Potentiometric measurements

The low values of the open circuit emf during the reaction (-15mV-250 mV) show that in general $a_o^2 < P_O$. This implies that thermodynamic equilibrium is not established between gaseous oxygen and oxygen adsorbed on silver during reaction. The activity of oxygen was found to decrease as P_{PrO} increases by keeping the temperature and the pressure of oxygen constant. On the other hand a_o increases with increasing P_{O_2} and with increasing temperature.

Several functional forms were examined in order to describe the dependence of a_o on gas composition. It was found that the a_o measurements could be correlated in a satisfactory way by the expression

$$\frac{a_o}{P_{O_2}^{1/2} - a_o} = \frac{K}{P_{PrO}} + K' \qquad [C5.1]$$

This is shown in figure (47). In figure (48) lnK is plotted vs. temperature; K increases with temperature according to

$$K = 2.4 \cdot 10^3 \exp(-9600/T) \qquad [C5.2]$$

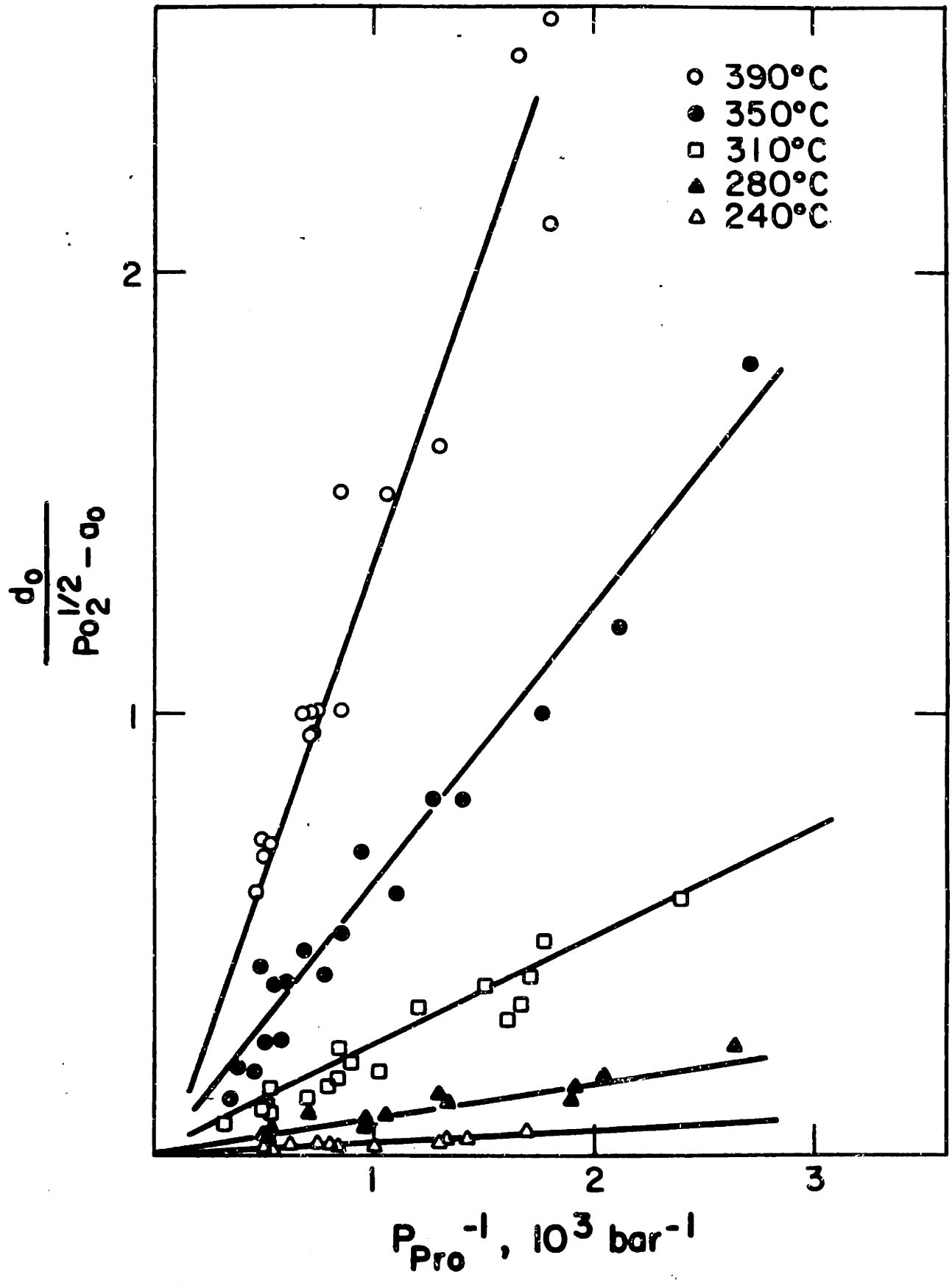

Figure 47: Surface oxygen activity dependence on gas phase composition

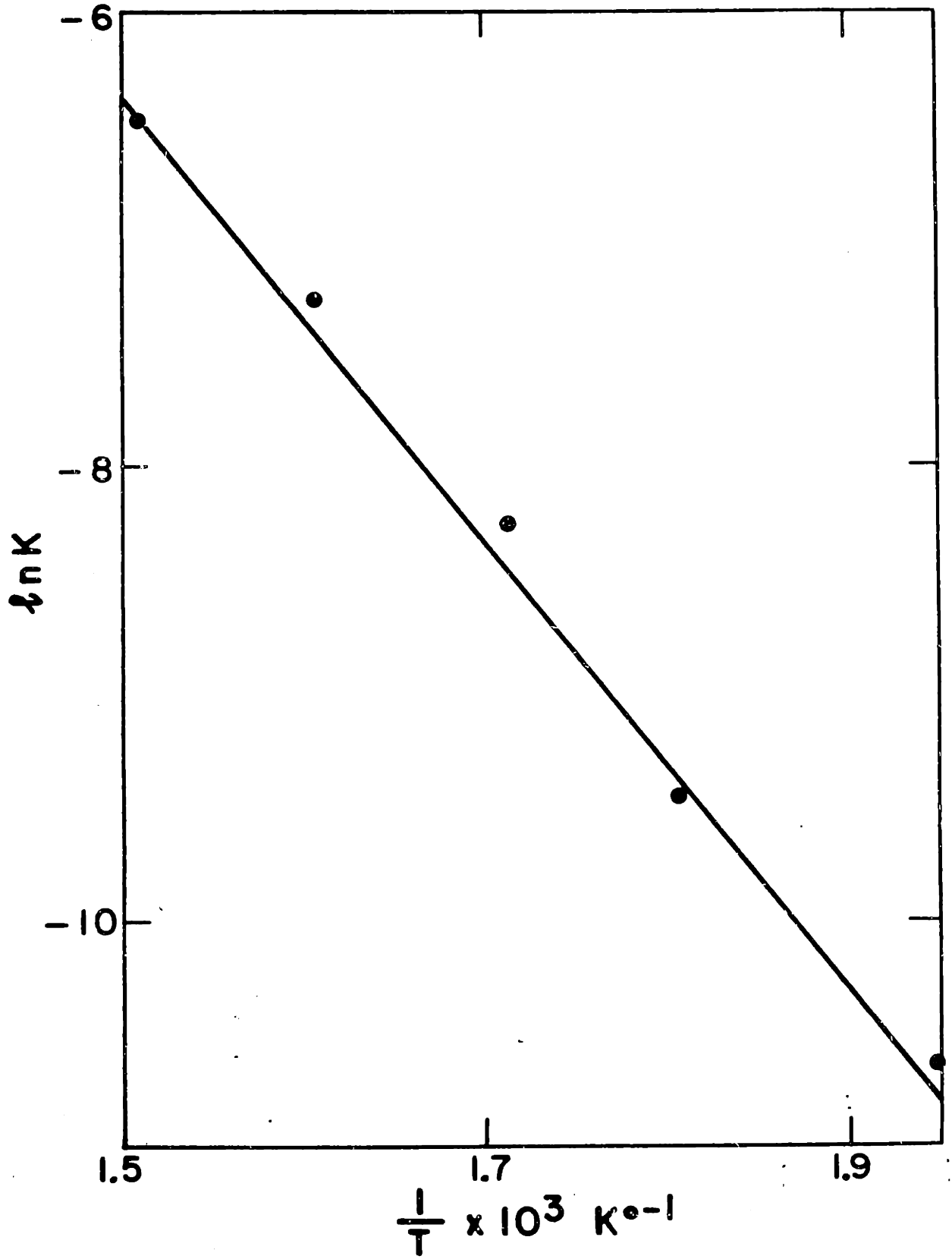

Figure 48: Temperature dependence of K

C5.b. Kinetic measurements

The kinetics were studied at temperatures between 240 and 390°C, propylene oxide partial pressures between $.4 \cdot 10^{-3}$ bar and $4.0 \cdot 10^{-3}$ bar and oxygen partial pressures between .02 bar and .2 bar.

The rate of the reaction was calculated from the equation

$$r = F' \left[X_{Pro(Reactants)} - X_{Pro(Products)}\right] \qquad [C5.3]$$

where F' is the total flowrate and X is the mole fraction of propylene oxide.

The rate is shown in figure (49) as a function of the partial pressure of oxygen in the gas phase, P_{O_2} for various temperatures examind. The rate is zero order in oxygen at all temperatures. In figure (50) the rate is shown as a function of the partial pressure of propylene oxide P_{Pro}. The rate is close to first order with respect to P_{Pro} at the highest temperature (390°C) but this simple first order dependence disappears at lower temperatures.

It was found that all the kinetic data could be expressed quite accurately by the rate expression

$$r = K_R \frac{K_{Pro} P_{Pro}}{1 + K_{Pro} P_{Pro}} \qquad [C5.4]$$

where r is given in moles/s and

$$K_R = 6.4 \quad \exp\left(-\frac{19{,}000}{RT}\right) \frac{\text{moles}}{S} \text{ and} \qquad [C5.5]$$

$$K_{Pro} = .010 \quad \exp\left(\frac{10{,}400}{RT}\right) \text{ bar}^{-1} \qquad [C5.6]$$

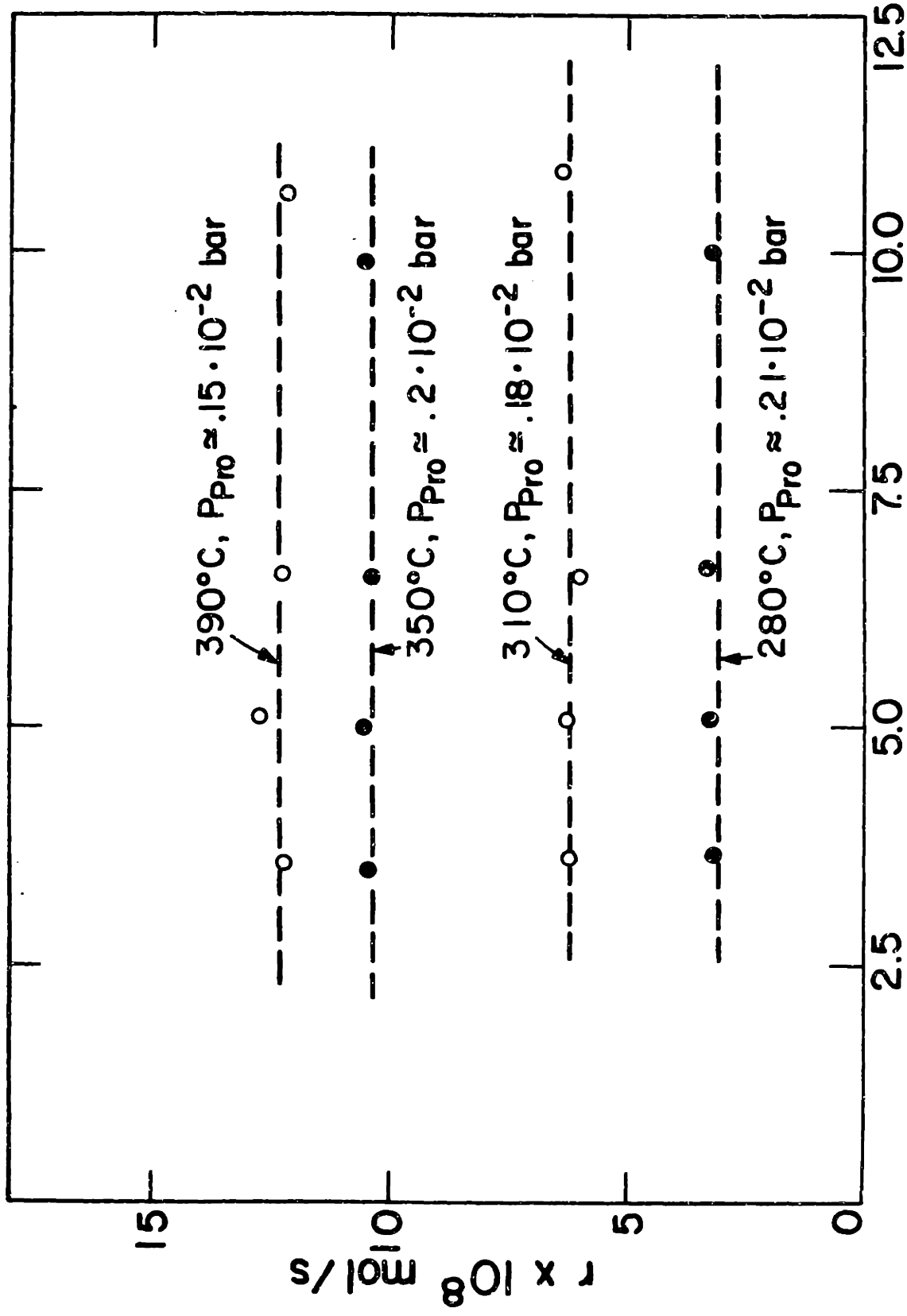

Figure 49: Oxidation rate of propylene oxide vs. P_{O_2}

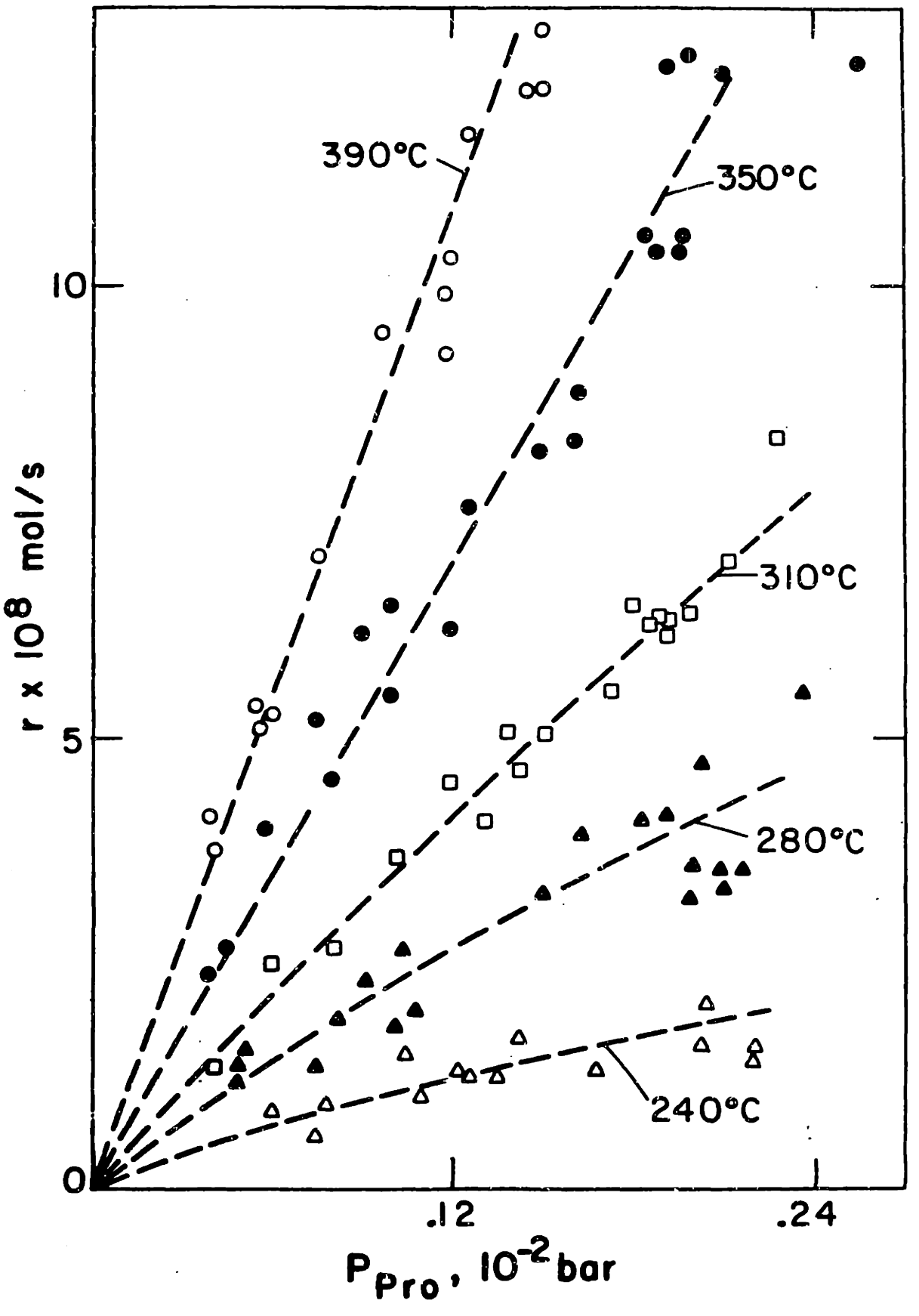

Figure 50: Oxidation rate vs. the partial pressure of propylene oxide

C5.c. Rate and oxygen activity oscillations

over a wide range of temperature, space velocity and gas composition the rate of CO_2 production as well as the surface oxygen activity exhibit oscillatory behavior (Fig.51). However since the amplitude of the rate oscillations is typically less than 15% of the steady state rate, eq. [C5.4] can be used as an estimate of the average rate of CO_2 formation in the oscillatory region as well.

The period and amplitude of the oscillations were found to depend on temperature, residence time as well as on gas composition. The oscillations were often quite complex. Typical periods were between 3 and 60 minutes. The rate of CO_2 production and the surface oxygen activity oscillate simultaneously, with increasing surface oxygen activity generally corresponding to increasing rate (figure 51). Typical amplitudes were 2-20 mV for the emf and up to $.5 \cdot 10^{-3}$ bar for the partial pressure of CO_2 in the effluent stream.

There are no specific temperature limits between which oscillations occur. Oscillatory phenomena were observed from 240°C, the lowest temperature studied, and over the entire range of temperatures examined. The effect of temperature at constant gas composition and residence time is shown in figure (52). In general as temperature increases both the period and the amplitude of the oscillations decrease.

The effect of the residence time on the frequency and amplitude of the oscillations is shown in Figure (53). By increasing the total molar flowrate at constant temperature

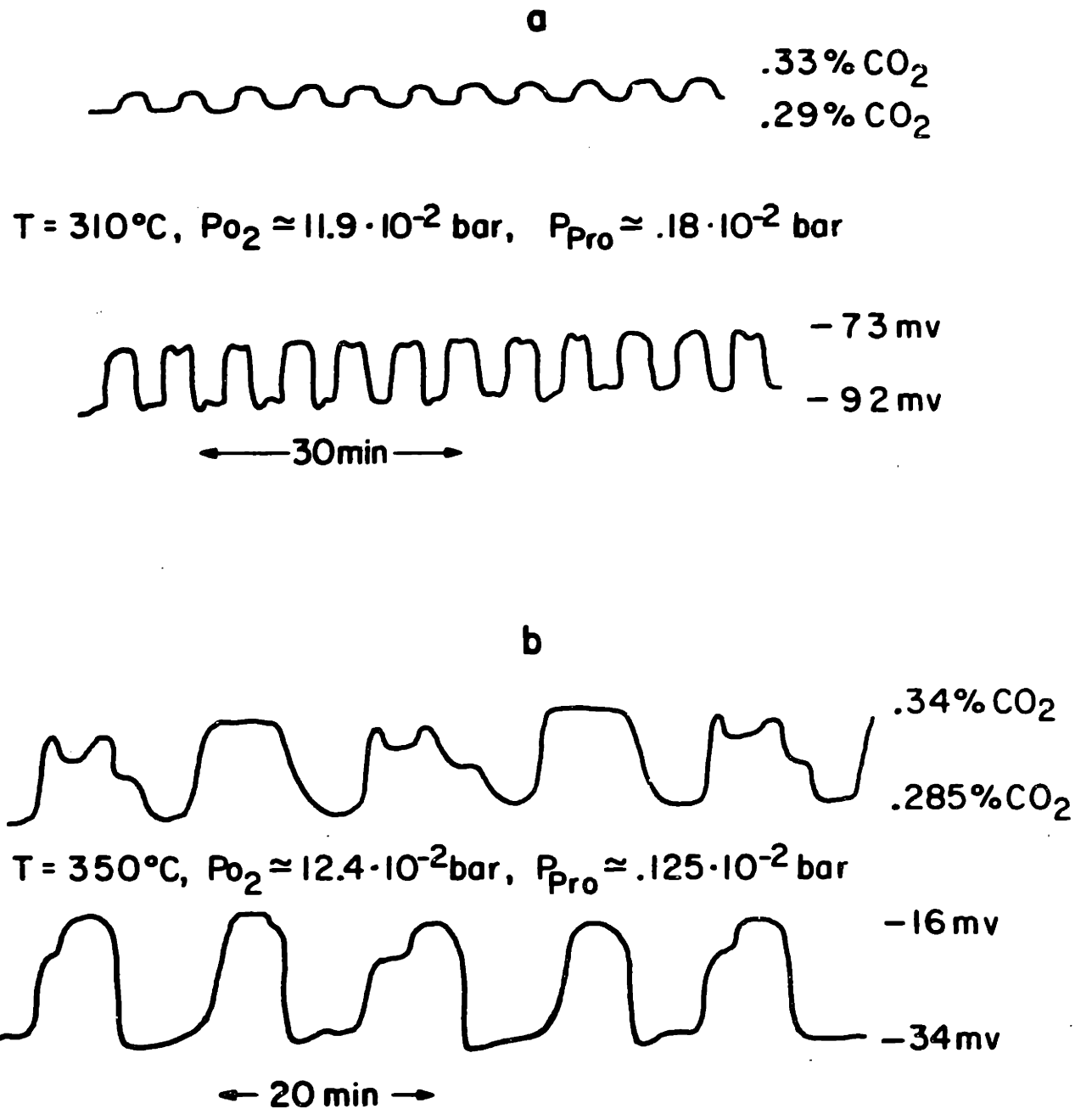

Figure 51 Typical rate and emf oscillations

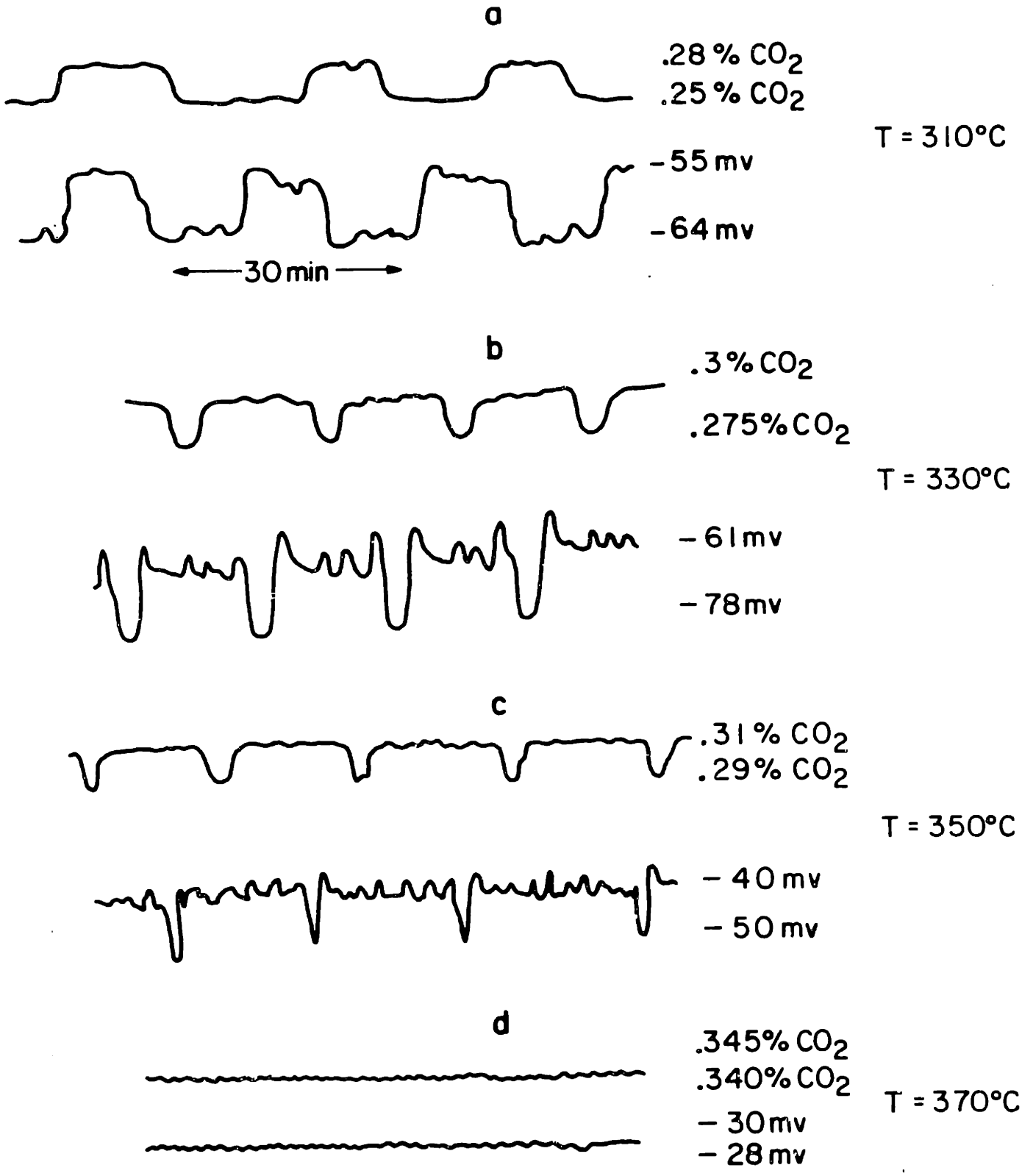

Figure 52 Temperature effect on rate and emf oscillations at constant flowrate and gas composition. There is no real phase lag as discussed in the text.

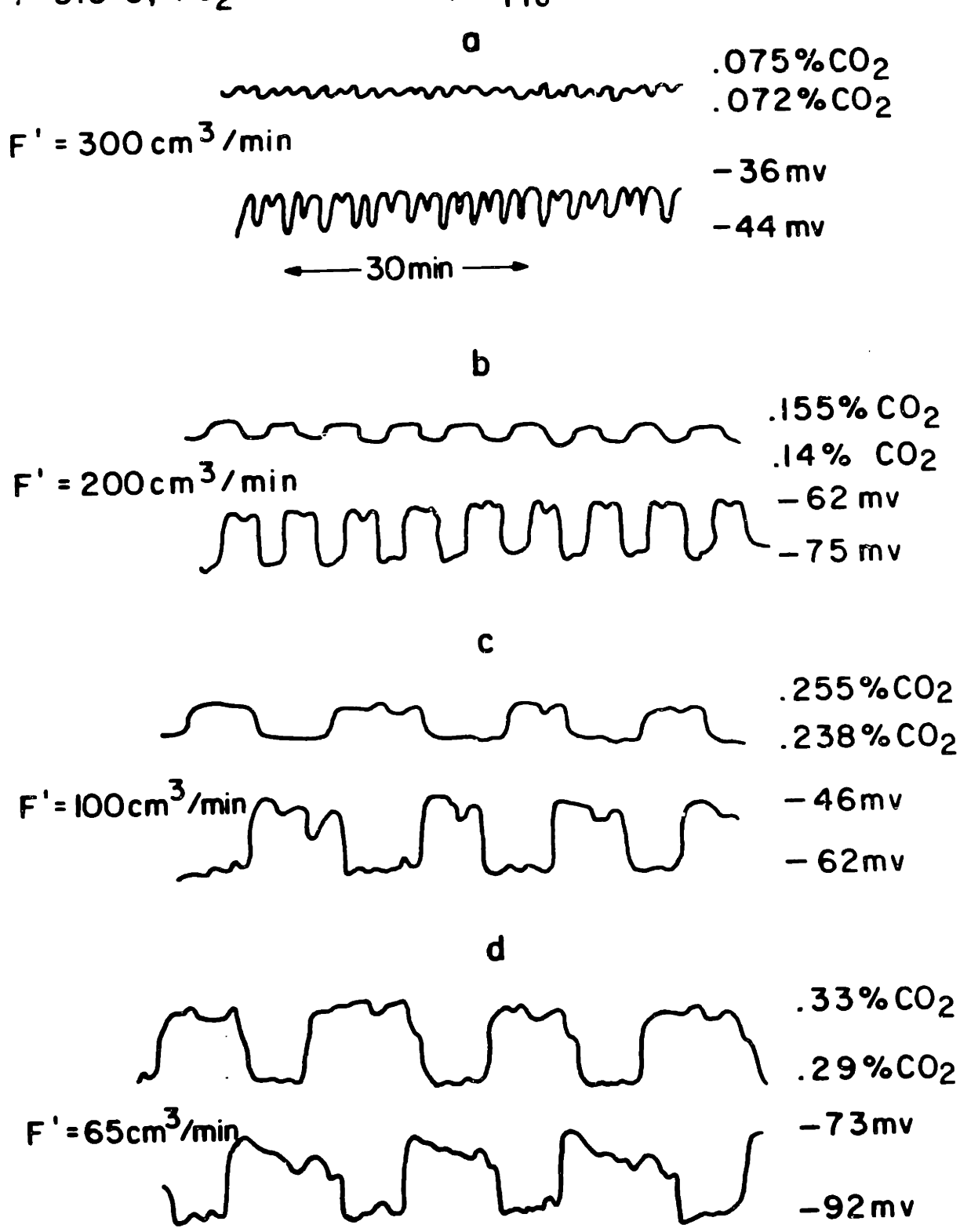

Figure 53 Effect of residence time at constant temperature and gas composition. There is no real phase lag as discussed in the text.

and gas composition, both the period and the amplitude of the oscillations decrease.

Table 8 shows the dependence of the period and amplitude of oscillations on the partial pressure of oxygen in the gas phase for constant temperature, P_{Pro} and residence time. The amplitude is expressed as % deviation from the average rate. The period decreases as P_{O_2} increases. No specific correlation was found between the period τ_c or the amplitude of the oscillations and the pressure of propylene oxide P_{Pro}. It was found however that for each temperature there is a specific range of $\frac{P_{Pro}}{P_{O_2}}$ within which oscillations occur. This is shown in fig. 54. Such a range was not found for the oxygen activity at any temperature.

The oscillations were isothermal. This was verified by attaching a thermocouple directly to the catalyst film and measuring a constant temperature within 1°C. This is expected since the heat released due to the reaction rate is negligible because of the very low partial pressures of propylene oxide employed in this study.

C5.d Discussion of results

The mechanism of the catalytic oxidation of propylene oxide can be now discussed on the basis of the reaction kinetics and the information provided by the solid electrolyte aided surface oxygen activity measurements. A satisfactory reaction mechanism should account not only for the kinetics (eq.[C5.4]) but also for the surface oxygen activity behavior (eq.[C5.1]). A reaction model explaining both kinetic and potentiometric observations in a semiquantitative manner is presented below.

Table 8

Effect of P_{O_2} on the period and amplitude of reaction rate oscillations

a) T = 350°C, F = 100 cm^3/min $P_{Pro} \simeq .00155$ bar

P_{O_2} (bar)	Period τ (min)	Amplitude (%)
.040	30	6.5
.055	10	3.1
.155	7.5	2.3

b) T = 350°C, F = 250 cm^3/min $P_{Pro} \simeq .002$ bar

P_{O_2} (bar)	Period τ (min)	Amplitude (%)
.031	17	3.2
.053	12	1.3
.112	8.5	.8

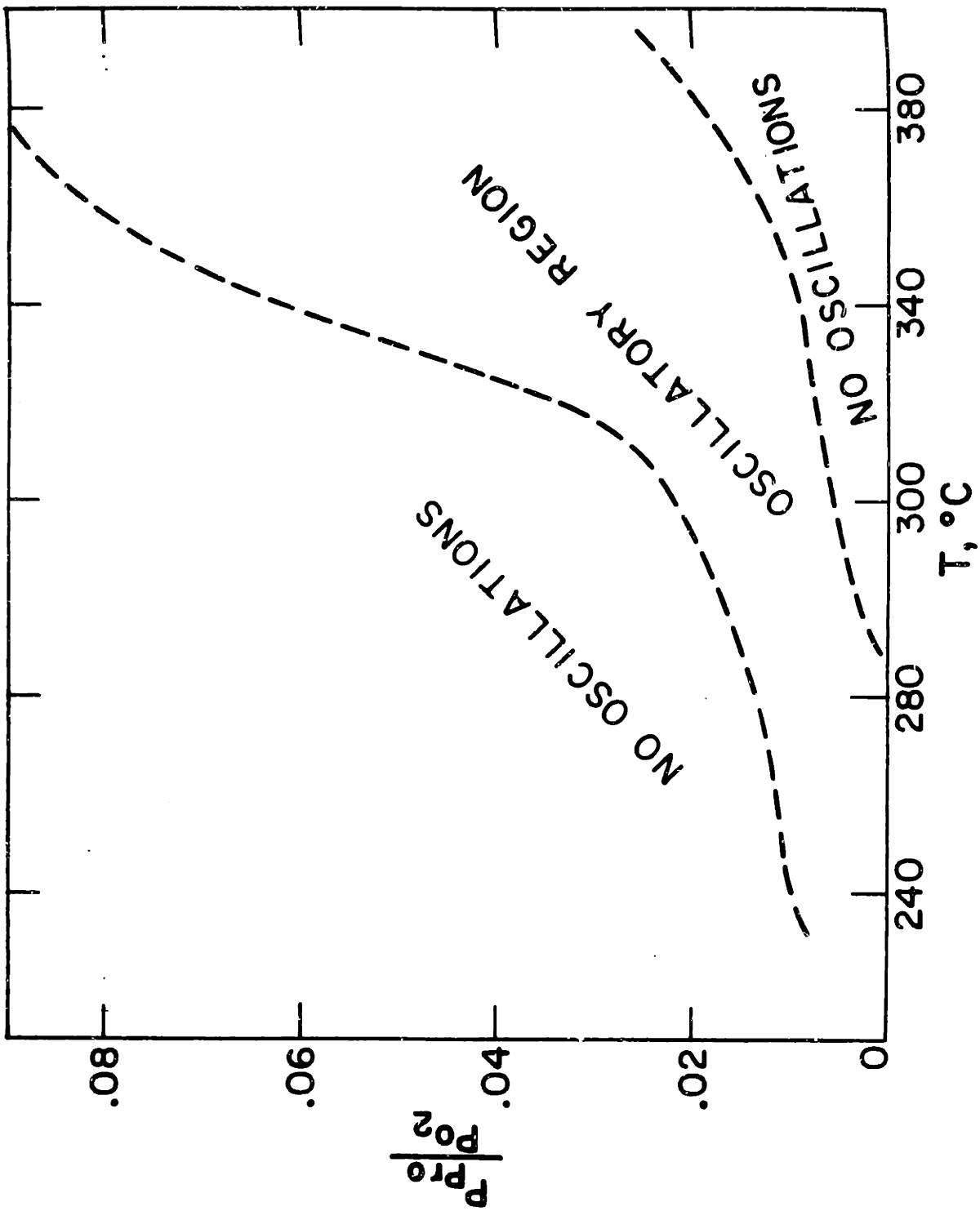

Figure 54 Temperature effect on the upper and lower propylene oxide/oxygen limits for oscillations

We will assume a Langmuir type adsorption for both atomic oxygen and propylene oxide. If thermodynamic equilibrium is established between surface and gaseous propylene oxide the coverage θ_{Pro} is given by the equation

$$\theta_{Pro} = \frac{K_{Pro} P_{Pro}}{1+K_{Pro} P_{Pro}} \qquad [C5.7]$$

where K_{Pro} is the adsorption coefficient of propylene oxide.

In the case of adsorbed atomic oxygen because of the definition of surface oxygen activity a_o [A4.4] and the Langmuir adsorption assumption it follows that

$$\theta_o = \frac{K_o a_o}{1+K_o a_o} \qquad [C5.8]$$

Note that eq.[C5.8]relates two intrinsic surface properties and is valid whether or not equilibrium with the gas phase exists.

On the basis of the above assumptions and considering the reaction to take place between adsorbed propylene oxide and adsorbed atomic oxygen one can write the rate expression as

$$r = K_R \cdot \theta_{Pro} \cdot \theta_o \qquad [C5.9]$$

Substituting the values of θ_o, θ_{Pro} from eq.[C5.7] and [C5.8] one obtains

$$r = K_R \frac{K_{Pro} P_{Pro}}{1+K_{Pro} P_{Pro}} \frac{K_o a_o}{1+K_o a_o} \qquad [C5.10]$$

which reduces to the experimental expression[C5.4] if $K_o a_o >> 1$

Since K_{Pro} is interpreted as the adsorption coefficient of propylene oxide on silver one can calculate from eq. [C5.6] an enthalpy of adsorption

$$\Delta H_{Pro} = -43.5 \text{ KJ/mol} \qquad [C5.11]$$

and an entropy of adsorption

$$\Delta S_{Pro} = -38.2 \text{ J/mol·K} \qquad [C5.12]$$

The surface oxygen activity behavior can be explained now by considering a steady state mass balance for adsorbed atomic oxygen

$$k_{ad} P_{O_2}^{1/2}(1-\theta_o) = K_d\theta_o + K_R \theta_{Pro}\theta_o \qquad [C5.13]$$

The left hand side term corresponds to atomic oxygen adsorption and the right hand side terms correspond to desorption of atomic oxygen and surface reaction respectively.

Taking into account eq. [C5.7] and [C5.8] and dividing eq.[C5.13] by $K_{ad}(1-\theta_o)$ one obtains:

$$P_{O_2}^{1/2} - a_o = \frac{K_R}{K_D} a_o \left(\frac{K_{Pro}P_{pro}}{1+K_{Pro}P_{Pro}} \right) \qquad [C5.14]$$

Dividing eq.[C5.14]by a_o and taking the reciprocal of both terms one obtains

$$\frac{a_o}{P_{O_2}^{1/2} - ao} = \frac{K_D}{K_R} + \frac{K_D}{K_R K_{Pro}} \frac{1}{P_{Pro}} \qquad [C5.15]$$

which describes the experimental observations [C5.1] with

$$K = \frac{K_D}{K_R K_{Pro}} \quad \text{and} \quad K' = \frac{K_D}{K_R} \qquad [C5.16]$$

Furthermore from the experimental values of K, K_R, K_{Pro}, eq. ([C5.2],[C5.5],[C5.6]) one can calculate K_D, the desorption rate of atomic oxygen

$$K_D = 155 \exp\left(-\frac{27500}{RT}\right) \text{ moles/s} \qquad [C5.17]$$

The activation energy of 27.5 Kcal/mole found for K_D is in good agreement with previous works (10,73).

The above model explains the steady-state behavior in a quantitative way but it fails to explain the oscillatory phenomena that were observed. Nevertheless since the amplitude of the oscillations is typically 2-15%, eq. [C5.1] and [C5.4] can be used approximately in both regions.

The origin of the limit cycles is not clear. Rate oscillations have not been reported previously for silver catalyzed oxidations. Oxidation of ethylene, propylene and ethylene oxide on the same silver surface and under identical temperature, space velocity and air-fuel ratio conditions did not give rise to oscillations. It thus appears that the oscillations are related specifically to the nature of chemisorbed propylene oxide. This is also supported by the lack of any correlation between the limits of oscillatory behavior and the surface oxygen activity. This makes the SEP measurements much less useful for interpreting the oscillations than in the case of ethylene oxidation on Pt (76) where the periodic behavior was due to the peculiarities of the platinum-oxygen interaction, i.e. surface platinum oxide formation.

Very little is known about the exact nature of propylene oxide chemisorption on silver. There is evidence for isomerization to acrolein and for polymer formation (77). Formation of a surface polymeric structure has also been observed during propylene oxidation on silver (52). It would appear possible, if not likely, that the rate oscillations are related to the ability of chemisorbed propylene oxide to form relatively

stable intermediates or polymeric structures. Thus chemisorbed monomer could account for the steady state kinetics discussed above whereas the superimposed fluctuactions on the rate could originate from periodic formation and combustion of surface polymeric residues. A mathematical model based on this assumptions and describing the oscillations in a qualitative manner will be presented later.

In summary, although the kinetic and potentiometric results of propylene oxide oxidation on silver can be interpreted within the framework of a simple Langmuir-Hinshelwood mechanism with two types of adsorption sites, further work is required to interprete the observed rate and oxygen activity oscillations. It is likely that the oscillations are related to the ability of propylene oxide to form polymeric structures. Understanding the origin of the oscillations may be quite important in obtaining a better picture of the oxidation of propylene on silver and devising methods to improve the selectivity to propylene oxide. We note that propylene oxide oxidation is the first known reaction which exhibits periodic behavior on sivler.

C.6 The catalytic oxidation of propylene

The catalytic oxidation of propylene was studied at temperatures 290-420°C and atmospheric and propylene varied between .03-.11 bars and .001-.01 bars respectively. Table 9 summarizes the kinetic and potentiometric data of this study.

C6.a. Kinetic measurements

The reaction network could be represented by the following scheme:

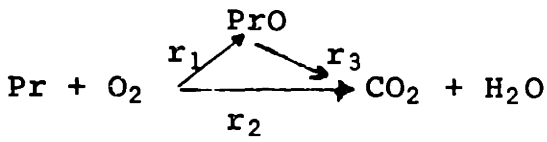

The three independent reaction rates r_1, r_2 (moles C_3H_6/s) and r_3 (moles C_2H_4O/s) are calculated as follows from the new kinetic data of the CSTR: First r_3 was calculated using the partial pressure of propylene oxide P_{Pro} in the products and the rate expression obtained in our previous work for the same catalyst.

$$r_3 = k_3 \frac{K_{Pro} P_{Pro}}{1+K_{Pro} P_{Pro}} \qquad [C5.4]$$

with $$K_3 = 6.4 \exp\left(\frac{-19000}{RT}\right) \frac{mole}{s} \qquad [C5.5]$$

and $$K_{Pro} = .010 \exp\left(\frac{10400}{RT}\right) bar^{-1} \qquad [C5.6]$$

The rate of propylene oxide oxidation r_3 was very small compared to r_2 ($r_3 \sim .001\ r_2$) thus essentially all CO_2 found in the products was produced from the direct propylene combustion. Unlike ethylene oxidation, the epoxidation rate was much smaller than the direct CO_2 formation as shown in table 9.

Taking into account that the reactor was a CSTR the reaction

Table 9

T (°C)	F_{tot} (cm^3/min)	P_{Pr} x10^3bar	P_O x10^3bar	a_O	r_1 (x10^6mole/s)	r_2 (x10^6moles/s)
420	700	8.9	95	.116	.08	1.76
420	700	5.56	98	.142	.048	1.06
420	700	3.25	88	.168	.031	.643
420	700	1.85	93	.204	.017	.30
420	700	5.42	67	.109	.046	1.03
420	700	5.7	47	.083	.057	1.14
420	700	6.1	33	.066	.054	1.07
375	700	9.3	95	.053	.063	1.33
375	700	5.67	93	.066	.039	.9
375	700	3.07	88	.090	.021	.515
375	700	1.91	93	.126	.015	.28
375	700	6.0	69	.045	.033	.92
375	700	5.7	47	.034	.028	.92
375	700	6.0	30	.0274	.032	.90
330	500	8.5	95	.014	.032	1.03
330	500	6.3	95	.022	.028	.78
330	500	3.2	86	.073	.018	.44
330	500	5.8	59	.012	.020	.78
330	500	6.5	40	.008	.025	.68
330	500	6.1	23	.0074	.072	.73
330	500	2.4	88	.044	.010	.30
290	360	9.1	110	.0078	.011	.60
290	360	5.4	102	.0090	.008	.45
290	360	3.4	113	.0151	.007	.31
290	360	1.9	112	.0186	.005	.22
290	360	5.6	62	.007	.115	.42
290	360	6.0	35	.0055	.009	.40
290	360	6.4	20	.0037	.011	.41

rates r_1, r_2 were calculated from the appropriate mass balances:

$$r_1 - r_2 = G \quad X_{PrO} \qquad [C6.1]$$

$$r_2 + r_3 \simeq r_2 = \frac{1}{3} G \, X_{CO_2} \qquad [C6.2]$$

where X_{PrO}, X_{CO_2} are the exit mole fractions of propylene oxide and CO_2 and G is the total molar flow rate. The values of r_1 and r_2 were also found to satisfy within 2% the mass balance requirement

$$r_1 + r_2 = G[X_{Pr,IN} - X_{Pr,OUT}] \qquad [C6.3]$$

where $X_{Pr,IN}$, $X_{Pr,OUT}$ are mole fractions of propylene in the feed and effluent stream respectively. Volume changes were calculated to be negligible due to the high partial pressure of diluent N_2 (>80%).

The rate of propylene oxide formation r_1 is plotted in fig. (55) vs. the partial pressure of oxygen P_{O_2} for constant P_{Pr}. The rate of deep propylene oxidation r_2 is plotted vs. P_{O_2} in Fig. (56). As in the case of ethylene oxidation both r_1 and r_2 are essentially independent of the partial pressure of oxygen for the range of gas compositions examined.

Figure (57) exhibits the dependence of r_1 on P_{Pr} for various temperatures. Similarly the dependence of r_2 on P_{pr} is shown in Fig. (58). At high temperatures both rates resemble simple first order depedence on P_{Pr} but at lower temperatures a deviation from first order kinetics is quite obvious.

It was found that all the kinetic data could be expressed rather accurately by the rate expressions:

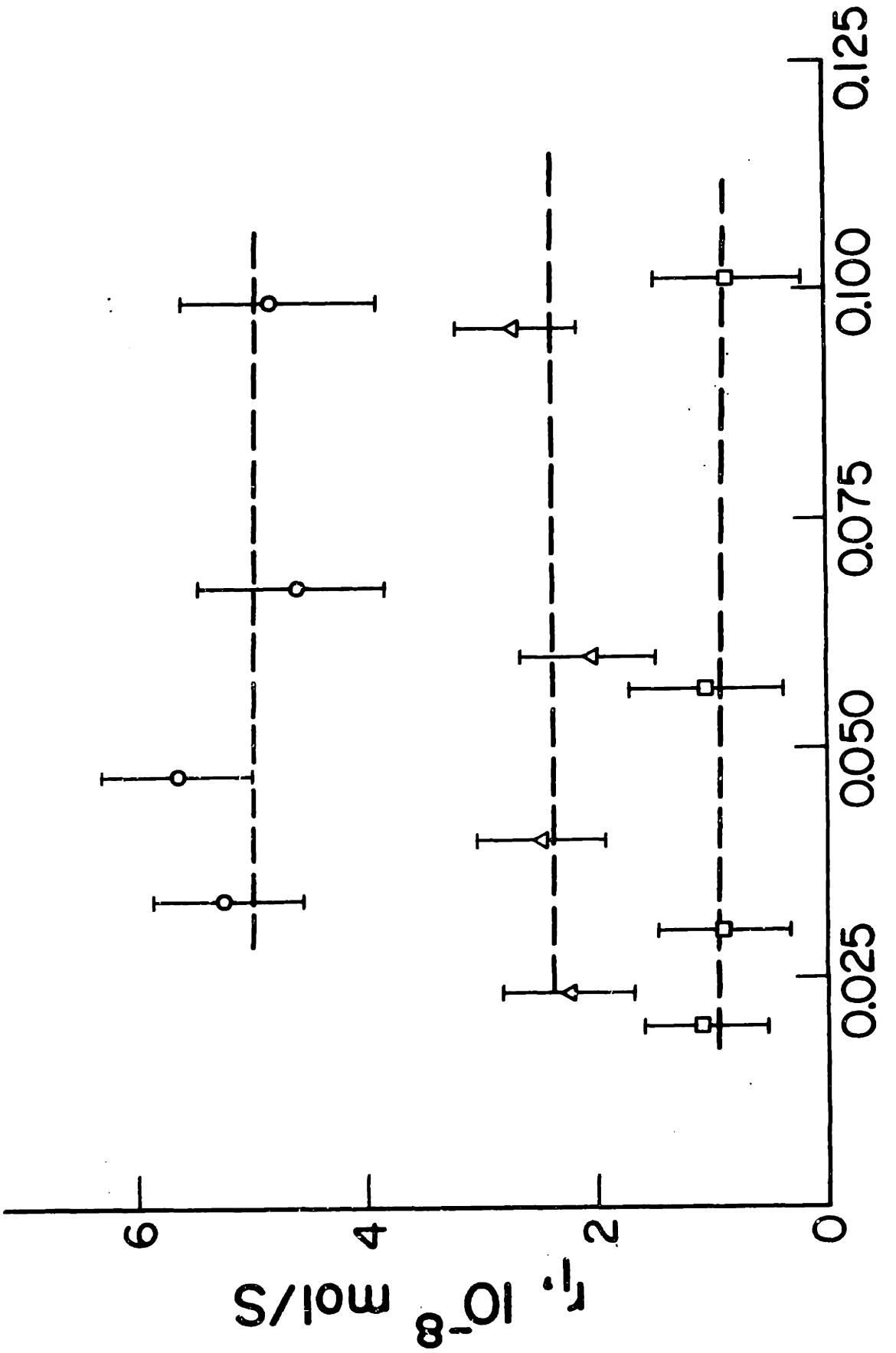

Figure 55: Rate of propylene epoxidation vs. P_{O_2}

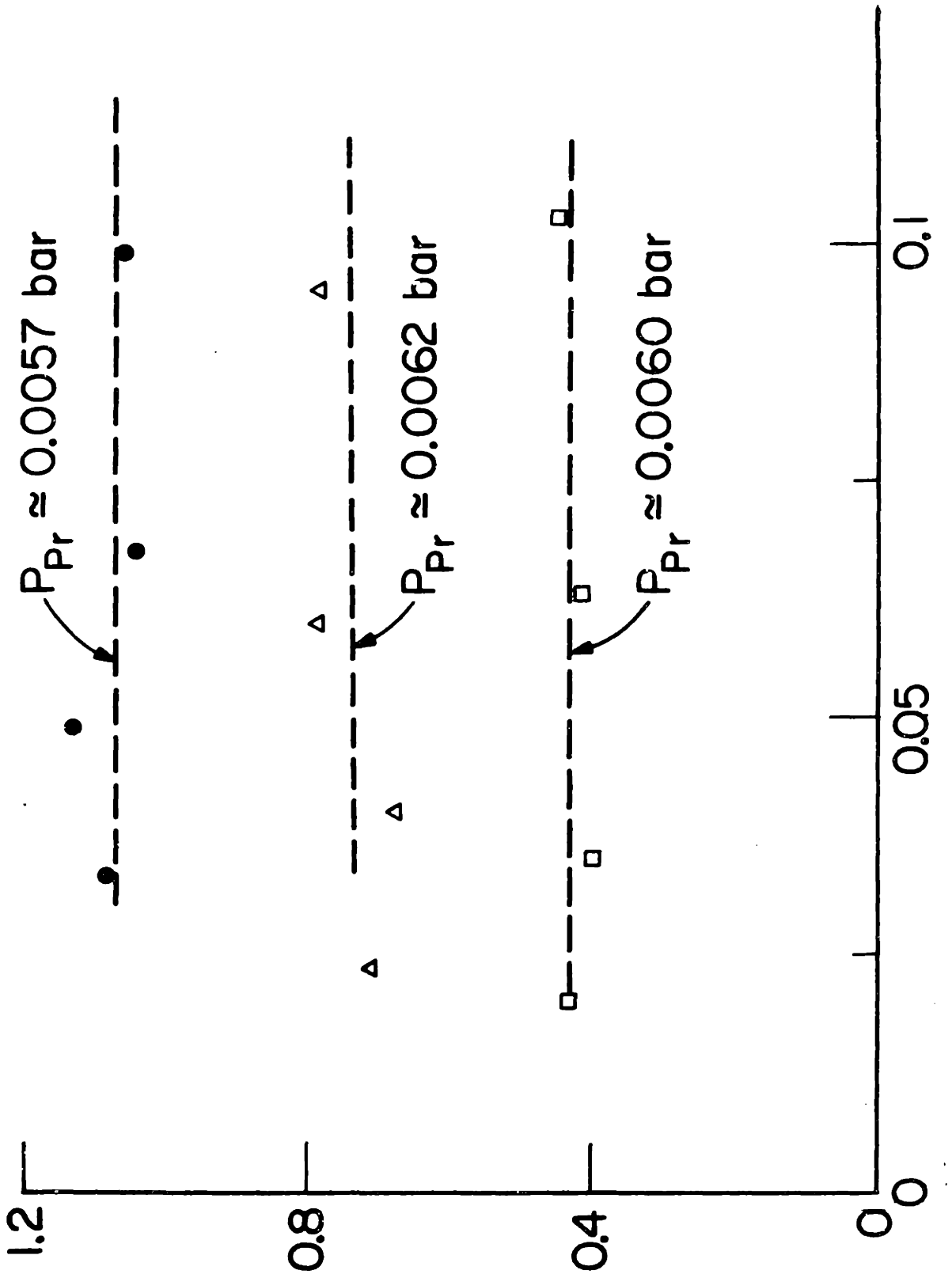

Figure 56: Rate of propylene deep oxidation vs. P_{O_2}

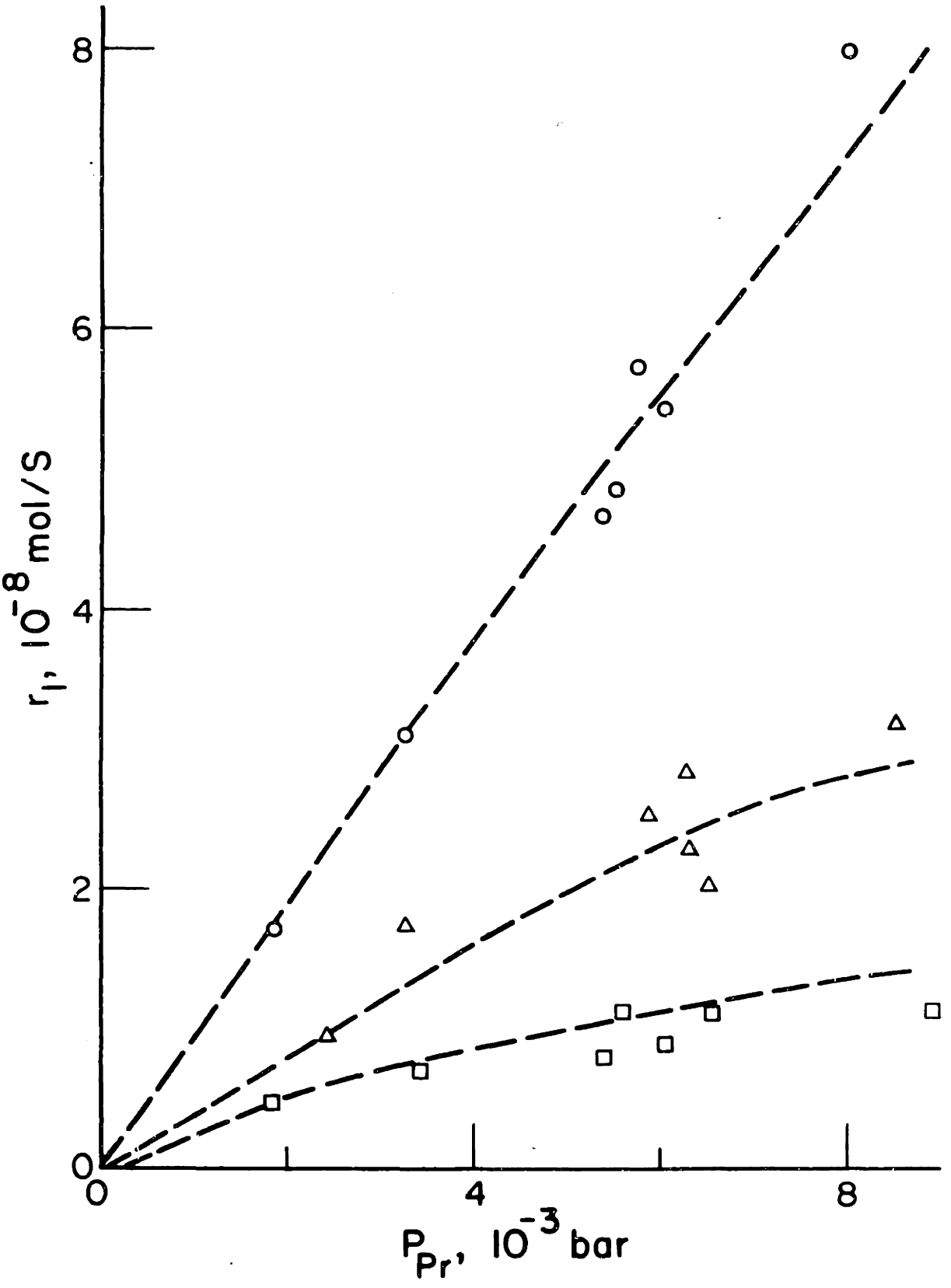

Figure 57: Rate of propylene epoxidation vs. p_{Pr}

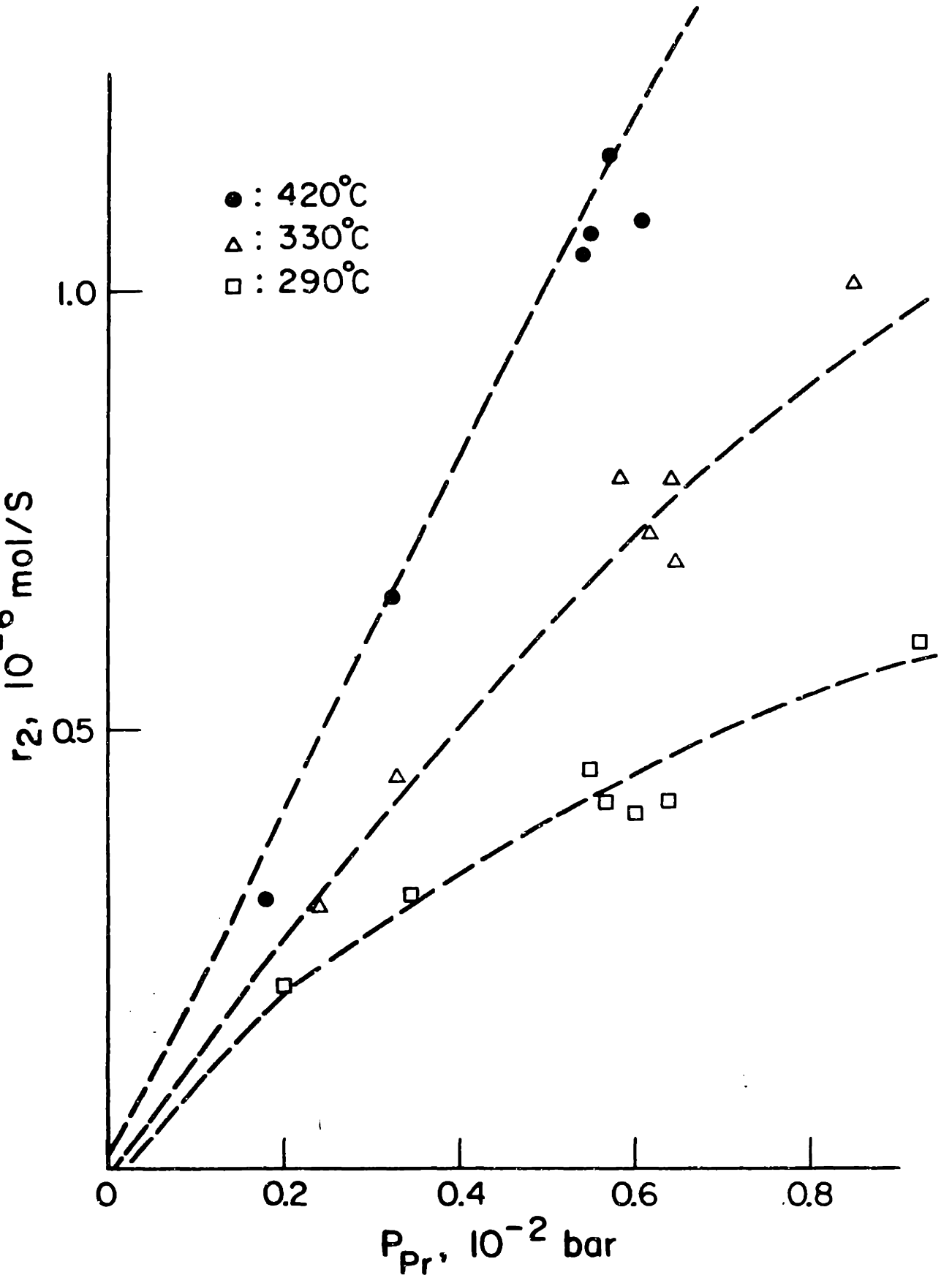

Figure 58: Rate of propylene epoxidation vs. P_{Pr}

$$r_1 = K_1 \frac{K_{Pr} P_{Pr}}{1+K_{Pr}P_{Pr}} \qquad [C6.4]$$

$$r_2 = K_2 \frac{K_{Pr}P_{Pr}}{1+K_{Pr}P_{Pr}} \qquad [C6.5]$$

with $$K_1 = 11.94 \exp\left(\frac{-22000}{RT}\right) \qquad [C6.6]$$

$$K_2 = 32.9 \exp\left(\frac{-19000}{RT}\right) \qquad [C6.7]$$

$$K_{Pr} = 1.2 \cdot 10^{-4} \exp\left(\frac{15000}{RT}\right) \qquad [C6.8]$$

Similar kinetic equations were found during the study of ethylene oxidation.

C6.b. Oxygen activity measurements

Like in the cases of ethylene, ethylene oxide and propylene oxide oxidation it was found that in general $a_O^2 < P_{O_2}$ during propylene oxidation, i.e., thermodynamic equilibrium was not established between adsorbed oxygen and oxygen in the gas phase. The dependence of the surface oxygen activity a_O on the partial pressure of propylene for constant P_{O_2} is shown in Fig. 59. In Fig. 60 a_O is plotted vs. P_{O_2} for constant P_{Pr}. From these figures it can be easily observed that

a) a_O increases as P_{O_2} increases at constant temperature and P_{Pr}

b) a_O decreases as P_{Pr} increases at constant temperature and P_{O_2}

c) a_O increases as the temperature increases at constant gas composition.

Several functional forms were examined in order to describe the dependence of a_O on gas-phase composition. It was found that all the a_O measurements could be correlated rather

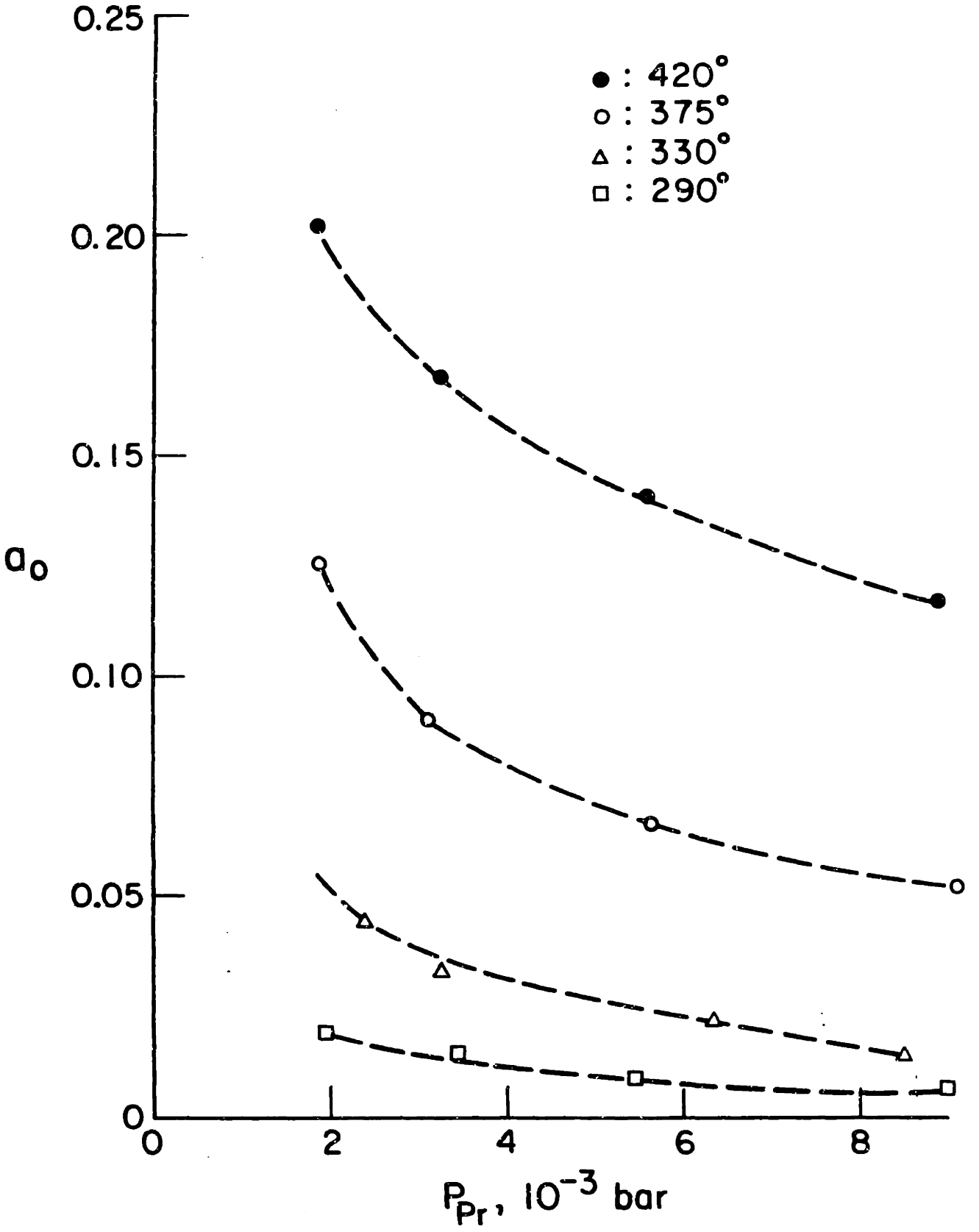

Figure 59: Dependence of oxygen activity a_o on P_{Pr}

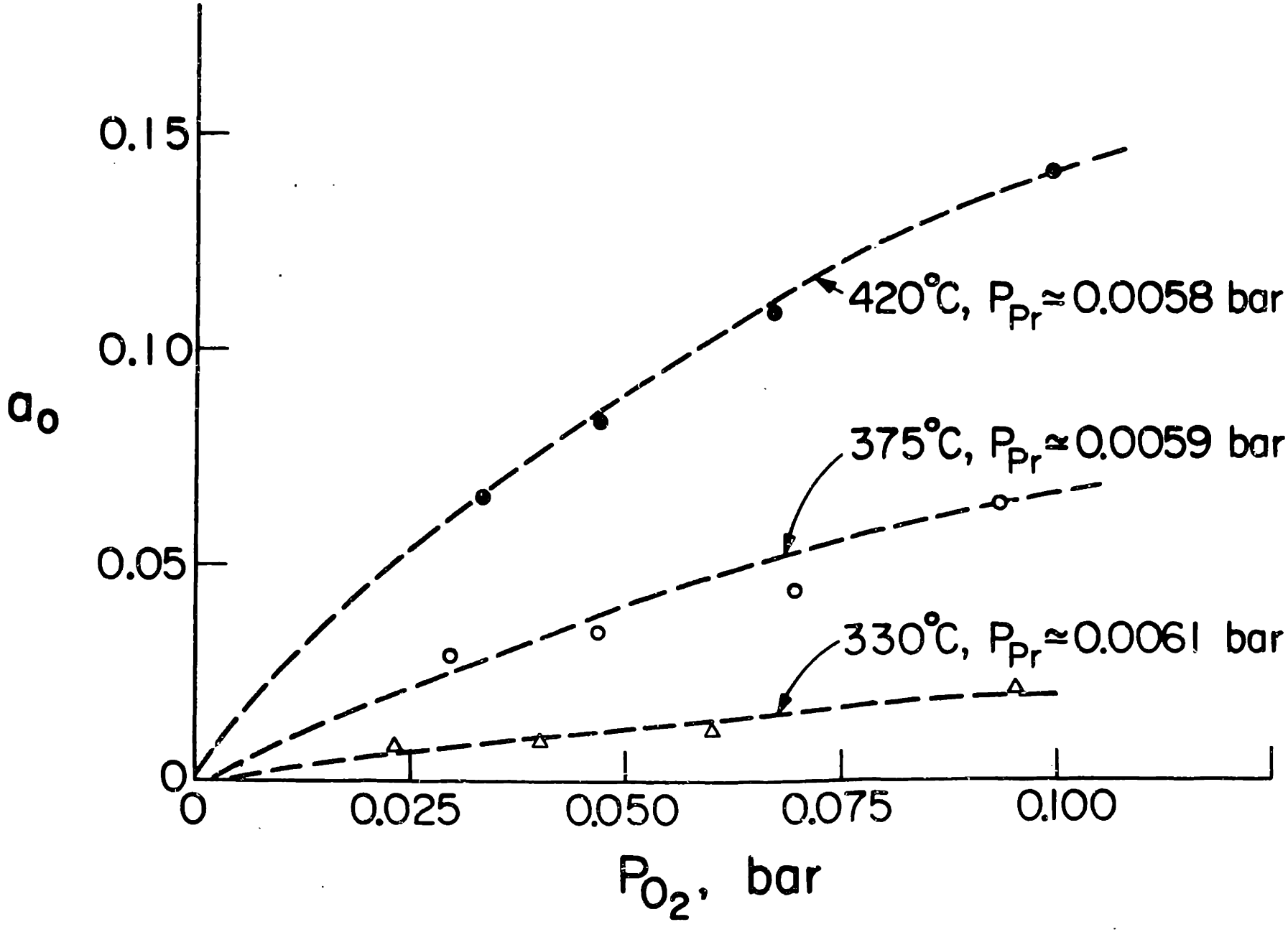

Figure 60: Dependence of oxygen activity a_o on P_{O_2}

satisfactory by the expression:

$$\frac{a_O}{P_O^{1/2} - a_O} = K\, P_{Pr}^{-1} + K' \qquad [C6.9]$$

with $K = 22800 \exp\left(\frac{-21.500}{RT}\right)$

This is shown in Figs. (61) and (62).

C6.c Discussion of results

A satisfactory kinetic model for the present study should account for both kinetics (Eqs.[C6.4],[C6.5]) and the surface oxygen activity behavior (Eq.[C6.9]).

In agreement with the previous results the existence of two kinds of adsorbed oxygen molecular and atomic, is assumed. Molecular oxygen which reacts to produce propylene oxide adsorbs on surface sites S_3 and atomic oxygen adsorption occurs on sites S_2. Propylene and propylene oxide adsorbe on sites S_1 of the silver surface. A Langmuir-type adsorption for propylene is assumed and furthermore that thermodynamic equilibrium is established between surface and gaseous propylene. It thus follows that the coverage θ_{Pr} of propylene on S_1 sites is given by

$$\theta_{Pr} = K_{Pr}P_{Pr}/(1 + K_{Pr}P_{Pr}) \qquad [C6.10]$$

where K_{Pr} is the adsorption coefficient of propylene, provided P_{PrO} is small enough so that $K_{Pr}P_{Pr} >> K_{PrO}P_{Pro}$ ($\theta_{Pro} << \theta_{Pr}$).

Similarly, assuming Langmuir-type adsorption for molecular oxygen on S_3 sited and thermodyanmic equilibrium between molecularly adsorbed and gaseous O_2

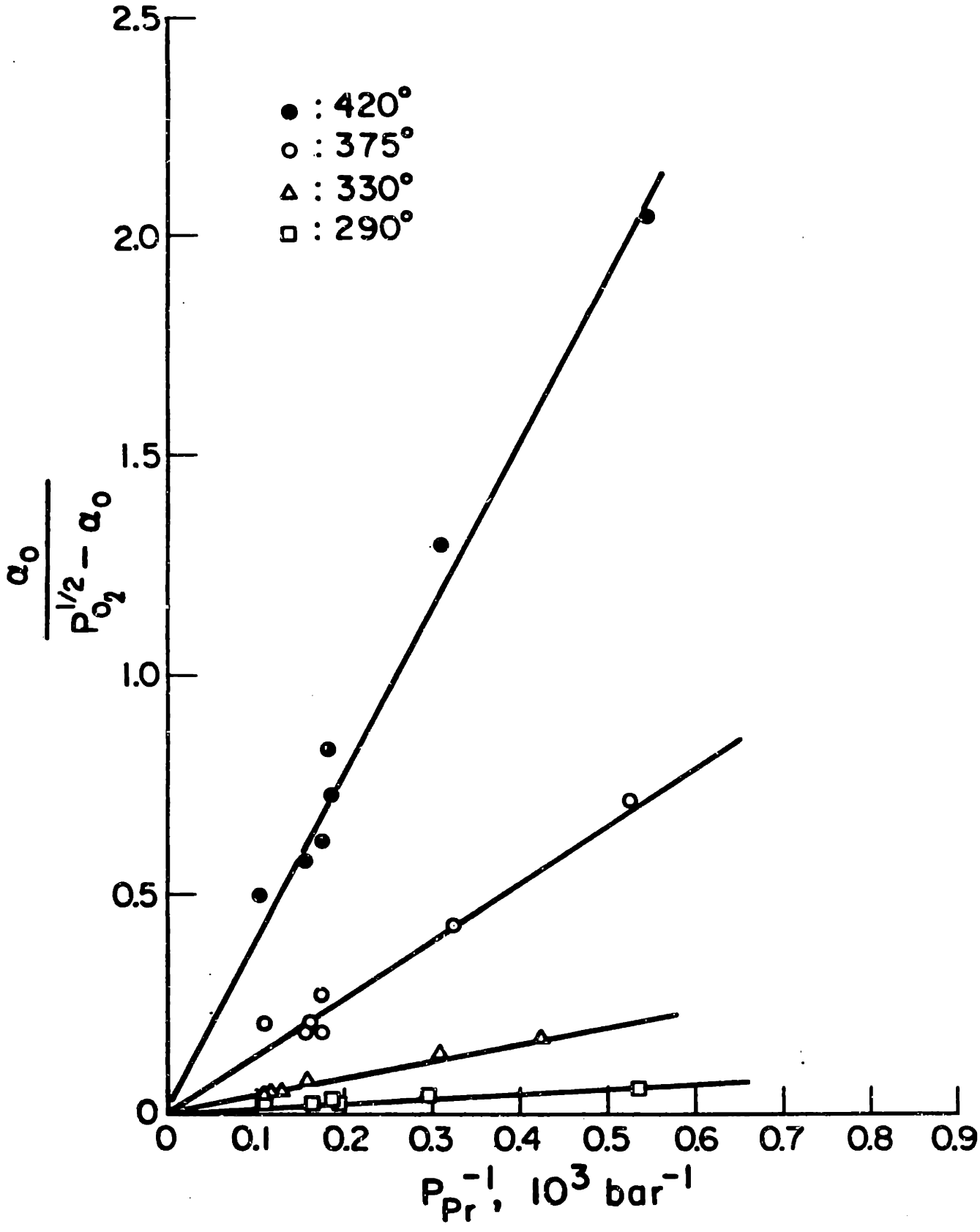

Figure 61: Dependence of a_o on gas phase composition

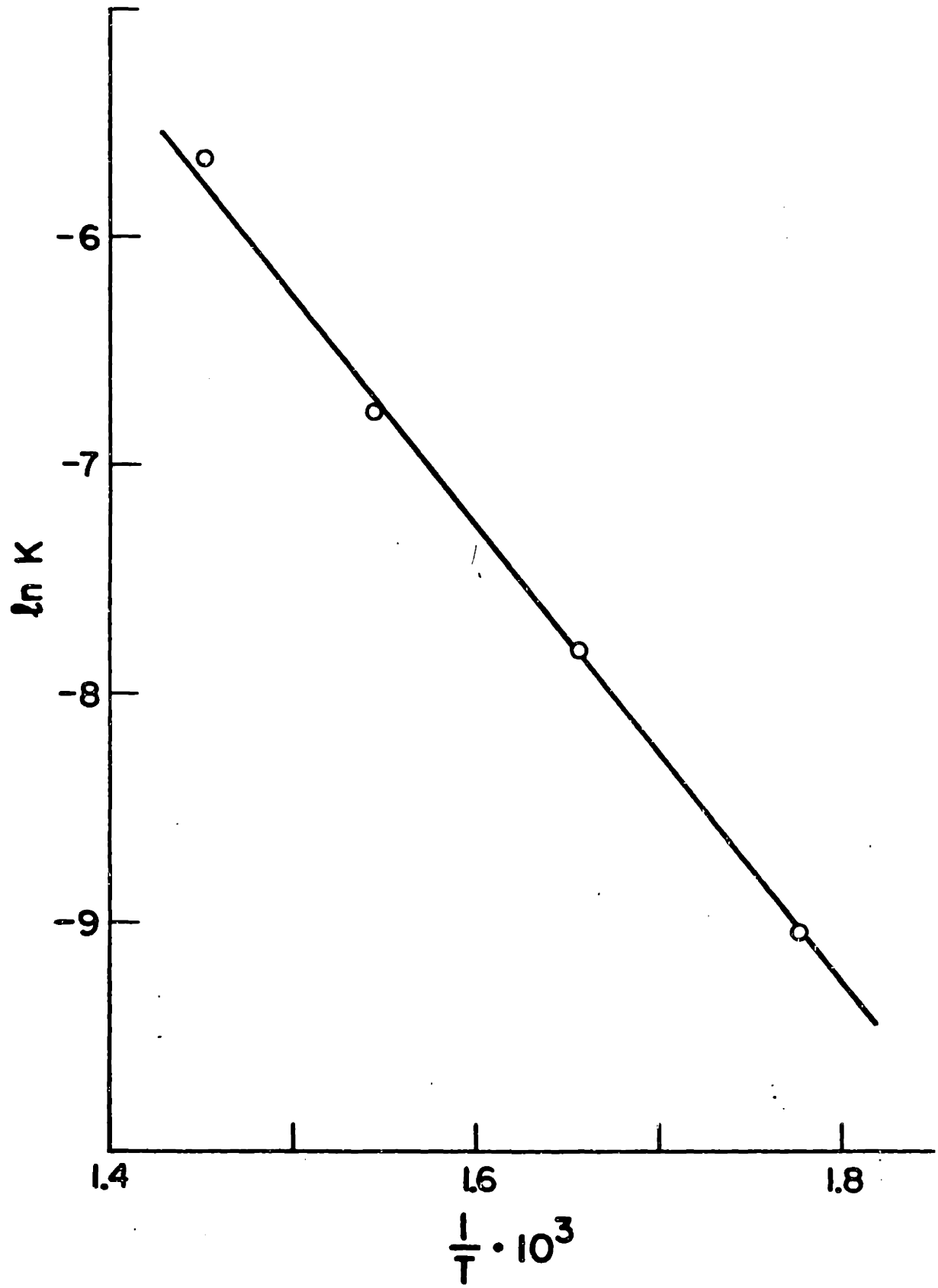

Figure 62: Temperature dependence of the parameter K

$$\theta_{O_2} = K_{O_2}P_{O_2}/(1 + K_{O_2}P_{O_2}) \qquad [C6.11]$$

where θ_{O_2} is the molecular oxygen coverage and K_{O_2} is the molecular adsorption coefficient of oxygen. Assuming that the electrochemically measured surface oxygen activity represents atomically adsorbed oxygen (62), the coverage θ_O of atomic oxygen adsorbed will be given from the equation

$$\theta_O = K_O a_O/(1 + K_O a_O) \qquad [C6.12]$$

irrespective of whether thermodynamic equilibrium is established between gaseous and atomically adsorbed oxygen or not.

On the basis of the above assumptions it follows that the rate of propylene oxide formation r_1 is given by

$$r_1 = K_1\theta_{Pr}\theta_{O_2} = K_1 \frac{K_{Pr}P_{Pr}}{1+K_{Pr}P_{Pr}} \cdot \frac{K_{O_2}P_{O_2}}{1+K_{O_2}P_{O_2}} \qquad [C6.13]$$

which reduces to the experimental rate expression [C6.4] if $K_{O_2}P_{O_2} >> 1$. This is quite reasonable since excess oxygen was used in all the experiments. Similarly the rate of propylene deep oxidation to CO_2 is given by

$$r_2 = K_2\theta_{Pr}\theta_O = K_2 \frac{K_{Pr}P_{pr}}{1+K_{Pr}P_{pr}} \cdot \frac{K_O a_O}{1+K_O a_O} \qquad [C6.14]$$

which reduces to the experimental expression [C6.5] if $K_O a_O >> 1$.

From eqns [C6.13] and [C6.14] it follows that the experimentally determined parameter K_{Pr} is the adsorption coefficient of propylene on silver. According to eq. [C6.8] it follows that the enthalpy and entropy of adsorption of propylene on sivler are

$$\Delta H_{Pr} = -15 \text{Kcal/mol} \qquad \text{and}$$

$$\Delta S_{pr} = -17.9 \text{ cal/mole}\cdot^{\circ}\text{K}$$

The surface oxygen activity dependence on temperature and

gas-phase composition can be explained now by considering a steady-state mass balance for adsorbed atomic oxygen

$$O = K_{ad} P_{O_2}^{1/2}(1-\theta_o) - K_d\theta_o - K_2\theta_{Pr}\theta_o \qquad [C6.15]$$

The first term corresponds to the atomic oxygen adsorption step using the same assumption made in the previous studies on silver catalyst (sections C2,C3). The second term corresponds to oxygen description under the same assumptions. In the absence of propylene eq. [C6.15] reduces to the common Langmuir isotherm with $K_o = \frac{K_{ad}}{K_d}$. The third term refers to atomic oxygen reacting with propylene to form CO_2. Dividing [C6.15] by $K_{ad}(1-\theta_o)$ one obtains:

$$P_o^{1/2} - \frac{K_d}{K_{ad}} \cdot \frac{\theta_o}{(1-\theta_o)} - \frac{K_2}{K_{ad}} \theta_{Pr} \frac{\theta_o}{(1-\theta_o)} \qquad [C6.16]$$

Taking into account eq. [C6.10] [C6.12] the above equation becomes

$$P_{O_2}^{1/2} - a_o = \frac{K_2}{K_d} \theta_{Pr} a_o \Rightarrow$$

$$\Rightarrow \frac{a_o}{P_{O_2}^{1/2} - a_o} = \frac{K_d}{K_2} \frac{(1+K_{Pr}P_{Pr})}{K_{Pr}P_{Pr}}$$

$$\Rightarrow \frac{a_o}{P_{O_2}^{1/2} - a_o} = \frac{K_d}{K_2} + \frac{K_d}{K_2 K_{Pr}} \frac{1}{P_{Pr}} \qquad [C6.17]$$

which describes the experimental observations [C6.9] with

$$K = \frac{K_D}{K_2 K_{Pr}} \text{ and } K' = \frac{K_D}{K_2} \qquad [C6.18]$$

Furthermore from the experimental values of K, K_2, K_{Pr} (eqs. [C6.7], [C6.8], [C6.9]) one can calculate K_D, the desorption coefficient of atomic oxygen

$$K_d = 89.5 \exp\left(\frac{-25500}{RT}\right) \qquad [C6.19]$$

The activation energy found here for atomic oxygen desorption (25.5 kcal/mole) is in very good agreement with both values found previously in this research (eqs. [C2.2],[C5.17] and values reported from previous workers (10).

Thus with the above study of propylene oxidation on silver following ethylene oxide, ethylene and propylene oxide (sections C2,C3,C5,C6) the conjuntion of kinetic and potentiometric measurements during these two important catalytic systems (ethylene and propylene oxidation) has been concluded. Similarities and differences between those two reaction networks are further discussed in section D .

C7. The effect of oxygen pumping during propylene oxidation

C7.a. Qualitative description

As in the case of oxygen pumping during Ethylene Oxidation (sec. C4) several different zirconia reactor cells were used in the course of these experiments. The electrolyte thickness of the cells was roughly between 150 and 300 μm. The cells differed in the surface area S of the silver catalyst electrode. The surface areas of the cells were measured in the way described in Section C1.d. and their values are given in table 10.

The effect of electrochemical oxygen pumping on the rates of propylene epoxidation r_1 and deep oxidation r_2 is shown in figure (63). At time $t < 0$ the circuit is open and the catalyst is at steady state chearacterized by $r_{20} = 2.53 \cdot 10^{-7}$ moles/s and $r_{1C} = .050 \cdot 10^{-7}$ mole/s. The temperature as well as ($390 \pm 1°C$) the gas phase composition ($P_{Pr} \sim 2.8 \cdot 10^{-3}$ bar, $P_{O_2} \sim .15$ bar) remain practically constant.

At $t = 0$ a constant current of +200 μA is applied to the cell. A transient increase on both reaction rates is observed. The increase in r_1 is higher than that in r_2 and thus the selectivity to propylene oxide increases. The system reaches a new steady state after approximately 30 minutes. At time $t = 50$ min the circuit is opened and the catalyst returns to its initial state indicating the reversibility of the phenomenon. At $t = 100$ min a constant current of -100 μA is applied through the cell so that oxygen is pumped from the catalyst. Both rates decrease and so does the selectivity. When the circuit is opened again the rates return to the original

Table 10

Catalyst-Electrode Surface Areas

Reactor Cell #	Reactive Oxygen Uptake Q(moles O_2)
RC12	$4 \cdot 10^{-7}$
RC13	$1.5 \cdot 10^{-7}$
RC14	$7.6 \cdot 10^{-7}$
RC15	$1 \cdot 10^{07}$
RC16	$10 \cdot 10^{-7}$

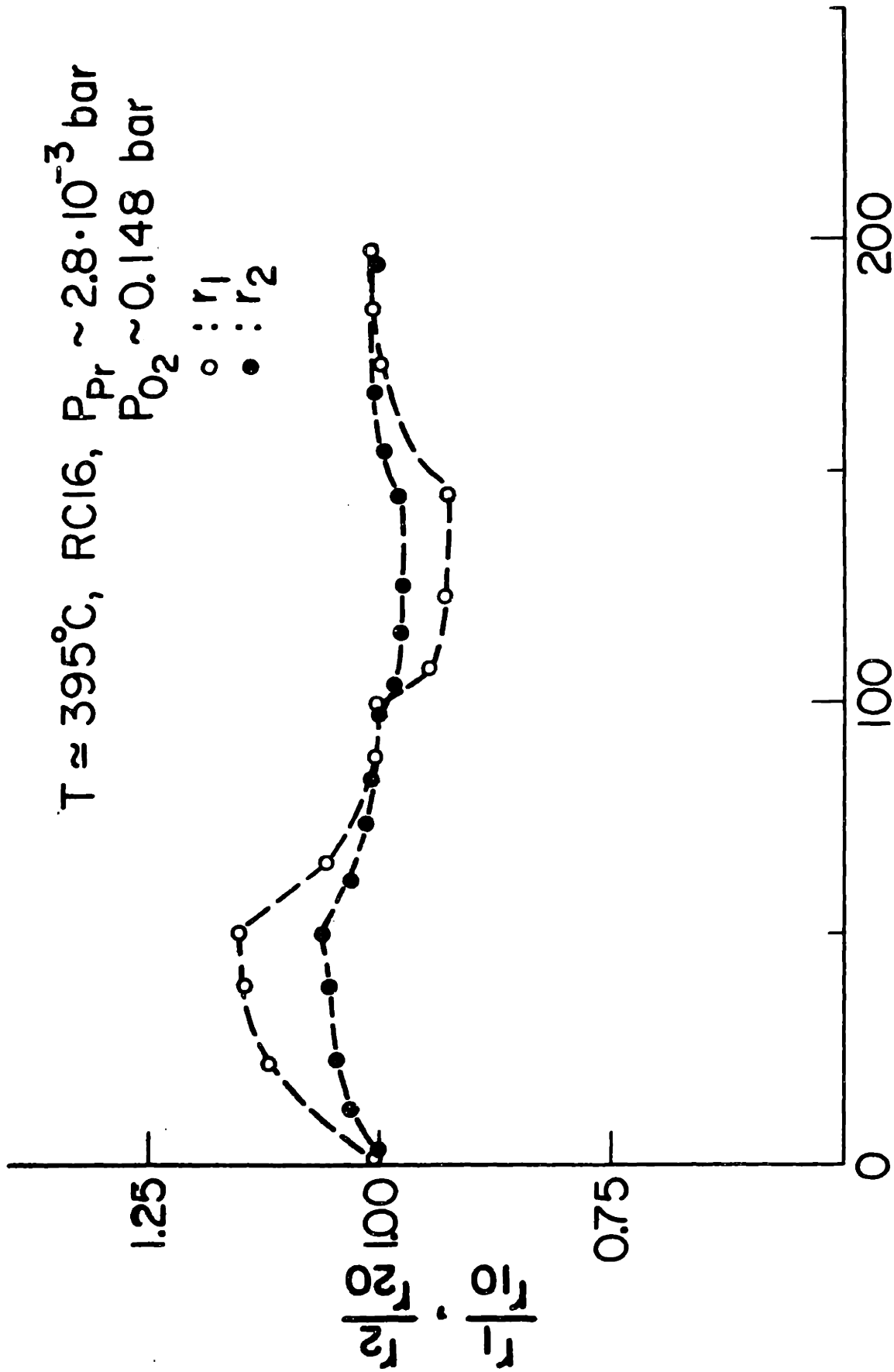

Figure 63: Effect of oxygen pumping during Propylene oxidation

steady state values r_{10} and r_{20}.

The rate of oxygen transport through the electrolyte G_O^{2-} can be calculated from the value of the imposed current i ($G_O^{2-} = \frac{i}{2F}$ moles oxygen/s). By calculating G_O^{2-} and comparing the value of G_O^{2-} with the increase in the reaction rate it was found that the total increase in the reaction rates exceeded G_O^{2-} by a factor of 100. The same interesting result was obtained during ethylene oxidation (Section C4). In general, as it will be shown and discussed below, the effect of oxygen pumping during propylene oxidation is quite similar to that observed during the oxidation of ethylene.

C7.b Effect of current i and overvoltage ΔV

In figure 64 the effect of the imposed current i is shown for two different reactor cells. In both cases the temperature and the gas phase composition were kept constant throughout the experiment. Figure (64) contains the final increase in r_1. The rate of propylene epoxidation increases as the current i increases until i reaches a value (250-300 μA) above which increase in i does not produce any further increase in the reaction rates. The effect of current i on r_2, the deep oxidation rate is shown in figure 65. From these two figures 64 and 65 it can be seen that in both cases the effect is qualitatively the same. Nevertheless the relative increase in r_1 is much larger than that in r_2 and thus the selectivity increases.

As shown in figure 64 the relative increase in r_1 for the reactor cells RC13 is higher than that in RC12 for the

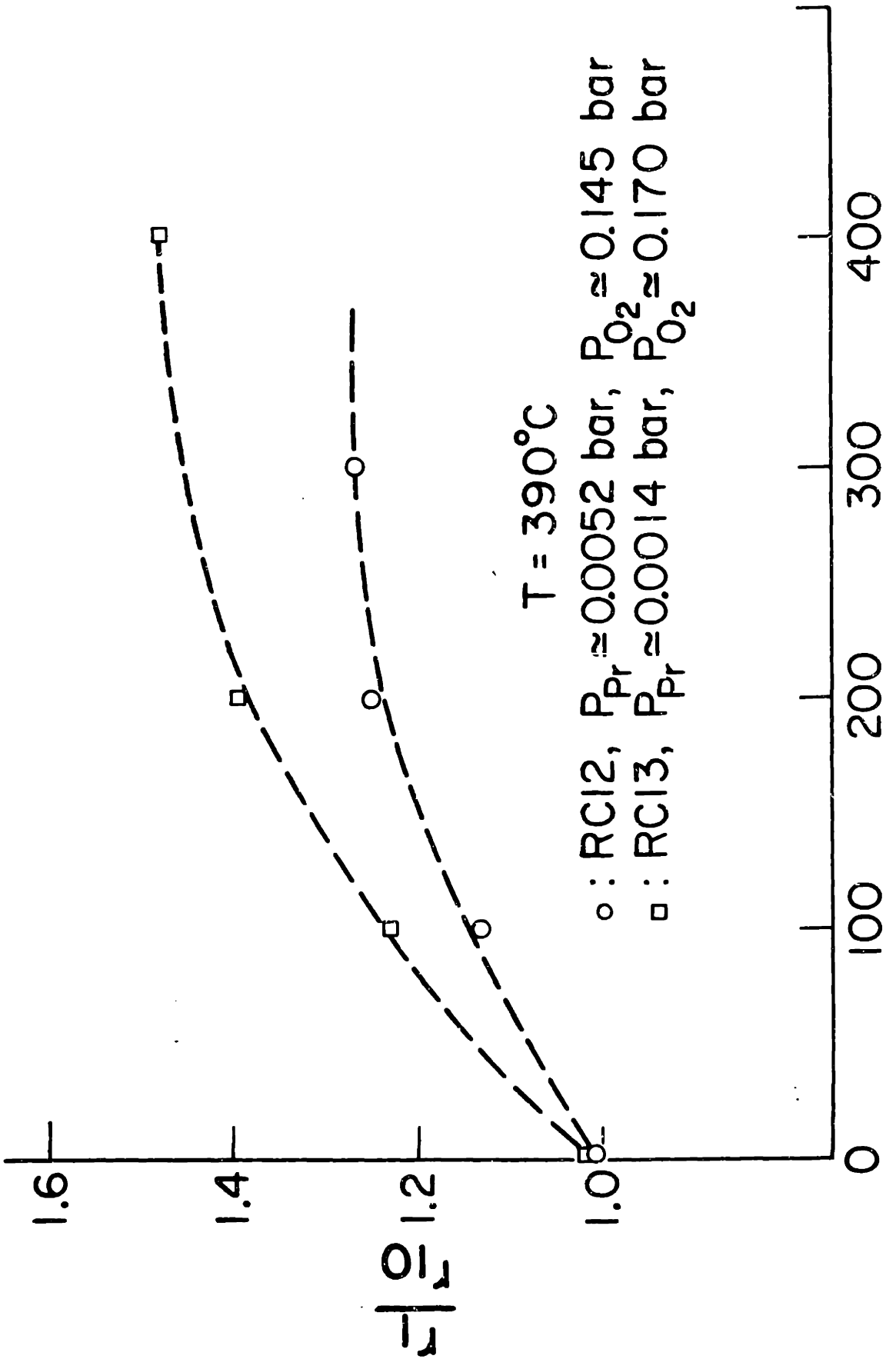

Figure 64: Increase of propylene epoxidation rate r_1 vs. current i

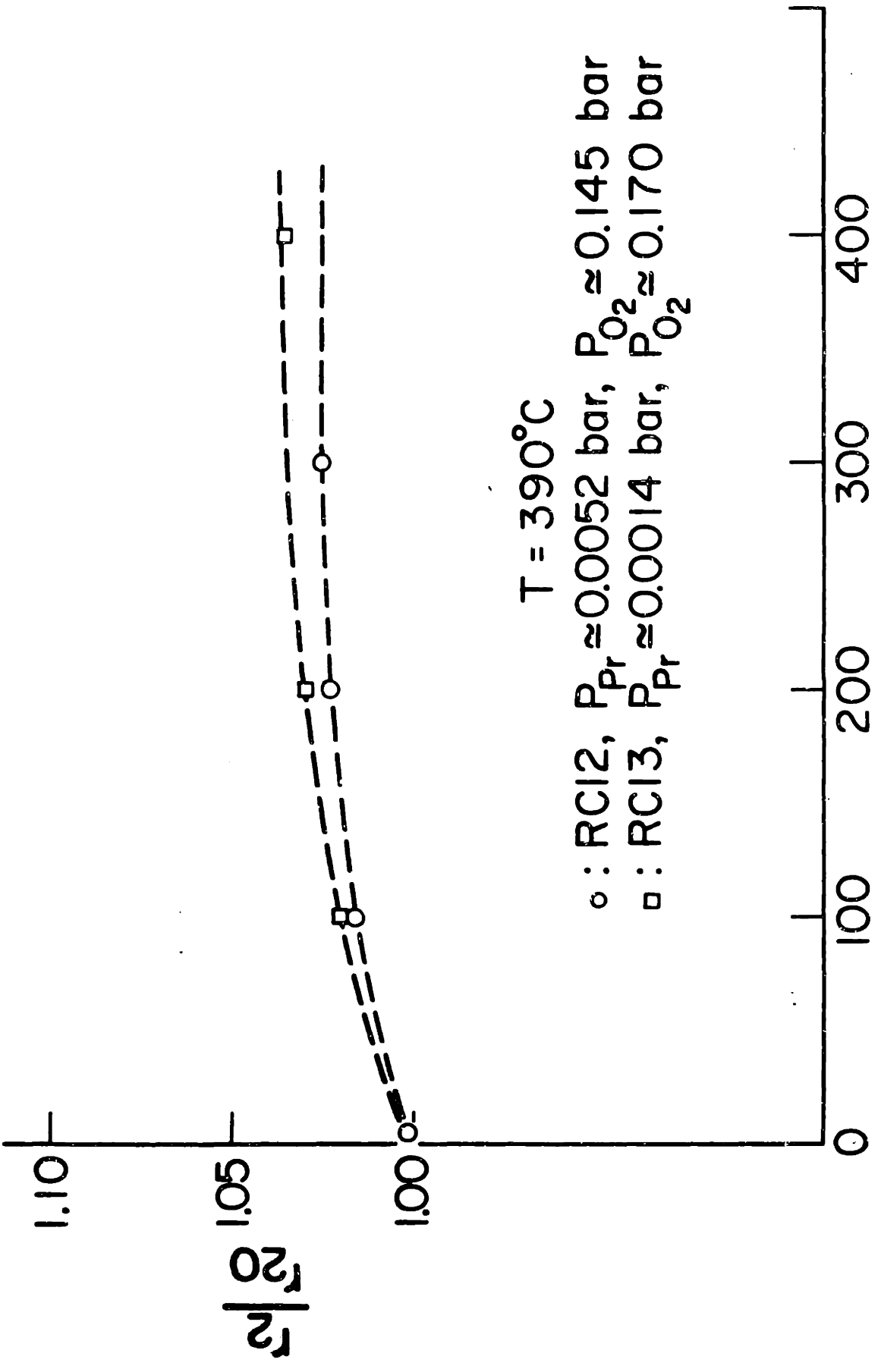

Figure 65: Increase of CO_2 formation rate r_2 vs. current i

same current imposed. It has to be pointed out, however, that these two reactor cells differed in the surface areas of their catalyst-electrodes. And furthermore the gas-phase composition was different during these experiments.

Figure (66) shows a typical transient cell voltage response when a constant current i is imposed to the cell. At $t < 0$ the circuit is open and the cell voltage equals the open circuit emf E given by eq.[A4.4]. At $t = 0$ the circuit is closed and a constant current of 200 μA is imposed. The initial sharp rise at $t = 0$ corresponds to the ohmic drop iR_c where R_c is the ohmic resistance of the solid electrolyte cell. The subsequent gradual increase ΔV to a final asymptotic value corresponds to formation of surface intermediates on the catalyst-electrode. A similar voltage behavior was observed during the oxidation of ethylene (fig. 32).

Figure 67 shows the transient cell voltage response in absence of propylene i.e., when air only is fed in the reactor inlet stream. It is interesting that even in this case a considerable overvoltage ΔV is observed although no chemical reaction takes place in the reactor. Figure 67 contains the overpotential transient behavior for various currents (between 25 and 150 μA). The time required for ΔV to reach the final asymptotic value depends on the imposed current as shown in figure 67 and the time constant τ_c (defined as the time required for the system to reach the 63.2% of its final steady state) as the current i increases. This is shown in figure 68. It is also interesting that the time constant τ_c shown in the

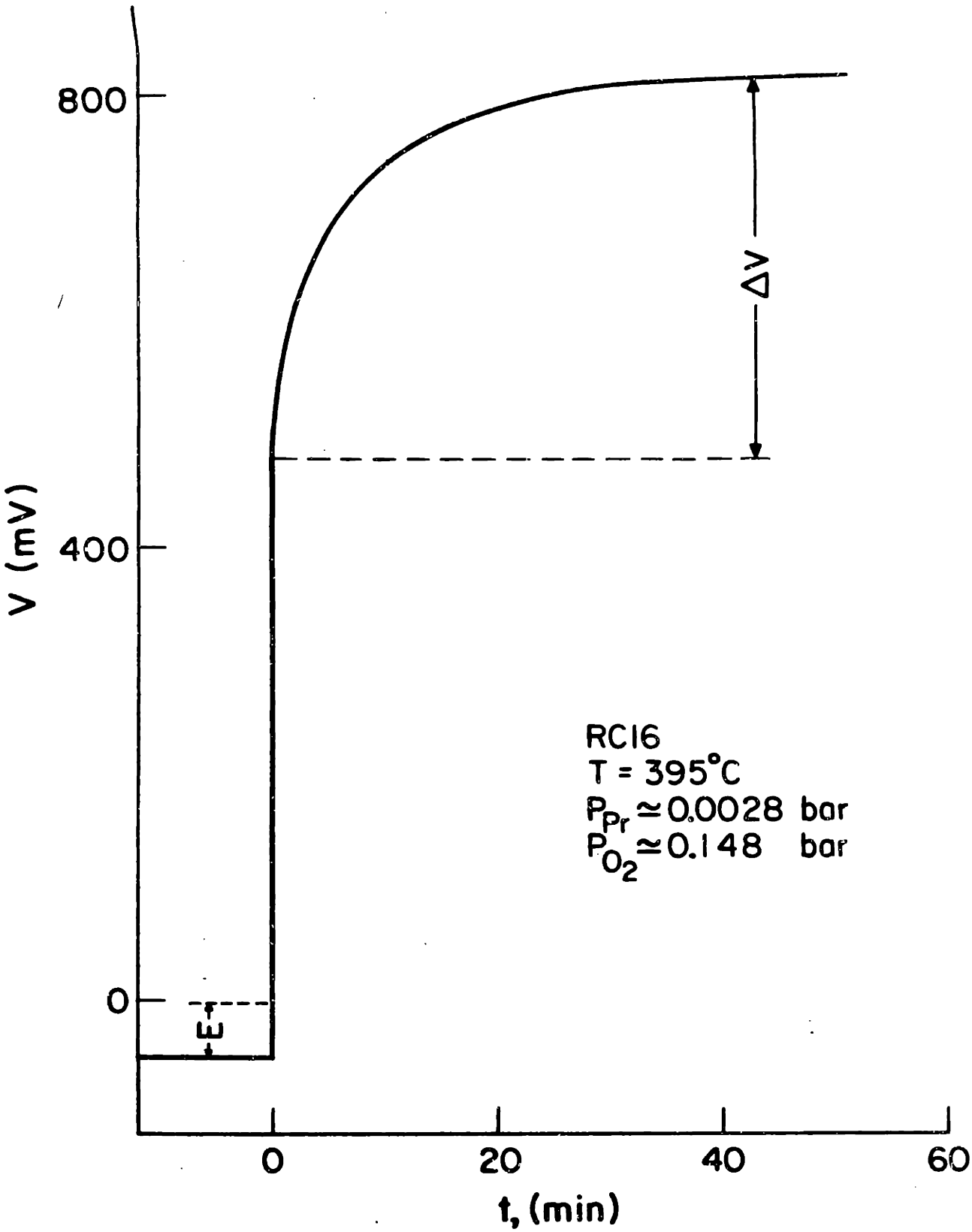

Figure 66: Galvanostatic transient voltage response

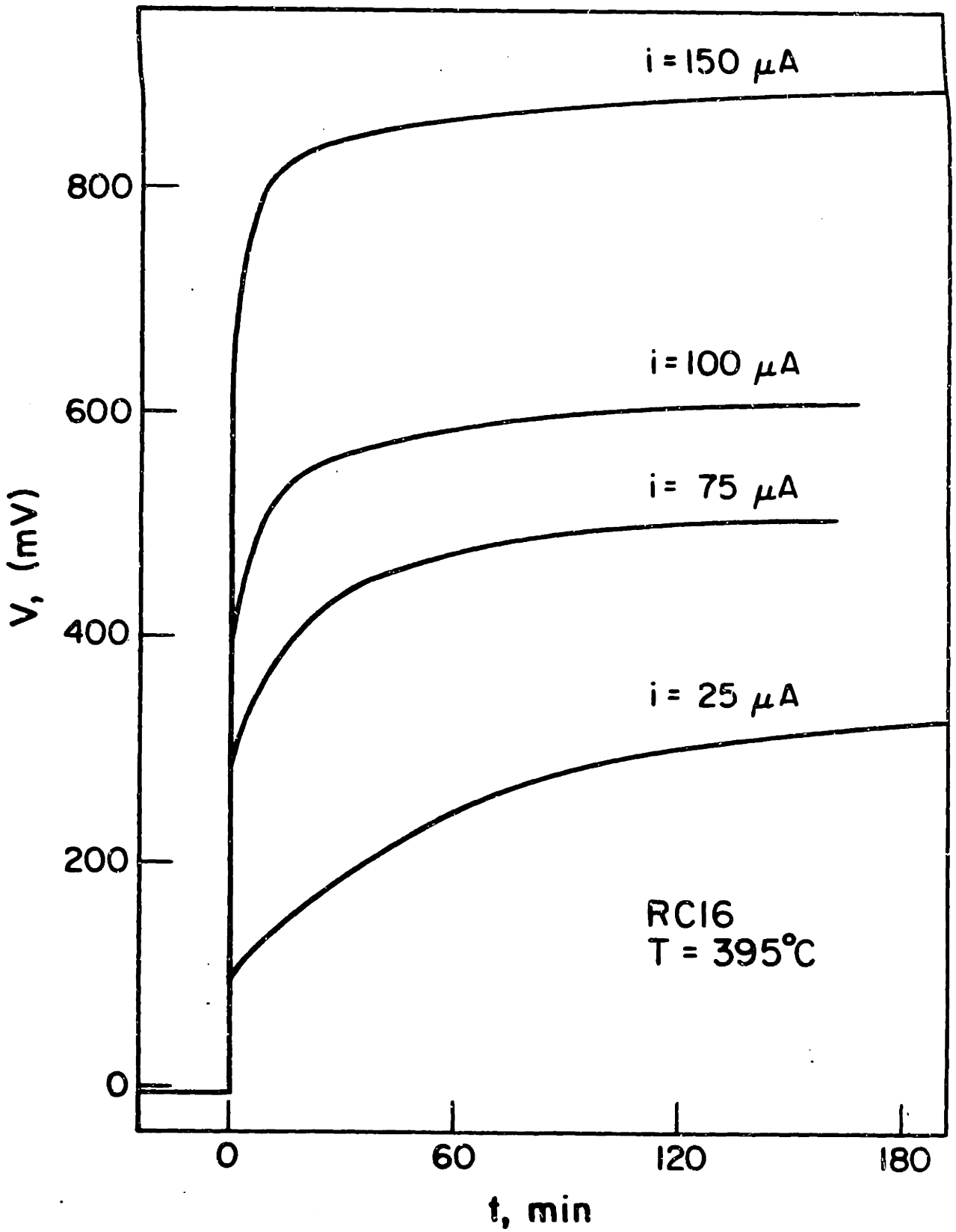

Figure 67: Overpotential rise for various currents i

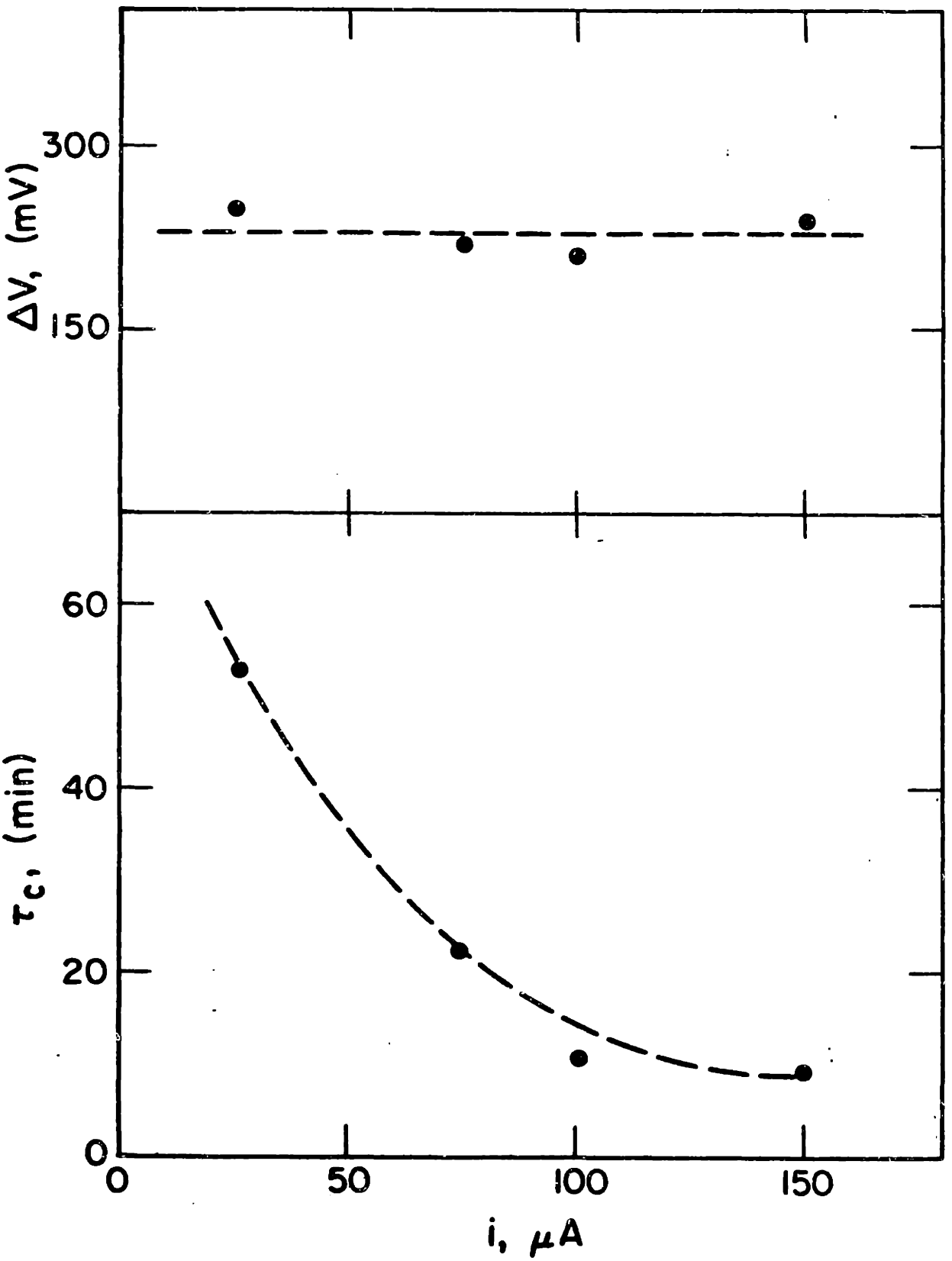

Figure 68: Dependence of relaxation time constant τ on the imposed current i

above figure is of the same order of magnitude with the time constant of the "pumping" process during propylene oxidation. As shown in the same figure the final steady state overpotential rise ΔV is practically independent of the imposed current i.

As in the case of ethylene oxidation, within the accuracy of the experimental data the galvanostatic transient response of ΔV is identical to the transient rate response Δr_1 and Δr_2. This is shown in figure 69 for two different reactors.

C7.c Surface area and gas phase composition effects

Table 11 contains data from 4 different reactor cells RC13, RC14, RC15 and RC16. The relative increase in the propylene epoxidation rate r_1 is shown as a function of the surface area of the catalyst-electrode and the gas-phase composition. Comparing data #2 and #3 which were taken with the same reactor cell, i.e. the same surface area, it can be seen that as the ratio $\frac{P_{Pr}}{P_{O_2}}$ increases the effect of of pumping on the epoxidation rate becomes less considerable. On the other hand lower surface area of the catalyst provides higher relative increase in the reaction rate. This can be seen by comparing the data #3 and #4 as well as data #1 and #5. Thus the effects of surface area and gas composition are the same with those found previously during ethylene oxidation on the same catalyst (sections C4c and C4e).

C7d. Discussion of results

The experimental observations from the electrochemical oxygen pumping during propylene oxidatin can be summarized as follows:

Table 11

Effect of Surface Area and Gas Composition on the reaction rates enhancement

Reactor Cell #	Surface Area (moles O_2)	P_{Pr} (bar)	P_{O_2} (bar)	i (μA)	$\Delta r_1/r_{10}$ (%)
RC13	$1.5 \cdot 10^{-7}$	.0014	.17	200	39
RC14	$7.6 \cdot 10^{-7}$	.0046	.145	200	11
RC14	$7.6 \cdot 10^{-7}$	.0088	.095	200	3
RC15	$1 \cdot 10^{-7}$	.0094	.09	150	20
RC16	10.10^{-7}	.0028	.15	200	11

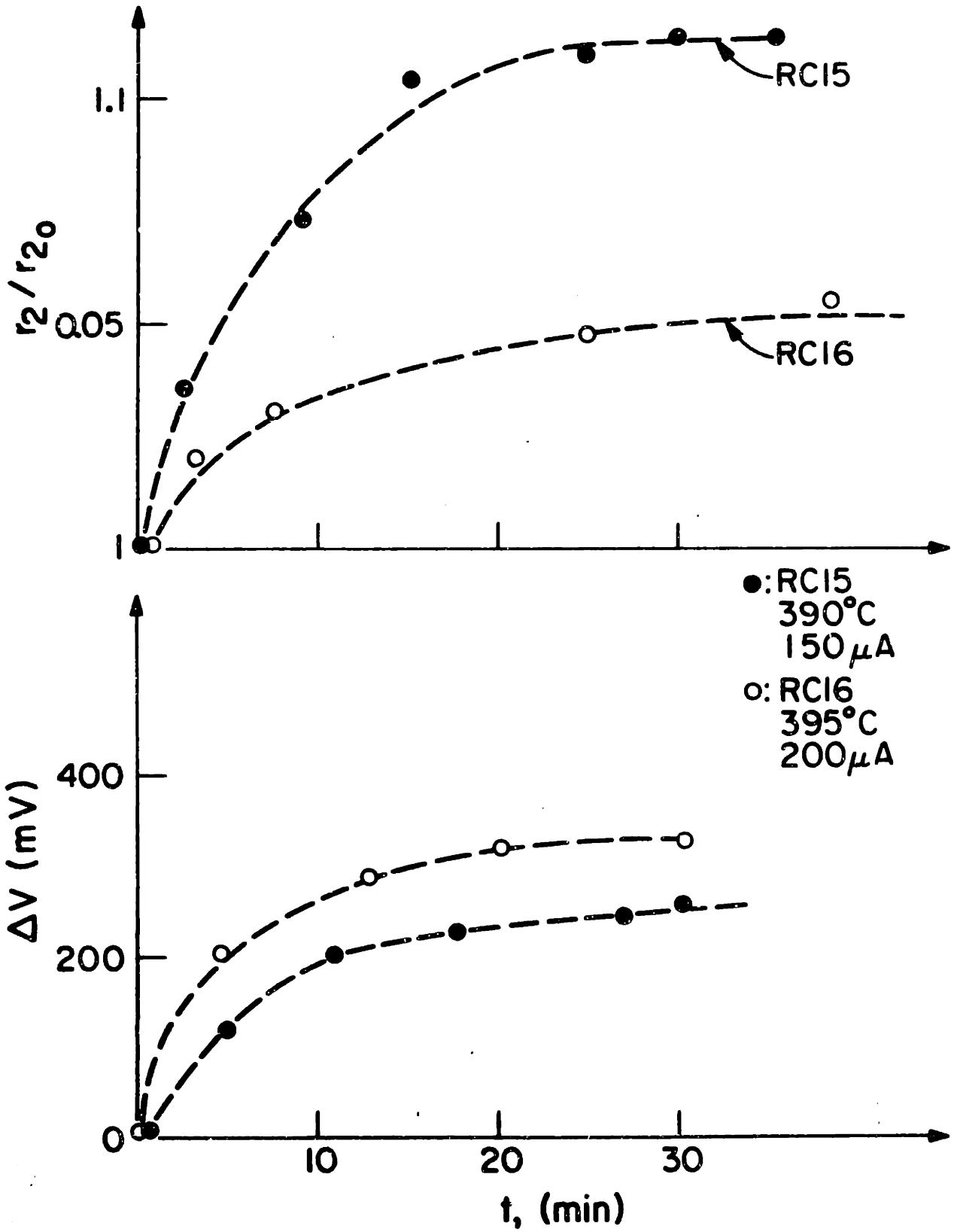

Figure 69: Galvanostatic transient overvoltage increase compared to the reaction rate enhancement

a) A positive current, i.e. pumping oxygen to the catalyst, causes an increase to both epoxidation and deep oxidation rates r_1 and r_2 while by imposing a negative current, i.e. pumping oxygen from the catalyst, both reaction rates are decreased. The selectivity of the reaction increases by imposing a positive current and decreases upon inversion of the polarity. The increase in the reaction rates is two orders of magnitude higher than the rate of oxygen transport across the solid electrolyte.

b) At constant current $\frac{\Delta r_1}{r_{10}}$ and $\frac{\Delta r_2}{r_{20}}$ decrease as $\frac{P_{Pr}}{P_O}$ increases. Also $\frac{\Delta r_1}{r_{10}}$ and $\frac{\Delta r_2}{r_{20}}$ increase by decreasing the surface area of the catalyst-electrode (table (10)).

c) For a given gas composition Δr_1 and Δr_2 are increased by increasing current i followed by roughly constant Δr_1 and Δr_2 for i greater than $\sim$200 μA (figure 64).

d) The transient rate change behavior parallels the transient overvoltage behavior (figure 69). A similar overvoltage rise was observed under galvanostatic conditions even in absence of propylene in the reactor.

The similarity of the above results with those obtained during ethylene oxidation (section C4) incidates strongly what has been previously suggested, i.e. that the effect of oxygen pumping to the rate and the selectivity of propylene epoxidation is associated with a change in the active oxygen species adsorbed on the silver surface during the reaction. In order to explain the effect of oxygen pumping during ethylene oxidation the assumption of active silver oxide formation was made. The activity and selectivity on that silver oxide was assumed

higher than that on reduced silver. The validity of these assumptions is reinforced by the recent results of propylene oxidation. Specifically the observed overvoltage increase upon imposing a constant current, even in absence of propylene, clearly indicates that the reaction rate increase or decrease is associated with changes in the state of oxygen adsorbed on the catalyst surface. This is in agreement with the fact that the dependence of the rate increase Δr_1 or Δr_2 on all the parameters examined (current i, gas phase composition, surface area, relaxation time constant) is qualitatively the same for both ethylene and propylene oxidation.

Thus, excluding the numerical values of the various constants, the model presented in section C4.h for the effect of oxygen pumping during ethylene oxidation is directly applicable in the case of propylene oxidation. Due to the very low intrinsic selectivities to propylene oxide (2-3%) it was quite difficult to determine the exact values of the various constants that appear in the model (see eq. [C4.13],[C4.13]). When the surface area of the catalyst was small the effect of pumping was considerable but the absolute values of the partial pressures of propylene oxide were very low and thus the error in measuring changes of P_{Pro} was very large. If on the other hand the surface area of the catalyst was high the previous problem was overcome but the effect of pumping was diminished.

D. SUMMARY OF RESULTS AND CONCLUSIONS

Two important catalytic systems have been examined in the present work under both open and closed circuit conditions, namely the oxidation of ethylene on silver and the oxidation of propylene on the same catalyst. Experimental results have already been discussed in section C. A summary of the experimental work will be presented herein and kinetic and potentiometric results for the two catalytic systems will be compared.

D.1 Steady State Kinetics

The oxidation of ethylene was studied at temperatures between 250 and 440°C., ethylene partial pressures between 10^{-3} and $2 \cdot 10^{-2}$ bar and oxygen partial pressures between $1.5 \cdot 10^{-2}$ and $15 \cdot 10^{-2}$ bar. The overall reaction network is of the following type

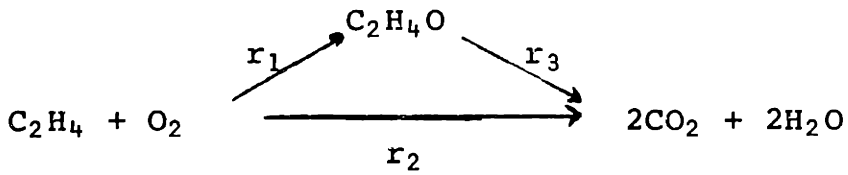

The kinetics of ethylene oxide oxidation to CO_2 and H_2O has been studied separately. The reaction rates r_1, r_2 and r_3 were found to satisfy the following equations: (78,79)

$$r_1 = K_1 \frac{K_{ET} P_{ET}}{1+K_{ET} P_{ET}} \qquad [D1]$$

$$r_2 = K_2 \frac{K_{ET} P_{ET}}{1+K_{ET} P_{ET}} \qquad [D2]$$

and

$$r_3 = K_3 \frac{K_{ETO} P_{ETO}^2}{1+K_{ETO} P_{ETO}^2} \qquad [D3]$$

where

$$K_1 = .28 \exp\left(-\frac{7300}{T}\right) \text{ mole/s} \qquad [D4]$$

$$K_2 = 2\cdot10^2 \exp\left(-\frac{11000}{T}\right) \text{ mole/s} \qquad [D5]$$

$$K_3 = 14.4 \exp\left(-\frac{10200}{T}\right) \text{ mole/s} \qquad [D6]$$

and

$$K_{ET} = 8.7\cdot10^{-4} \exp\left(\frac{5800}{T}\right), \quad K_{ETO} = 3.3\cdot10^{-5}\exp\left(\frac{10600}{T}\right) \qquad [D7]$$

on a porous film that could adsorb a total of $2\cdot10^{-6}$ moles O_2.

The kinetics of propylene oxidation were studied on the same catalyst film at temperatures between 240 and 420°C. The reaction network can be written as: (80)

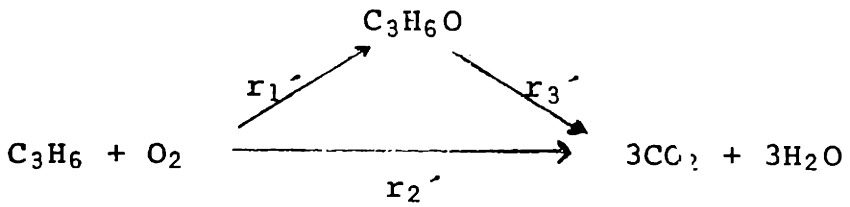

with

$$r_1 = K_1' \frac{K_{Pr}P_{Pr}}{1+K_{Pr}P_{Pr}} \qquad r_2 = K_2' \frac{K_{Pr}P_{Pr}}{1+K_{Pr}P_{Pr}} \qquad [D8]$$

and $r_3' = K_3' \frac{K_{Pro}P_{Pro}}{1+K_{Pro}P_{Pro}}$ where

$$K_1' = 11.94 \exp\left(\frac{-11000}{T}\right) \text{ mole/s} \quad K_2' = 32.9 \exp\left(\frac{-9500}{T}\right) \text{ mole/s}$$

$$K_3' = 6.4 \exp\left(\frac{-9500}{T}\right) \text{ mole/s} \quad \text{and}$$

$$K_{Pro} = .01 \exp\left(\frac{5200}{T}\right) \text{ bar}^{-1}, \quad K_{Pr} = 1.2\cdot10^{-4}\exp\left(\frac{7500}{T}\right)\text{bar}^{-1} \qquad [D9]$$

The rates r_3 and r_3' of ethylene oxide and propylene oxide oxidation respectively were found to be much smaller than r_2 and r_2', i.e. almost all the CO_2 produced during ethylene or propylene oxidation comes from the direct olefin oxidation. In the case of ethylene oxidation r_3 is practically negligible and thus the reaction network reduces to

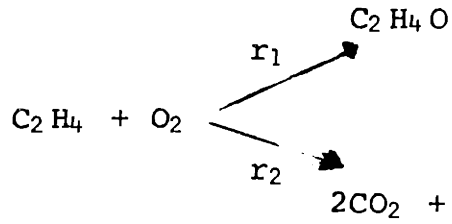

The two rates r_1 and r_2 were of comparable values in the case of ethylene oxidation. Using eqns. [D8] [D9] the selectivity S defined as moles of ETO produced over the total moles of ET reacted is given by the expression

$$S = \frac{r_1 - r_3}{r_1 + r_2} \quad \frac{r_1}{r_1 + r_2} = \frac{K_1}{K_1 + K_2} \qquad [D10]$$

Thus the selectivity is essentially a function of temperature only and it decreases at high temperatures (Section 3). Typical values for S in case of ethylene oxidation were between .4 and .7 (40%-70%).

In the case of propylene oxidation the selectivity was much smaller (between 2% and 3%). The rate of propylene oxide oxidation r_3', although much smaller than r_2' was comparable to r_1', and the selectivity is given by the equation:

$$S = \frac{r_1' - r_3'}{r_1' + r_2'} \qquad [D11]$$

Nevertheless even by neglecting r_3' and considering $S = \frac{r_1'}{r_1' + r_2'}$, the selectivity remains quite small (usually < 5%). This verifies what had been suggested by previous investigators, i.e. the reason for low selectivity of silver for propylene oxide formation is not primarily due to the instability of propylene oxide under reaction conditions (33).

Equations [D1] through [D9] are valid for small partial pressures of CO_2 in the reactor. If the temperature is low and the CO_2 pressure quite high (see section 3.C) there is a consider-

able inhibition effect of CO_2 on the epoxidation rate only which thus causes a decrease in the epoxide selectivity.

Self sustained rate oscillations were observed during the oxidation of propylene oxide to CO_2 and H_2O. It is interesting to be pointed out that under similar conditions none of ethylene, propylene or ethylene oxide oxidations exhibited oscillatory behavior. The period and amplitude of the oscillations were found to depend on temperature, residence time as well as on gas composition (Section 5).

D.2 Oxygen activity measurements

The potentiometric observations (SEP) can be summarized as follows:

a) Generally $a_o < P_{O_2}^{1/2}$, i.e. in presence of ET, ETO, Pr or PrO thermodynamic equilibrium was not established between gaseous oxygen and oxygen adsorbed on the catalyst surface.

b) The surface oxygen activity a_o was found to increase with increasing P_{O_2} at constant hydrocarbon partial pressure.

c) a_o decreased with increasing P_{ET} (or P_{Pr}) at constant P_{O_2}.

d) a_o approaches $P_{O_2}^{1/2}$ with increasing temperature at constant P_{O_2} and P_{ET} (or P_{Pr}). (78, 79, 80)

Specifically for each oxidized compound that was studied the following correlations were found between a_o and the gas phase composition.

$$\frac{P_{O_2}^{1/2}}{a_o} = 1 + K \frac{P_{ET}}{P_{O_2}} \quad \text{(ethylene oxidation)} \qquad [D1.2]$$

$$\frac{P_{O_2}^{1/2}}{a_o} = 1 + K' P_{ETO}^{2} \quad \text{(Ethylene oxide oxidation)} \quad [D13]$$

$$\frac{a_o}{P_{O_2}^{1/2} - a_o} = K_1 P_{Pr}^{-1} + K_2 \quad \text{(propylene oxidation)} \quad [D14]$$

$$\frac{a_o}{P_{O_2}^{1/2} - a_o} = K_1' P_{Pro}^{-1} + K_2' \quad \text{(propylene oxidation)} \quad [D15]$$

where all K's are functions of the temperature only. The kinetic models proposed for the oxidation reactions should be in agreement with the experimental observations [D12] through [D15] which were independently obtained. This limited the number of possible mechanistic models. Specifically in the case of ethylene oxide oxidation eq [D13] indicated the formation of ethylene oxide dimer on the silver surface and this was in agreement with the kinetic results (section 2). The fact that a_o was essentially independent of the partial pressure of CO_2 in the reactor during ethylene oxidation (section 4) showed indirectly the existence of molecular and atomic oxygen adsorbed on the catalyst surface in agreement with previous workers (7)(10). In the case of propylene oxide oxidation during which rate oscillations were observed it was found that the surface oxygen activity a_o and the rate of reaction were oscillating with the same frequency and generally increasing a_o corresponded to increasing rate (figure 51). Combining kinetic and potentiometric measurements it was possible to derive a value for the atomic oxygen desorption rate constant K_d. The values thus obtained for K_d from three separate studies were

$$K_d = 14.4 \exp\left(\frac{-10200}{T}\right) \quad \text{(ETO oxidation)} \qquad [D16]$$

$$K_d = 155 \exp\left(\frac{-13700}{T}\right) \quad \text{(PrO oxidation)} \qquad [D17]$$

and

$$K_d = 89.5 \exp\left(\frac{-12800}{T}\right) \quad \text{(Pr oxidation)} \qquad [D18]$$

The agreement between these three values of K_d independently derived is very good. (For a very wide range of temperatures eqns [D16], [D17] and [D18] provide values of K_d of the same order of magnitude). The activation energies found for K_d (21-28 Kcal/mole) are quite close to those reported previously in the literature ([10]).

D.3 Oxygen pumping

The selectivity and ethylene oxide yield of ethylene oxidation on Ag can be affected significantly by electrochemical oxygen pumping. When external voltages are applied to the cell and O^{2-} is "pumped" to the catalyst, the ethylene oxide selectivity and yield increase consierably. The opposite effect is observed upon inversion of the voltage polarity. The increase in the rate of C_2H_4O production can exceed the rate of O^{2-} pumping by a factor of 400, indicating a dramatic change in the properties of the silver catalyst. The phenomenon is reversible and typical relaxation times are of the order of several minutes. A similar behavior was observed during propylene oxidation on the same catalyst.

Specifically the dependence of the rate increase on the various parameters examined can be summarized as follows:

a) The galvanostatic transient response of the cell overpotential ΔV is identical to the transient rate response Δr_1 and Δr_2 .

b) The relative increase in the reaction rates $\frac{\Delta r_i}{r_{io}}$ decreases as $\frac{P_{ET}}{P_{O_2}}$ (or $\frac{P_{Pr}}{P_{O_2}}$) increases.

c) The relative increase in the reaction rates is inversely proportional to the electrode surface area.

d) Δr_i increases by increasing the imposed current i until a value of i is reached above which Δr_i remains essentially unchanged by increasing the current i. (81,82)

A simple model has been proposed that explains all the experimental observations. The model is based on the hypothesis that oxygen pumping to the catalyst causes an increase in the surface concentration of active silver oxide. The activity and selectivity on the surface of this silver oxide is assumed higher than that on reduced silver. A mass balance for this active oxide (eqn. [C4.13] leads to the following equation for the increase in the reaction rate (Section C4.h)

$$\frac{\Delta r_i}{r_{io}} = \frac{K_i K_2 \ (i/4F) \cdot P_{O_2}}{K_{iO} \cdot S} \left\{ \left[\frac{i}{4FSC_m} + K_1 \theta_{O_2} + K_2 P_R \right] \left[K_1 \theta_{O_2} + K_2 P \right] \right\} \qquad [D19]$$

S = surface area of the catalyst-electrode

i = current

F = Faraday constant

$P_R = P_{ET}$ or P_{Pr}

θ_{O_2} = surface coverage of molecular oxygen

K_i, K_2, K_1 reaction rate constants

D4. Conclusions

The present results from the steady state kinetic and oxygen activity measurements provided some new information

about the catalytic oxidation of ethylene and propylene on silver. The use of solid electrolyte potentiometry in conjunction with other surface-sensitive techniques, such as ir spectroscopy, could improve considerably the understanding of this important catalytic systems. SEP measurements have been proved to contribute considerably in investigating oscillatory phenomena as the observed rate and oxygen activity oscillations during propylene oxide oxidation. We note that propylene oxide oxidation is the first known reaction which exhibits periodic behavior on silver.

Study of the above reactions under closed circuit conditions showed that oxygen pumping alters the nature and the catalytic properties of silver. We note that this is the first known application of electrochemical oxygen pumping through a solid electrolyte to alter the selectivity of a heterogeneous catalytic reaction. The present study was limited to temperatures above 300°C because of the severe increase in the electrolyte resistance with decreasing temperature. Thinner (<100 μm) electrolyte components must be used to study the temperature range of industrial interest, i.e. 220° to 290°C. The application of external voltages to solid electrolyte cells with appropriate catalyst electrodes may be a powerful technique for influencing the selectivity of other partial catalytic oxidations as well.

E. LITERATURE

1. Chem. Eng. Prog. 76 (1), 53, (1980)
2. Zomerdijk, J.C., and Hall, M.W., Cat. Rev. - Sci. Eng. 23 (1), 163, (1981)
3. Twigg, G.H., Proc. Roy. Soc. A., 188, 92 (1946)
4. Twigg, G.H., Tans. Faraday Soc. 42, 284 (1946)
5. Chilton, C.H., Chem. Eng. 65, 100, (1958)
6. Landau, R. Petrol. Refiner 32, (9), 146 (1953)
7. Voge, H.H., and Adams, C.R., Avd. Catal. 17, 154, (1967)
8. Force, E.L. and Bell, A.T., J. Catal. 38, 440 (1975)
9. Force, E.L. and Bell, A.T., J. Catal. 40, 356 (1975)
10. Kilty, P.A., Rol, N.C. and Sachtler, W.M.H., Proc. 5th Int. Congr. Catal. Miami, Fla. (J.W. Hightower, Ed.)
11. Kilty, P.A. and Sachtler, W.M.H., Cat. Rev.-Sci.Eng., 10 (1), 1 (1974)
12. Imre, L., Ber. Bunsenges. Phys. Chem., 74, 220 (1970)
13. Kenson, R.E., and Lapkin, M., J. of Phys. Chem. 74 (7) 1943 (1970)
14. Flank, W.H. and Beachell, H.C., J. Catal. 8, 316 (1967)
15. Spath, H.T., Proc. 5th Int. Congr. Catalysis, Miami, Fla. (J.W. Hightower, Ed.) Paper 64, p. 929, American Elservier, N.Y. 1972
16. Temkin, M.I., Kinetika i Kataliz. 18 (3), 544 (1977)
17. Herzog, W., Ber. Bunsenges. Phys. Chem. 74, 216 (1970)
18. Law, G.H., and Chitwood, H.C., U.S. Patent 2, 279, 469 (1942)
19. Metcalf, P.L. and Harriot, P., Ind. Eng. Chem. Proc. Des. and Develop. 11, 4 (1972)
20. McKim, F.L., and Cambron, A. Can. J. of Research 27B 814 (1949)

21. Kurilenko, A.I., et.al., Zhur. Fix. Khim. 32, 1048 (1958)

22. Hayes, K.E., Can. J. of Chem. 38, 2256 (1960)

23. Temkin, M.I., Kinetika i Kataliz 3, 189 (1963)

24. Ionov, Y.V., Rastatruin, V.A., and Kurochkin, Y.Y., Zh. Prinkl. Khim. 44 (3), 606 (1971)

25. Wachs, I.E., and Kelemen, S.R., J. Catal. 71, 78, (1981)

26. Kummer, J.T., J. Phys. Chem. 60, 66, (1956)

27. Carberry, J.J. Kuczynski, G.C. and Martinez, E., J. Catal. 26, 247 (1972)

28. Clarkson, R.B., and Cirillo, A.C., J. of Catalysis 33, 332 (1974)

29. Sato, N. and Seo, M., J. of Catalysis 24, 224 (1972)

30. Harriot, P., J. Catal. 21, 56, (1971)

31. Wu, J.C. and Harriot, P., J. Catal. 39, 395 (1975)

32. Verykios, X.E., Stein, F.P. and Coughlin, R.W., J. Catal. 66, 368 (1980)

33. Cant, N.W., and Hall, W.K., J. Catal. 52, 81, (1978)

34. Dettwiller, H.D., Baiker, A. and Richarz, W., Helv. Chim. Acta 62, 1689 (1979)

35. Sherwood, P., Chem. et Industrie 87 (6), 764, (1962)

36. Bryce-Smith, D., and Blues, E., C.E. News 50, 48,(1972)

37. Kaliberdo, L.M., et al. Kinetika i Kataliz 8(2) 463 (1967)

38. Kaliberdo, L.M., Vaabel, A.S., and Torgasheva, A.A., Kinetika i Kataliz 8 (1) 105 (1967)

39. Manara, G., And Parravano, G., J. of Catalysis, 32, 72 (1974)

40. Kaliberdo, L.M., Dorogova, V.B., Pashegorova, V.S., Neftekhimiya 11 (5) 719 (1971)

41. Rouchaud, J., and De Pavw, M., J. of Catalysis 14, 114, (1969)

42. Invi, T., et al, J. Chem. Soc. Faraday Trans. 74 (10) 2430 (1978)

43. Kano, H., et al., Muroran Kogyo Daigaku Ken. Hok. 6 (2) 555 (1968)

44. Vaabel, A.S., Kaliberdo, L.M., Milman, F.A., Khim Aromat Nepredel'n Soedin, 187, (1972)

45. Kaliberdo, L.M., Dorogova, V.B., Chenets. V.V., Ref., Zh. Khim. Abstr. No. 9B1314, (1973)

46. Vaabel, A.S., Kuvakina, P.R., Kaliberdo, L.M., Izv. Nauch-Issled. Inst. Neft-Uglekhim. Sin. Irkurtsk. Univ. 11 (1) 27 (1969)

47. Vaabel, A.S., et al., Kinet. i. Katal. 9 (5), 1053, (1968)

48. Kaliberdo, L.M., and Zhukova, G.G., Izv. Nauch.,-Issled. Inst. nefte-Uglekhim. Sin. Irkutsk. Univ. 9 (1), 136, (1967)

49. Yamamoto, T.A., Kano, H., Muroran Kogyo Daigaku Kenkyu Hokoku, Rio Hen 9 (1), 229, (1976)

50. Dorogova, V.B., Kaliberdo, L.M., Izv. Nacuh-Issled. Inst. Nefte-Uglekhim. Sin. Irkutsk. Univ. 11 (1) 31 (1969)

51. Imachi, M., et al., J. Catal. 70, 177, (1981)

52. Kobayashi, M., Can. J. of Chem. Eng. 58, 588, (1980)

53. Subbarao, E.C., "Solid Electrolytes and their Applications", Plenum Press, New York (1980)

54. Kiukkola, K., and Wagner, C., J. Electrochem. Soc. 104, 379, (1957)

55. Etsell, T., and Flengas, S., Chem. Rev. 70, 339, (1970).

56. Schmalzried, H., Z. Phys. Chem. 38, 87, (1963)

57. Steele, B., and Alcock, C., Trans. Metal. Doc. A.I.M.E., 233, 1369, (1965)

58. Baker, R., and West, T., J. Iron Steel Inst. 204, 212, (1966)

59. Peters, H., and Mobius, H., Z. Phys. Chem. 209, 298, (1958)

60. Peters, H., and Mann, G., Z. Electrochem. 63, 2, (1959).

61. Weissbart, T., and Ruka, R., J. Electrochem. Soc. 109, 723, (1962)

62. Wagner, C., Adv. in Catalysis 21, 323, (1970)

63. Vayenas, C.,and Saltsburg, H., J. Catal., 57, 296, (1979)

64. Vayenas, C., and Saltsburg, H., Col. and Interface Sci. 3, 261, (1976)

65. Vayenas, C.G., Lee, B., and Michaels, J., J. Catal., 66, 36 (1980)

66. Weissbart, T., Smart, W. and Waydeven, T., Aerospace Medicine 40, 136, (1969)

67. Pancharatnam, S., Huggins, R. and Mason, D., J. Electrochem. Soc. 122, 869, (1975)

68. Gur, T., and Huggins, R., J. Electrochem. Soc. 126, 1067, (1979)

69. Vayenas, C.G., and Farr, R.D., Science 208, 593, (1980)

70. Farr, R.D., and Vayenas, C.G., J. of Electrochem. Soc. 127 (7) (1980)

71. Nault, G.N., et.al., in Ind. Eng. Chem. Process Des. Develop. 1 285 (1962)

72. Czanderna, A.W., J. Coll. Interface Sci. 24, 500 (1967)

73. Ostrovskii, V.E., and Temkin, M.I., Kinet. Katal. 7 (3), 529 (1966)

74. Bockris, J. O'M., Reddy, A.K.N., "Modern Electrochemistry", New York, 1973, p. 1020-1036; 1190-1195

75. Holbrook, L.L. and Wise, H., J. Catal. 38, 294 (1975)

76. Vayenas, C.G., Georgakis, C., Michaels, J. and Tormo, J., J. Catal. 67, 348 (1981)

77. Freriks, I.C., Bouwman, R., and Geenen, P.V., J. Catal. 65, 311 (1980)

78. Stoukides, M., and Vayenas, C., J. Catal. 64, 18, (1980)

79. Stoukides, M., and Vayenas, C., J. Catal. 69, 18, (1981)

80. Stoukides, M. and Vayenas, C., J. Catal., in press, 1982

81. Stoukides, M., and Vayenas, C., in "Catalysis under transient conditions" (A.T. Bell and L.L. Hegedus, Eds.). ACS Symp. Series, in press, 1982.

82. Stoukides, M., and Vayenas, C., J. Catal. 70, 137, (1981)